Acetabular Defect Augmentation with Kryptonite Bone Cement in Total Hip Replacement: Stability Analysis

BY

STEFANIE BROVIAK

B.S., University of Illinois at Chicago, Chicago, 2010

THESIS

Submitted as partial fulfillment of the requirements

for the degree of Master of Science in Bioengineering

in the Graduate College of the

University of Illinois at Chicago, 2012

Chicago, Illinois

Defense Committee:

Farid Amirouche, Mechanical & Industrial Engineering, Chair and Advisor

David Eddington

Andreas Linninger

ACKNOWLEDGEMENTS

First and foremost, I want to thank my adviser, Dr. Farid Amirouche, for his never-ending support and expertise. He took me in as an undergraduate student and introduced me to the field of biomechanics, for which I will be forever grateful. Most importantly, he always asks the questions that I never think to ask, which has helped me to develop tremendously as an engineer.

I am sincerely grateful to Dr. Giovanni F. Solitro, who has always been there to answer all of my questions, no matter how big or small. His encouragement and patience with me has helped in more ways than I can even begin to describe.

I also want to thank my committee members, Dr. David Eddington and Dr. Andreas Linninger, who have agreed to take the time out of their busy schedules to take an interest in my research.

Lastly, I am grateful to the other students in the lab who have always provided support and friendship when I needed it the most.

TABLE OF CONTENTS

LIST OF TABLES

LIST OF FIGURES

LIST OF ABBREVIATIONS

3D	Three dimensional
BW	Body Weight
BMD	Bone Mineral Density
CAD	Computer Aided Design
DAQ	Data Acquisition
DICOM	Digital Imaging and Communications Medicine
FEA	Finite Element Analysis
DOF	Degree of Freedom
LVDT	Linear Variable Differential Transformer
OA	Osteoarthritis
OP	Osteoporosis
PMMA	Polymethylmethacrylate
RA	Rheumatoid Arthritis
SD	Standard Deviation
THR	Total Hip Replacement
THA	Total Hip Arthroplasty
UHMWPE	Ultra High Molecular Weight Polyethylene
VI	Virtual Instrument

SUMMARY

The pelvis connects the upper and lower extremities of the body's musculoskeletal system and plays an extremely important role in locomotion, balance, and stability, as well as load transfer across the joint. The hip joint is a ball and socket joint which fits into the acetabulum of the pelvis, and is able to support as much as five times the body weight with a smooth articulation within the joint itself. The repetitive loading of the hip joint leads to degeneration of the surrounding articular cartilage and cortical bone and can result in acetabulum bone defect and osteoarthritis. In order to restore normal hip function, a number of patients undergo a total hip replacement surgery.

Both experimental studies utilizing cadaveric specimens and finite element analysis studies usually complement well the clinical investigation of cup fixation. In this thesis research, a finite element model suitable for patient-specific analysis was developed and validated with in-vitro measurements. The use of a finite element model helps to quantify the effect of various factors including the amount of under-reaming and the force used to insert the acetabular cup on the micromotion and stress due to simulated initial post-operative loading. The results indicate that for a lesser amount of under-reaming less cup insertion force is needed, and approximately the same percentage of surface contact at the cup-bone interface can be achieved with only a slight difference in micromotion of the cup occurs.

Furthermore, acetabular defects and repair in the presence of total hip replacement are seen in patients with severe arthritis or extensive bone loss at the hip joint because aseptic loosening of the acetabular cup component following initial THR

can lead to additional bone loss over time. The study aims to quantify the displacement and rotation of the acetabular cup into the acetabulum following THR using the mechanical testing of cadaveric specimens with and without the presence of an acetabular wall defect augmented with Kryptonite bone cement. The results suggest that defect augmentation with Kryptonite bone cement during acetabular wall reconstruction allowed for a successful reconstruction of the wall, but that the response is dependent on the loading conditions.

Finally, a finite element model was developed in which an acetabular defect was introduced in order to have an understanding of the initial cup fixation and stress on the bone during immediate post-operative loading and for various bone apparent densities. The results show that defect reconstruction with bone screws and Kryptonite results in a re-distribution of stress into the bone, particularly at the site of defect reconstruction. The results of this study can provide useful information for clinicians performing total hip replacement with and without the presence of acetabular wall defects.

1. INTRODUCTION

1.1 Introduction

In a healthy human hip joint, the coverings of the bone are evenly masked with a covering of articular cartilage, which can become worn over time, causing degeneration of the protective coating that it provides to the acetabulum (Noguchi et al., 1999). In order to relieve the pain caused by the degenerated interface, a total hip replacement (THR) surgery is often performed. This section describes the surgical process of THR, as well as the materials properties of implant components, and the occurrence of post-operative failure.

1.2 The Healthy Hip Joint

Although often used interchangeably, the pelvis and hip are two separate and distinct, yet integrated parts of the body (McKinley and O'Loughlin, 2006). More specifically, the pelvis is a semicircular rigid bony complex designed to support the weight of the upper body while transferring that weight evenly to the leg bones through the hip joint. The pelvis is composed of the sacrum and the coccyx, as well as a left and right coxal bone. The pair of two separate os coxae, which are often referred to as the coxal bones or "hip bones," each contain three fused bones - the ilium, ischium, and pubis. The labeled anatomy of the pelvis bones are shown in Figure 2. The largest, the ilium, is located on the lateral side of each coxal bone, or hemi-pelvis, and is formed in the shape of a wing. The superior portion of the ilium forms the iliac crest, which begins at the anterior superior iliac spine and extends posteriorly to the posterior superior iliac spine. The ischium makes up the posterior inferior portion of the pelvis. Bony formations

along the posterior end form the ischial tuberosity and aid in supporting the weight of the body in a sitting position. The flattened portion of the ischium, also known as the ramus, joins with the inferior ramus of the pubis, which forms the base of the pelvis. The rough area on the anterior surface of the pubis is called the pubic symphysis and marks the site of connection between the two coxal bones. In addition to supporting the weight of the upper body, the pelvis assists in all types of upright movement and locomotion. The ilium, ischium and pubis each come together to form the acetabulum.

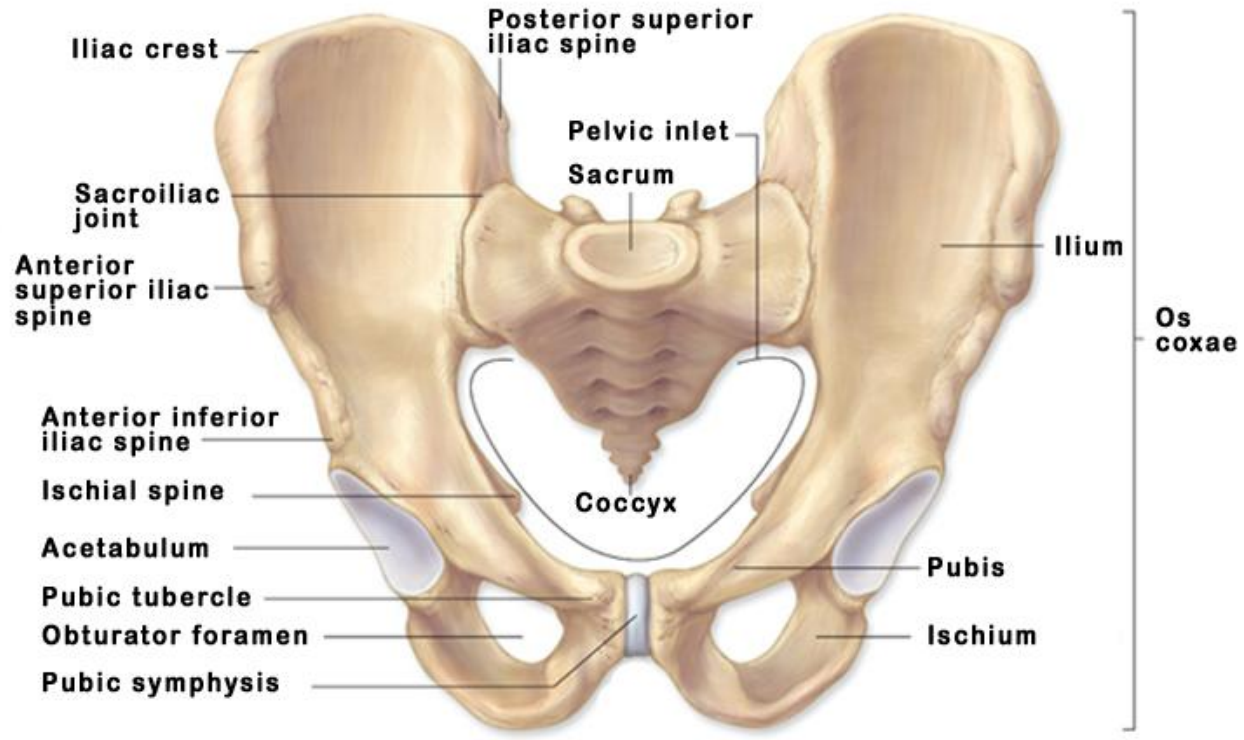

Figure I. Anatomy of the complete pelvis, consisting of the os coxae, the sacrum, and the coccx. Cited from (McKinley and O'Loughlin, 2006)

The hip joint is referred to as a ball and socket joint, which means that it allows for a 360° range of motion for the femur. In total, four bones make up the hip joint. The acetabulum is a cup-shaped portion located on the lateral side of the pelvis, into which the femur head inserts to create the ball and socket interaction. When standing in the upright position, the center of gravity passes directly through the hip joint and into the center of the femoral head of the femur.

1.2. 1 Cortical Bone

The cortical bone is a thin shell of dense bone which in the pelvic region ranges from 1.04 to 2.01 mm thick in a healthy person (Richards et al., 2010). Cortical bone is typically a highly dense material, with a bone mineral density of 1.215±0.1 g/cm^3 in the femur (Wachter et al., 2002). Cortical bone is composed mostly of a highly structured system of osteons, which contain lamellae surrounding the Haversion canal (McKinley and O'Loughlin, 2006). The organizational alignment of the lamellae for the long bone to undergo slight torsional forces without breaking (Jepson et al., 1999). According to literature reviews (Table 1), compression testing on cortical bone has resulted in strength values ranging from 133 to 195 MPa and a Young's modulus ranging from 11.4 to 29.2 GPa. Under tensile testing, the strength and Young's modulus are significantly decreased, and range from 90 to 188 MPa and 7.1 to 28.2 MPa, respectively. The Poisson's ratio of cortical bone has most often been found to be 0.3 (Spears et al., 2001). The cortical shell surrounds a less dense trabecular bone, as shown in Figure 1.

Table I. Literature Review of Cortical Bone Material Properties.

Bone	Strength (Mpa)	Elastic Modulus (Gpa)	Reference
Compression			
Femur (2x2x6 mm dumbbell)	167-215	14.7-19.7	Reilly et al., 1974
Femur (2x2x6 mm dumbbell)	179-209	15.4-18.6	Burstein et al., 1976
Femur (3 mm diam. dumbbell)	205-206	-	Cezayirlioglu et al., 1985
Distal Femur (8.1 mm cylinder)	321 ± 213	-	Burgers et al., 2008
Femur Mid-shaft (1 cm section)	-	17.73 ± 0.22	Turner et al., 1999
Proximal Tibia	-	5.54 ± 1.25	Choi et al., 1990
Tension			
Femur (2x2x6 mm dumbbell)	107-140	11.4-19.7	Reilly et al., 1974
Femur (2x2x6 mm dumbbell)	120-140	15.6-17.7	Burstein et al., 1976
Femur (3 mm diam. dumbbell)	133-136	18.9-29.2	Cezayirlioglu et al., 1985

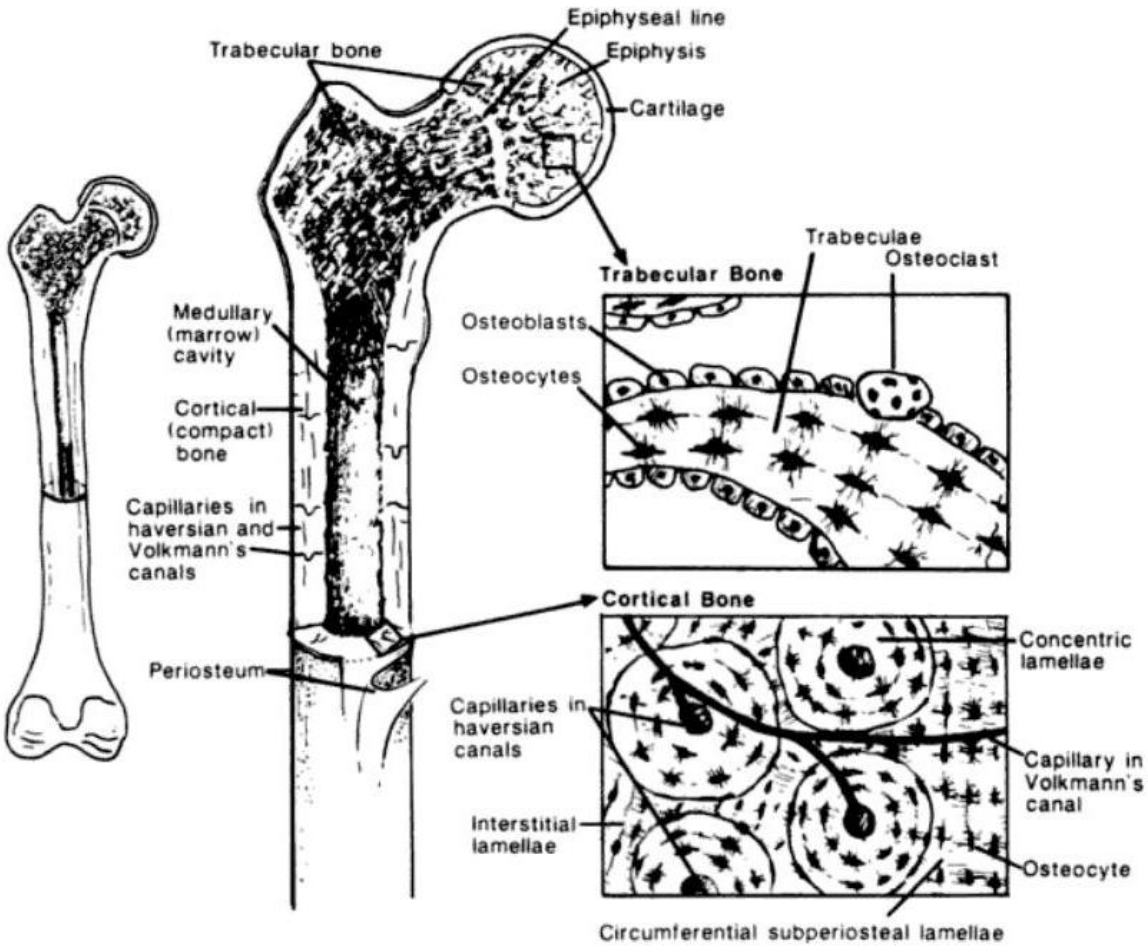

Figure II. Network of cancellous bone and cortical bone.

Cited from Hayes et al., 1991.

1.2.2Trabecular Bone

In the femur, trabecular bone, also known as cancellous bone, aids in supporting the compressive loads of the bodily weight (McKinley and O'Loughlin, 2006). It is composed of a porous network which is aligned along the directions of stress loading in long bones. In contrast to cortical bone, trabecular bone is much less dense, with a

bone mineral density of 0.245±0.02 g/cm^3 in the proximal femur (Jiang et al., 1998). The mechanical properties of trabecular bone, including Young's modulus and strength are heavily dependent on the apparent density of the bone (Gibson, 1985; Rice et al., 1988), and are shown in Table 2.

Table II. Literature Review of Trabecular Bone Material Properties.

Bone	Ultimate Strength (Mpa)	Elastic Modulus (Gpa)	Reference
Femoral Head (9 mm diam. Cyl)	3.3	-	Li et al., 1997a
Femoral Head (8 mm diam. Cyl)	6.6 ± 6.3	0.9± 0.71	Martens et al., 1983
Proximal Femur (8 mm diam. Cyl)	5.6 ± 3.8	0.616 ± 0.707	Martens et al., 1983
Proximal Tibia (7,5:7.5 mm. Cyl)	5.3 ± 2.9	0.445 ± 0.257	Linde et al., 1989
Proximal Tibia (127.1x118.7 microns)	-	4.59 ± 1.6	Choi et al., 1990

1.3 Indications for Total Hip Replacement Surgery

Diseases of the hip joint can affect persons of many ages and can present in a number of forms, including arthritis, osteoarthritis, rheumatioid arthritis, or osteonecrosis (Kaufer, 1980) and are often indications for a total hip replacement surgery.

1.3.1 Arthritis

Although the term arthritis is defined as an inflammation of the joints, this term is often used to characterize any condition in which the joint or surrounding cartilage has

been damaged, regardless of the presence of inflammation, and has been known to increase with age (Badley et al., 1994). In the early stages of arthritis, any pain is most likely due solely to inflammation of the joint; however, chronic, long-term pain caused by arthritis is more often due to the mechanical friction between the surfaces of two articulating bones after their cartilage has been eroded (Lewis, 1991).

1.3.2 Osteoarthritis

In a healthy human hip joint, the coverings of bones are very even and protectively lined with a defensive tissue called cartilage. The most common type of degeneration of the hip joint is known as osteoarthritis (OA), which is a degenerative disease that affects the entire joint (Callaghan, 2007). A comparison of a healthy hip joint versus a joint affected with OA is shown in Figure 2. The occurrence of osteoarthritis often causes devastation to the bone coverings and cartilage where the femoral head and acetabulum contact and rub together. More specifically, OA is characterized by the degeneration of articular cartilage located on the load bearing portions of the joint (Radin, 1995). When this occurs, the interface between the bones is damaged, causing the joint to become eroded and uneven, which can eventually result in joint stiffness and pain, as well as instability (Griffin et al., 2005). In extreme cases, joint mobility may also be limited by the occurrence of bone spurs, or osteophytes around the joint (Radin et al., 1991). For example, individuals with physically demanding professions, especially those in which the hip joint sees repetitive motion, have been found to be more likely to experience early onset joint degeneration (Anderson et al., 1993; Felson et al., 1994).

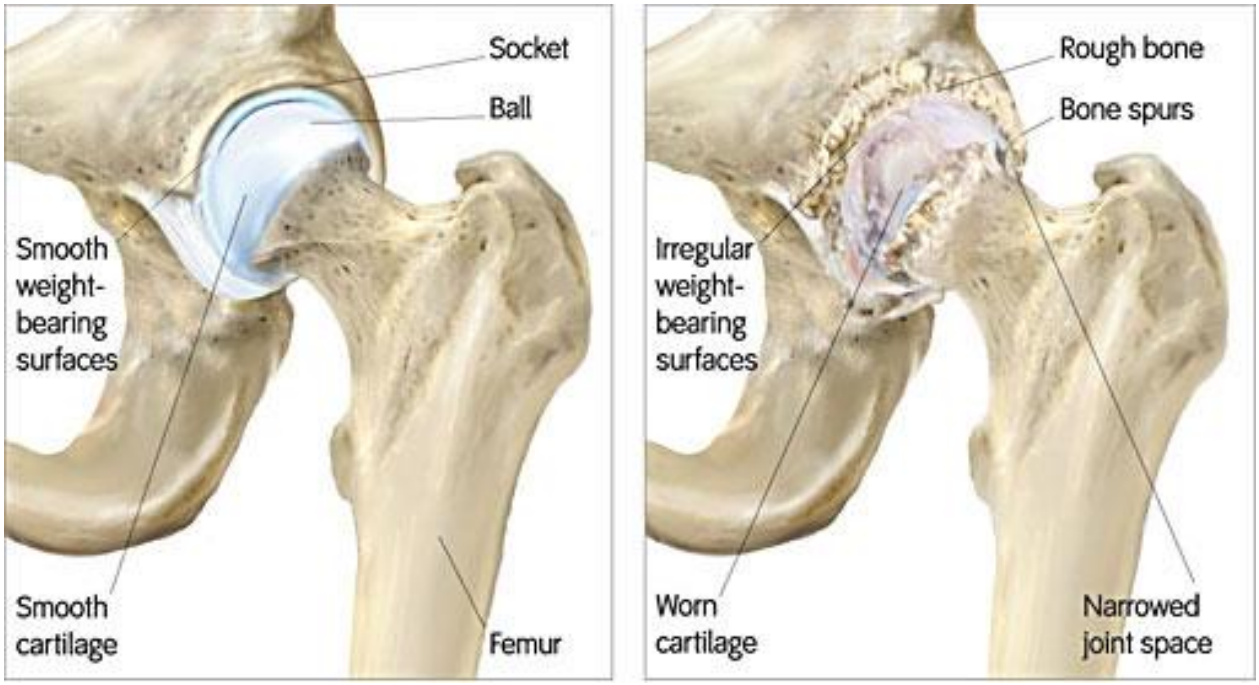

A B

Figure III. Healthy hip joint (A) and hip joint affected by osteoarthritis (B).
http://www.sonoranhipcenter.com/patient-education-hip-pain.shtml

There are a number of ways to treat joint pain as a result of osteoarthritis. In less extreme cases, the patient may be given anti-inflammatory drugs or nutritional supplements to reduce pain and swelling (Ausiello et al., 2002). If severe OA, or if non-surgical techniques are unsuccessful, a total hip replacement, or hip arthroplasty, is often the next step (ACR, 2000).

1.3.3 Osteoporosis

As an age related degenerative disorder of the bone, osteoporosis (OP) commonly affects middle-aged and elderly individuals, (Mäkinen et al., 2007) although women are at a greater risk for OP compared to men of the same age (Kanis et al., 1992). Studies have shown that while only 29.1% of men over the age of 85 are affected, while 60.5% of women of the same age are affected by OP (Kanis et al., 1994). OP is characterized by the occurrence of bony fractures (Seeley et al., 1991). The results of several studies have shown that the likelihood of fractures is directly related to the decrease of bone mineral density (BMD) (Melton, et al., 1993; Hui et al., 1988). In an individual affected by OP, the BMD is at least 2.5 standard deviations below the mean BMD of a healthy young adult, whereas the BMD of severe OP is greater than 2.5 SD below (Kanis et al., 1994). Figure 3 shows a radiograph image of a hip joint affected with decreased bone density due to OP. The fractures occurring due to increased fragility of the surrounding bone can occur as a result of decreased bone mass due to resorption (Raisz, 2005). Bone resorption can affect cortical bone or trabecular bone (Parfitt et al., 1995). For women between the ages of 75 to 81, the occurrence of pelvic fracture due to OP increased from 18% to 64% (Baron et al., 1996).

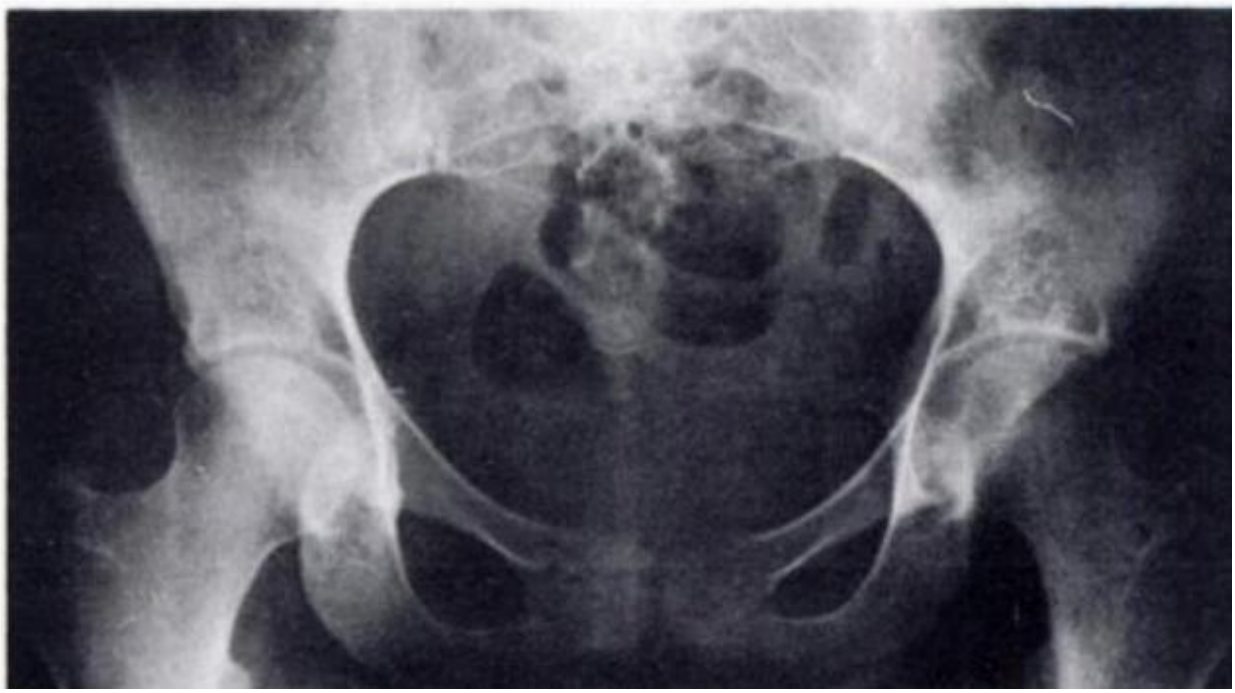

Figure IV. A radiograph image of a decreased bone density in the left hip, evidenced by an indistinguishable femoral head edge. Cited from Shifrin et al., 1987.

1.3 Total Hip Replacement and Acetabular Defect Repair

Total hip replacement (THR), also known is total hip arthroplasty (THA), is an operative technique that is used to replace the weight-bearing surfaces of the hip joint to reduce the pain and instability caused by osteoarthritis of the hip. A total hip replacement consists of an acetabular cup inserted into the acetabulum of the pelvis which articulates with a ultra high molecular weight polyethylene (UHMWPE) liner and a femoral stem, which is inserted into the femur (Figures 4-5). This explanation of total hip replacement is described in terms of the posterolateral approach. The total hip replacement procedure is described as follows (DePuy Orthopaedics, 2006).

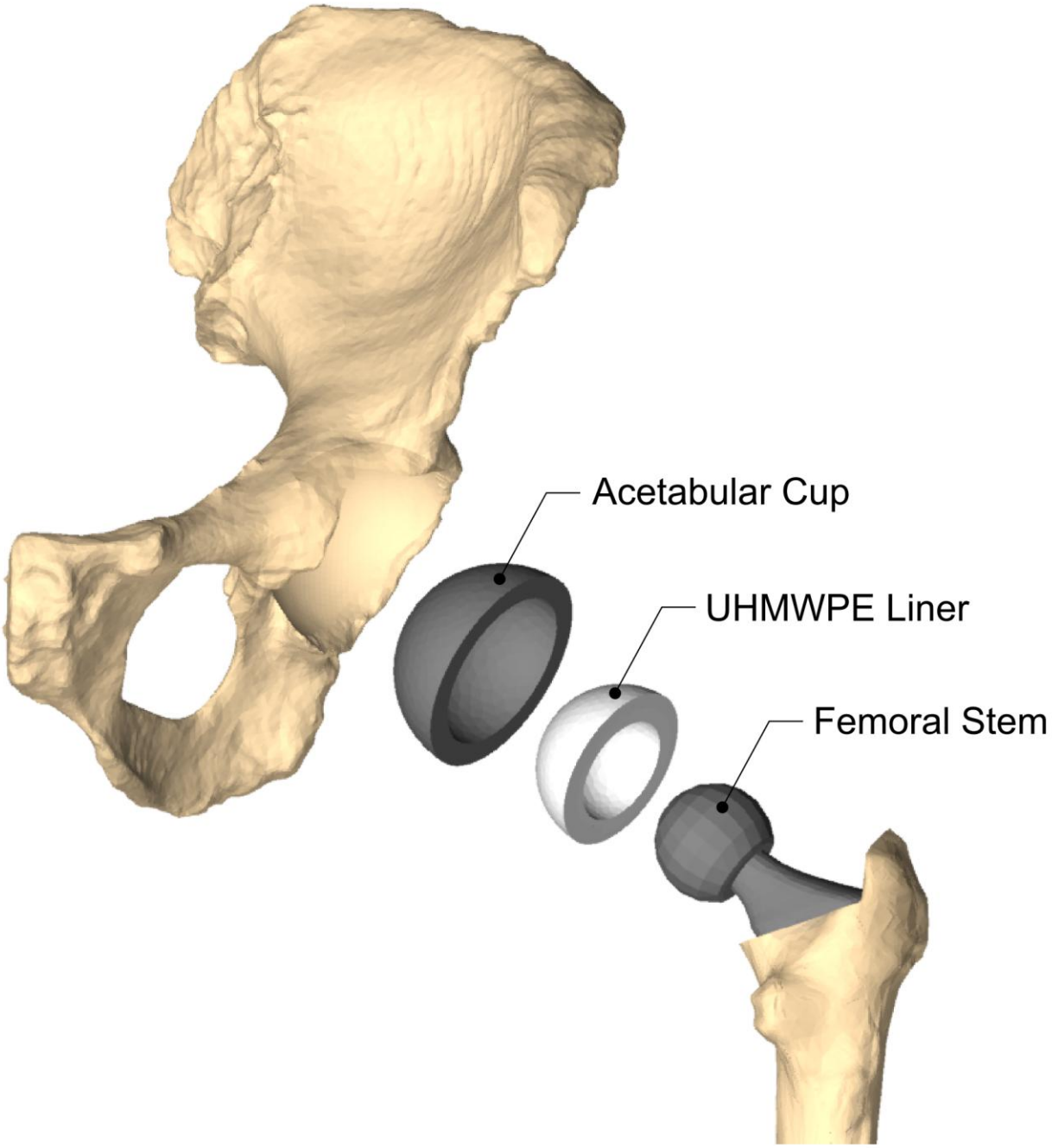

Figure V. The components of a total hip replacement.

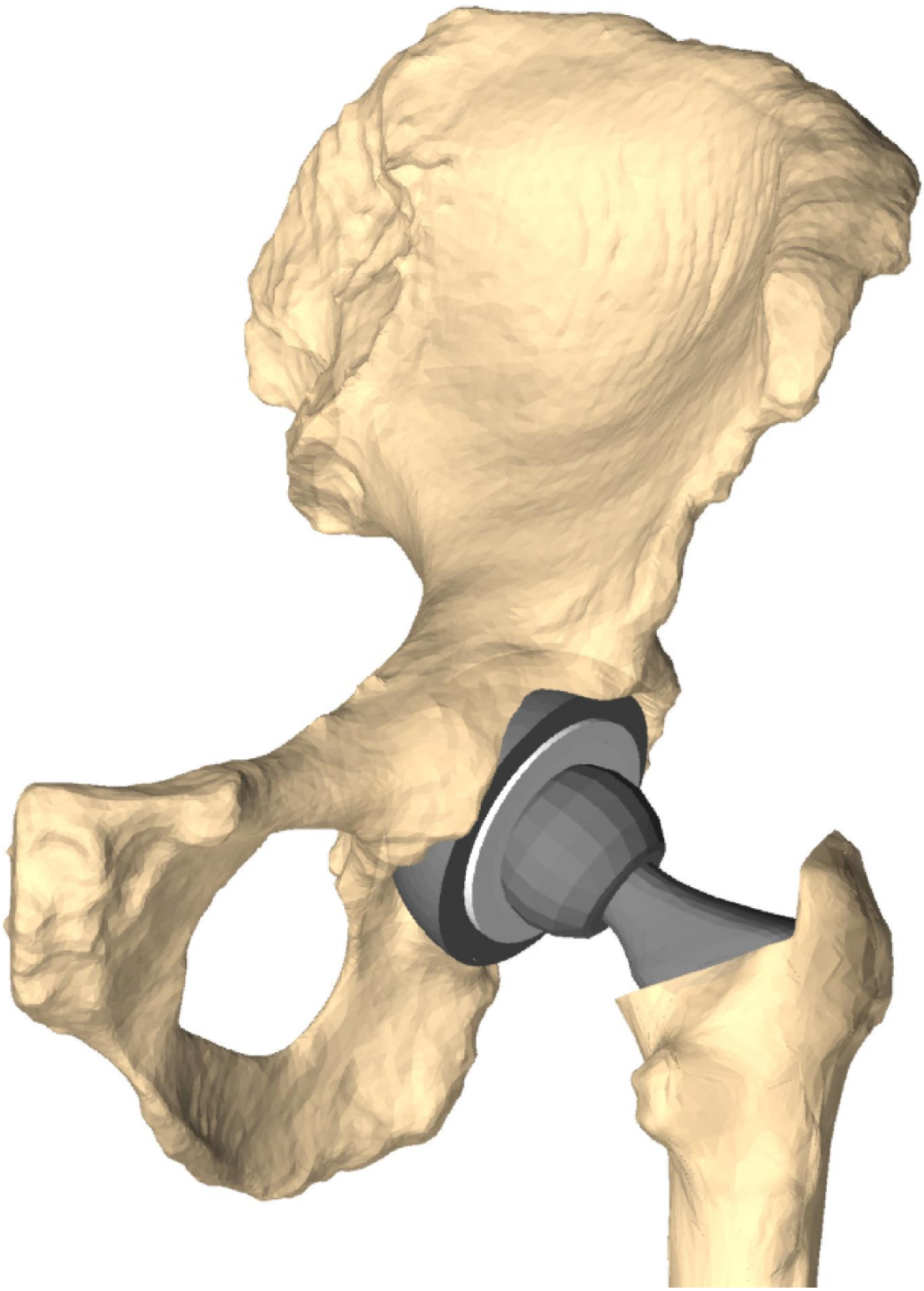

Figure VI. Frontal view of a computer rendering of a hemi-pelvis and femur following total hip replacement.

In the postero-lateral approach, the skin incision is located slightly towards the anterior rim of the greater trochanter and extending over the tip along the axis of the femur. Below that, the incision of the subcutaneous tissue follows the same line. The vastus lateralis and gluteus medius muscles are detached from the greater trochanter to expose the underlying bone. The femoral neck is marked for removal, and an oscillating saw is used to completely remove the femoral head in two osteotomies. The junction between the femoral head and neck marks the site of the first osteotomy, and the second occurs on the lateral portion of the femoral neck.

After the acetabular socket has been exposed through circumferential retraction the acetabular cup may be implanted. In order for the acetabular cup to be completely contained within the acetabulum, the socket must be deepened, or reamed, prior to implantation. For correct reaming, the reamers should be directed horizontally in order to preserve the anatomical center of the acetabulum. Initially, a small reamer, usually 42-46 mm is directed transversely to expose the inner floor of the acetabulum.

Once the acetabulum has reached an adequate depth through medical reaming, the circumference is concentrically enlarged using additional reamers in increasing increments of 1 to 2 mm. In the un-cemented total hip replacement, the acetabulum is commonly under-reamed to allow for a press-fit implantation technique. That is, the diameter of the final reamer is approximately 1 to 2 mm smaller than the anterior-posterior diameter of the acetabulum. Because the prosthesis is also approximately 1 mm smaller in diameter, the interface between the acetabular component and the acetabulum is often a snug fit. This technique also reduces the need for additional screw fixation. An insertion device is used to insert the prosthetic shell at approximately

40 degrees of abduction and 20 degrees of anteversion into the acetabulum. After the cup has been implanted, a liner can be used to interface between the acetabular shell and the femoral head component.

While most surgeons agree that a larger implant diameter in relation to the anterior-posterior diameter of the acetabulum allows for a more snug fit of the implant (Rohrl et al., 2004), the ideal level of under reaming is debatable. For hemispherical titanium cups, under reaming of more than 2 mm results in a number of complications, the first of which is fracture of the acetabular rim. In a study conducted by Kwong et al, acetabulum with diameters of less than 52 mm were prone to fracture when under reamed by 2 mm or more (Kwong et al., 1993). In contrast, clinical and cadaveric studies have shown a very low occurrence of fracture when the acetabulum is reached by 1 to 2 mm (Kim et al., 1995; McKenzie et al., 1994).

To prepare the femur for implantation of the femoral stem, the femoral canal is opened and a box chisel is used to remove a portion of the proximal femur. The canal is made progressively wider, also known as broaching, using increasing chisel sizes. Broaching continues until the chisel can no longer advance, and adequate cortical bone contact has been achieved. The size of the implanted femoral stem generally matches the size of the last broach which was used. The implant is inserted until good cortical contact is achieved, usually between 12 to 15 degrees of anteversion. A mallet is commonly used to fully insert the femoral stem implant.

1.3.1 Load Transfer across the Hip Joint Following THR

Just as load is transferred across the femoral head and into the hip joint in a healthy hip, a joint resurfaced with total hip replacement must do the same (Widmer,

2007). Additionally, the prosthesis must continue to allow for an adequate range of motion at the joint.

While performing daily activities such as walking or climbing stairs, the hip joint often experiences forces ranging on the order of two to three times the body weight (BW) (Bergmann et al., 2001). Table 3 details the loads seen in the acetabulum of the hip joint during a variety of daily activities. An ideal implant must be capable of bearing loads of this magnitude, as well as those even higher. On some occasions, the joint may experience peak loads of up to nine times the body weight (Bergmann et al., 1993).

Table III. Peak loads of a patient with a body weight of 702 N during various daily activities.

Activity	Peak Hip Contact Force (%BW)
slow walking	244
normal walking	242
fast walking	275
up stairs	272
downstairs	316
standing up	182
sitting down	149
knee bend	147

Additionally, the quality of load transmission through the hip joint must not be affected by THR (Wright et al., 2001; Periasami et al., 2011). Because the material stiffness of metal implants is considerably large compared to that of the surrounding bone, the prosthesis is often prone to stress shielding (Wright et al., 2001; Goodman et

al., 1987; Vasu et al., 1982), which means that the increased stiffness of the metallic implant allows for it to absorb a large amount of the transmitted stress, which in a healthy hip joint would be absorbed completely by the regional bone. Over time, the lack of loading on the surrounding bone could cause resorption according to Wolff's law. This resorption of the bone causes a decrease in bone mineral density and further decreased stiffness, which could eventually compromise the stability of the prosthesis (Huiskes, 1987; Beapupre et al., 1990). An ideal implant is composed of materials which not only help to reduce high levels of stress shielding, but also do not produce reactive stresses that would exceed the ultimate yield strength of the surrounding bone.

1.3.2 Prosthesis Material Properties

1.3.2.1 THR Implant Designs

Because the hip is a ball and socket joint, the articulating surfaces of the implant components must be allowed to slide relative to one another while simultaneously transmitting the load from one component to the other (Widmer, 2007; Katti, 2004). Because a number of factors can influence the friction and fatigue resistance between components, a number of different combinations of materials are currently on the market. The four combinations of materials are: metal-on-polymer, metal-on-metal, ceramic-on-metal and ceramic-on-ceramic.

Metal-on-polymer implants are considered among the gold standard for total hip replacements, especially in older patients, and can be used for both cemented and uncemented implantation (Dowson, 2001). First introduced by Charnley in 1959, metal-on-polymer implants allow for a low friction articulation at the hip joint. These implants are composed of a UHMWPE acetabular cup and a stainless steel femoral head.

Despite their status as the gold standard, metal-on-polyethylene implants have a relatively low survival rate, with only 94.2% of implants lasting 10 years post-operatively and 88.7% lasting 15 years post-operatively (Yoshi et al., 1998).

Beginning in the 1960s, cementless metal-on-metal designs made of steel were commonly used in THR, in which the femoral stem components was made of cobalt chromium casts.[august] By 1991, both the acetabular and femoral components of metal-on-metal implants were composed of metal (McMinn et al., 1996). Early metal-on-metal implants were prone to failure due to poor articulation at the interface. Common concerns regarding the use of metal-on-metal implants are the possibility of metal wear particles (Shimmin et al., 2009). During walking and every day activities, the metal ball and acetabular cup come into contact and slide against one another, producing small wear particles over time. Some studies have reported the occurrence of high levels of metal ions within the blood stream due to wear particles, which could eventually cause negative immune response in some people. However, more recent studies have shown that the long-term wear rates for metal-on-metal implants using cobalt chromium molybdenum alloys are actually quite low, reaching around 0.36 mm^3 per 10^6 cycles in both the cup and femoral head components (Goldsmith et al., 2000).

Ceramic-on-ceramic implants were first introduced by Boutin in 1970 and were later revised by Mittlemeier in 1974 (Semlitsch et al., 1997). Alumina is a commonly used material for this type of implant. Initially, industrial grade alumina was used, which resulted in a coarse grain size and insufficient purity of the implant. Between 1970 and 1976, fracture rates of the femoral head as high as 13.4% were reported (Griss et al., 1981; Knahr et al., 1987). Guidelines for the production of ceramic implants were

created in 1984 in order to produce high quality implants suitable for medical use. Recently, studies have shown that ceramic-on-ceramic implants result in a low wear rate, and have a increased survival rate, especially in patients under the age of 50 (Sedel et al., 1994). Downsides of ceramic-on-ceramic implants include the likelihood of neck socket impingement if exact positioning is not achieved. In time, this impingement could lead to fractures of the ceramic lining, particularly at the rim surface (Santavirta et al., 2003).

Despite the type of material implant that is used, the wear rate for each component should not be greater than 0.1 mm per year (Tanaka et al., 2003). Because the wearing properties and stability of the implant have a direct correlation with the material properties, extensive studies have been done to better understand the influence that these parameters have. Table 4 summarizes the Young's modulus and static strength of bone, as well as the materials that are commonly used in THR.

Table IV. Indicative values of Young's Moduli and Static Strength of most materials and interfaces used in THR reconstruction (MOW 1997).

Cup Material	Young's Modulus	Static Strength
Titanium	100-130 GPa	800-1500 GPa under tension
CoCr alloy	200-220 GPa	800-1000 GPa under tension
UHMWPE	1 GPa	20-30 MPa under tension
Hydroxyapatite-bone interface	-	30-50 MPa under shear

1.3.2.2 Hydroxyapatite Coating

The porous coating of the acetabular shell cup allows for a good interface with surrounding bone (Geesink et al., 1987). The surface of the cup is coated with titanium sintered metal beads, which encourage biological fixation of the bone into the porous coating over time (Stephenson et al., 1991; Soballe et al., 1992; Soballe, 1993). This is achieved through bone in-growth, which refers to formation of new bone within the porous surface of the implant. Biological implants with bone to implant interfaces which promote bone in-growth are generally more stable over time. The shells are coated with plasma sprayed hydroxyapatite (HA, $Ca_{10}[PO_4]_6[OH]_2$) over the porous coating, shown in Figure 6. HA coatings are commonly applied to metallic implants, particularly those of titanium alloys and stainless steel. Studies show that calcium phosphate ceramics, such as hydroxyapatite, has proven to be a successful coating for cementless metallic implants because it allows for a quick and strong fixation (Geesink et al., 1987; Geesink et al., 1995). In acetabular components coated with HA, it has been discovered that bone formation is induced not only on the side of the bone, but also from the side of the implant (Geesink et al., 1992).

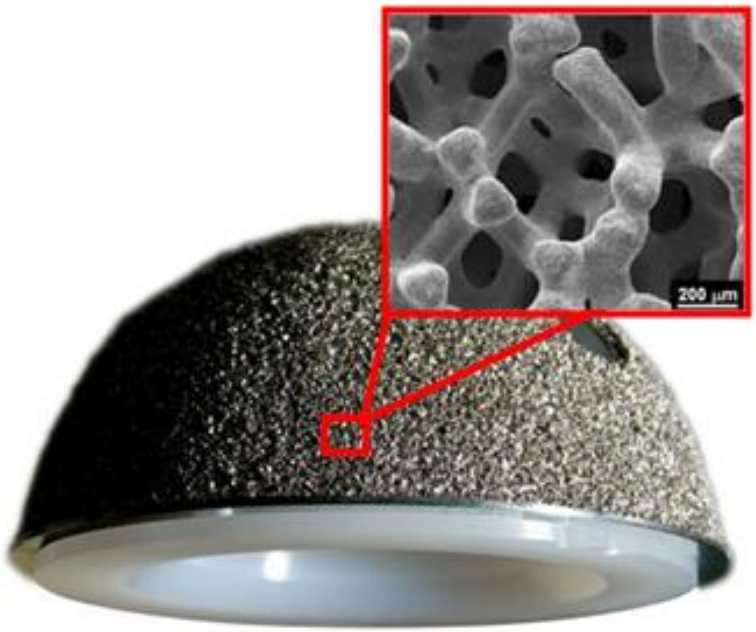

Figure VII. Close-up image of the porous hydroxyapatite coating on hemisphereical acetabular cup.

The effectiveness of HA in reducing micromotion at the bone-femoral prosthesis interface was studied post-operatively (Kroon et al., 1992). At one year following THR, the HA coated prosthesis had migrated less than 1 mm, which was significantly less than the migration seen in the non-coated implants. Similarly, a study was conducted to analyze the amount of bone remodeling following THR around a HA coated, porous femoral stem implant (Coathup et al., 2000). In comparing the amount of in-growth and bone attachment on the coated prosthesis surface to the non-coated surface, there was significantly more in-growth and attachment on the entire surface of the coated implant. The evenness of attachment reduces the amount of stress shield seen in the surrounding bone, which limits the occurrence of wear particles and osteolysis.

Conversely, in-growth on the non-coated implant occurred only on certain regions of the implant, which can increase micromotion over time, leading to the occurrence of wear particles located at the interface.

1.3.3 Failure in THR

THR can have a number of post-operative complications, including dislocation of the implant, prosthetic failure, or sepsis (Breusch et al., 2005; Amstz, 1970; Mallory, 1972; Eftekhar et al., 1976; Hallel et al., 1976; Lowell et al., 1978). Almost 10% of patients with a total hip replacement undergo a revision surgery within the first ten years following the initial surgery, many of which are due to aseptic loosening of the implant prosthesis (Herberts, 1992; Anhfelt et al., 1990).

1.3.3.1 Cup Migration

Migration, which is a permanent displacement between the implanted prosthesis and the surrounding host bone, is especially common in un-cemented THRs during the first year following implantation. During a normal gait cycle, the bone is loaded in a cyclic manner, which can eventually lead to miniscule cracks in the nearby trabecular bone (Burr et al., 1985). Additionally, insufficient initial fixation of the acetabular cup component can lead to migration over time (Mjoberg, 1991). Over time, decreased strength of the bone causes the prosthesis to shift positions relative to the original location.

1.3.3.2 Dislocation

Following THR, loosening of the components surrounding the implant components may lead to eventual dislocation of the prosthetic femoral head from the

acetabular cup in the pelvis (Bozic et al., 2009). This situation, which results when the femoral head no longer articulates with the acetabular component correctly, can result from loosening of the ligaments or muscles surrounding the joint capsule. Impingement of the acetabulum, caused by a smaller femoral head to neck ratio, can also cause dislocation of the femoral head if range of motion exceeds the restricted range of motion.

1.3.3.3 Infection

Although the occurrence of deep wound infection such as sepsis following THR is usually low, infection is a risk following any surgery (Schutzer et al., 1988). However, increased care regarding operative and post-operative techniques has reduced the rate of infection to less than 1 percent (Garvin et al., 1995). Furthermore, the infection of the laminar flow operating room, which utilizes filters to provide for the inflow of clean, bacteria free air, has reduced the likelihood of bacteria entering the open wound during surgery.

1.3.3.4 Aseptic Loosening

Aseptic loosening accounts for approximately 75% of failed total hip replacements (Malchau et al., 2002). Aseptic loosening can occur for a number of reasons, including poor fixation during the time of THR, as well as lack of adequate bone fixation thereafter. If the resulting micromotion at the cup-bone interface is greater than the size of the porous surface of the acetabular component (typically 100-400 microns) not only is bony in-growth of the surrounding bone limited, but it can also lead to wearing of the component surface (Bobyn et al., 1980; Harris, 1986). Furthermore, studies have shown that when micromotion of the cup is reduced to less than 28 microns, bony in-growth is

not stunted (Pilliar et al., 1986). Over time, this wearing can result in accumulation of particulate matter. These particulates can eventually migrate between the interface and lead to osteolysis and degradation of the interface. Most drastically, this can also lead to aseptic loosening of the acetabular cup component (Bartel et al., 1985; Saikko et al., 2002; Kurtz et al., 1992).

Stress shielding of the cortical bone near the interface of the components can also lead to aseptic loosening over time. Because the stiffness of the implant is high in comparison to that of the surrounding cortical and trabecular bone, it consequently bears a large portion of the weight bearing load. In accordance with Wolff's law, which states that bone will adapt to the loads that are placed upon it, the bone surrounding the implant begins to thin, and is therefore able to withstand less strain.

1.3.4 THR in the presence of high-grade acetabular defects

Often, acetabular defects are seen in patients with severe arthritis or extensive bone loss at the hip joint due to injury or osteoporosis. Aseptic loosening of the acetabular cup component following initial THR can lead to bone loss over time, resulting in either minor or severe bone deficiencies at the hip joint (Haydon et al., 2004; Sporer et al., 2005; Chen et al., 2000; Paprosky et al., 1994; Van der Linde et al., 2001). The occurrence of bony deficiencies can be problematic for the stability of the implant because of reduced stability of the surrounding posterior or anterior acetabular walls (Rees et a., 2011). Approximately 15% of patients undergoing a THR must undergo a second replacement surgery due to eventual failure of the initial component (Blackley et al., 2001).

1.3.4.1 Classification of bony defects

The severity of bony defects can be classified into different scales using the basic guidelines outlined by the Paprosky classification system (Paprosky et al., 1994). These guidelines of this system are based on the presence or lack of structures at the hip joint to classify defects into three types of categories. These structures include the acetabular rim, the superior dome, medial wall, and posterior and anterior columns. Type I defects occur when there minimal bone loss has occurred, and most supporting structure are still fully intact surrounding the acetabulum. Type II defects occur when some damage has occurred at the acetabular rim, but both the anterior and posterior columns are intact. This type of defect can be sub-categorized into three additional categories depending on the location of the defect, which are A,B, and C. Type III defects occur when severe bone loss can be seen at the supporting structures. In Type III defects, the stability and integrity of the hip joint is almost fully compromised due to bone loss at the interface. Type III defects can be subdivided into Types IIIA and IIIB depending on the amount of contact that the revision provides for the joint. Table 5 fully outlines the Paprosky classification system for each type of defect.

Table V. Classification of Types I, II, and III defects according to the Paprosky classification system (Johanson et al., 2010).

Type I	Supportive rim with no bony lysis or migration
Type II	Intact columns with acetabular rim damage
	Superomedial defect
	Superolateral defect (no dome)
	Medial defect only
Type III	Severege ischial and medial osteolysis and bone degeneration
	30-60% of component is supported post-revision
	>60% of component is supported post-revision

1.3.4.2 Stabilization of the acetabular cup in the presence of defects

The most efficient and effective method of management stability following bone loss remains controversial among the orthopaedic community (Johanson et al., 2010). Currently, several different methods of corrective products exist, and are in use. One method of reconstructive surgery is through the use of bone grafts. Another is through revision THR with the use of screw fixation.

1.3.4.3 Acetabular revision with bone grafts

Bone grafting has become a largely used method of fixation because acetabular revision without the use of grafting has shown to have an aseptic loosening rate of at least 50% over time (Kavanagh et al., 1985). These grafts are used to provide additional stability by filling defects. Bone grafting was first used in 1975, when Hastings and Parker developed a method in which bone grafts were used to treat bone loss and help restore bone loss in patients with rheumatoid arthritis (Hastings, 1975). In 1978, bone grafts were again used to treat bone defects in protrusion acetabuli with morselized allografts (McCollum et al., 1978). In 1983, bone grafts were used in conjunction with a

cement layer in animals, and studies found that bone chips survived beneath the surface of the cement (Roffman et al., 1983). This technique was later successfully used in THR for acetabulum reinforcement and all patients showed signs of bone growth at the interface following surgery (Mendes et al., 1984). The term impaction bone grafting was used to describe the compaction of bone grafts beneath the acetabular cup and a layer of pressurized cement during THR (Sloof et al., 1984). Cancellous bone has commonly been used as a bone graft material because many believe that the trabecular structure of cancellous bone would encourage bone in-growth and would drive remodeling of the cortical bone (Goldberg, 2000). However, various types of grafts have been used, including morselized cortical allografts, bovine bone, and human bone mixed with Hydroxyapatite (Kuiper et al., 1998).

In studies conducted by Slooff, only 5 of 56 patients treated for acetabular revision due to Type II defects required additional revision. That is, at 11.8 years post-operatively, only 6% of patients presented with aseptic loosening of the acetabular component. The survival rate 13 years post-operatively was as high as 89%.

Impaction grafting is also used as a method of improving mechanical stability at the implant site, and been reported as having approximately a 94% survival rate, even more than 10 years post-operatively (Schreurs et al., 2004; Toms et al., 2004). Cancellous allografts have also been used with an 85% survival rate (Bohm et al., 1999; Della Valle et al., 2005). Another grafting method is through the use of bulk allografts. Although bulk allografts may achieve a large percentage of union with the host bone, one downside of this method is the occurrence of bone resorption over time (Kwong et al., 1993). Also, because this type of grafting does not encourage bone fixation, it does

nothing to encourage contact between the bone and implant, despite that caused by the initial implantation. Allografts can sometimes be problematic in the case of an especially irregularly shaped defect, in which creating a near perfect contact surface would be difficult. Furthermore, some studies have reported that the bulk allograph is prone to failure at high loads (Kwong et al., 1993). Additional concerns regarding the use of grafts to stabilize the acetabular cup in the presence of defects involve the prevalence of negative immune responses, as well as the cost of harvesting and storing grafts (Zipfel et al., 2003).

1.3.4.4 Acetabular revision without bone grafts

A number of studies have been done to show that acetabular revision without the use of bone grafts can be successful as well. Rees et al (Rees et al., 2011) conducted a total of 107 acetabular revisions without bony grafts for a total of 99 patients over the course of thirteen years. Of those patients, 33 presented with moderate to severe bone deficiencies, and were classified as having Type II or III defects. In each case, the acetabulum was under-reamed by 1 or 2 mm depending on the evaluation of existing stability. As in all THR procedures, the acetabular was reamed for the purpose of creating a uniform contact surface for the implant. In this case, the intention was to also increase the contact at both the anterior and posterior columns. Titanium acetabular cups were inserted using the press-fit technique and secured with screw fixation. The number of screws used was dependant on the surgical evaluation at the time of implantation. At the time of patient follow-up, the stability of the implant where a bony defect was present was evaluated. Out of 53 patients available for follow-up, only 3 presented with mechanical failure of the implant. In one patient, migration of the

acetabular component occurred through the medial wall of the acetabulum, and aseptic loosening occurred in 2 additional patients. Overall, the survival rate of implants at 1 year was 96.9% and 95.2% after 2 years.

Moskal et al used porous coated acetabular cup implants without bone grafting for the fixation of the acetabular component in 11 patients with a Type III defect (Moskal et al., 2004). In particular, the patients of this study had defects which had significant failure in the posterior and/or anterior columns. The majority of patients presented with the need for revision surgery due to aseptic loosening of the acetabular cup following initial THR. In this study, Bilobed Oblong cups (Depuy, Warsaw, IN) were used and were implanted and secured with screw fixation with an average of 5 screws per patient. As far as three years following surgery, none of the patients showed signs of further loosening, and average pain scores improved post-operatively.

1.4 Kryptonite bone cement

Kryptonite bone cement (Doctors Research Group, Inc. Southury CT) is an injectable liquid which hardens upon mixing in order to act as an adhesive for the purpose of providing a stable interface between two surfaces. Kryptonite was created to allow for a strong bond between bony articulations, as well as chemical adhesion. Ideally, kryptonite would achieve a stable interface by preventing slippage on not only the micromotion level, but also macromotion.

1.4.1 Kryptonite chemical composition

Kyrptonite is composed of three separate components, each of which plays an essential role in Kryptonite's properties. Component A is a prepolymer composed of a naturally occurring fatty acid with a terminating hydroxyl group. This prepolymer is

derived from a castor oil, and is synthesized with NCO groups in order to ready the tricyleride chains for polymerization. This polymerization occurs when Component A is mixed with Component B. Component B, which is a poylol, is also composed of a fatty acid chain with a terminating hydroxyl group and is derived from castor oil, using the addition of a catalyst and water. Upon the addition of water, the water molecule reacts with the NCO group of Component A, causing the release of carbon dioxide. The release of carbon dioxide not only allows for the material to expand, but also allows for Kryptonite to remain a porous material, even upon hardening. The porosity of further increased using Component C, a calcium carbonate, which also aids in achieving the unique mechanical and structural properties of the cement, which are similar to that of bone. Laboratory and animal studies conducted by the Doctors Research Group has shown in that over time, the osteoclasts of bone have penetrated the porous structure of Kryptonite, allowing for a good bony in-growth.

1.4.2 Kryptonite mechanical properties

Studies conducted by the Doctors Research Group have compared the mechanical properties of Kryptonite to an intact cadaveric bone and polymethylmethacrylate (PMMA). In comparing the yield strength of Kryptonite to bone and PMMA, it was concluded that the yield strength of kryptonite was comparable to PMMA, as shown in Figure 7. The yield strength of kryptonite and PMMA were approximately 11,000 N and 12,000 N, respectively. A comparison of material stiffness is shown in Figure 8. It was concluded that the stiffness of Kryptonite and intact bone differ by only about 10%. Mechanical testing shows the Elastic Modulus of Kryptonite Bone Cement to be approximately 800 MPa (Santanglo et al., 2010) (Figure 9).

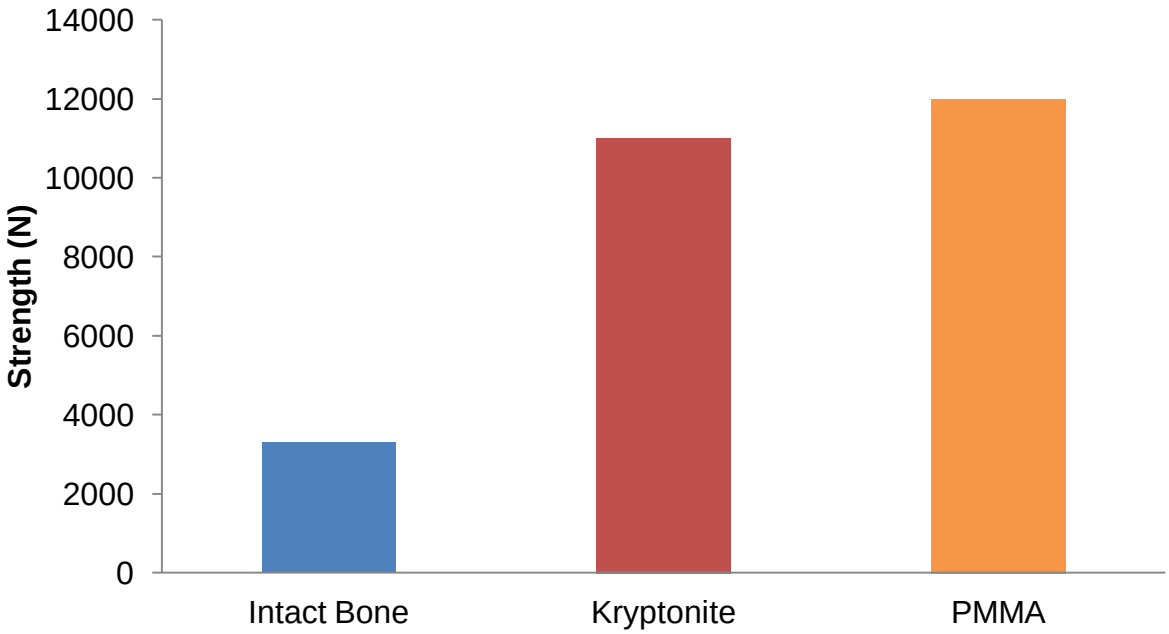

Figure VIII. Results of mechanical testing conducted by The Doctors Research Group showing the yield strength of Kryptonite Bone Cement in comparison to intact bone and PMMA (Santanglo et al., 2010).

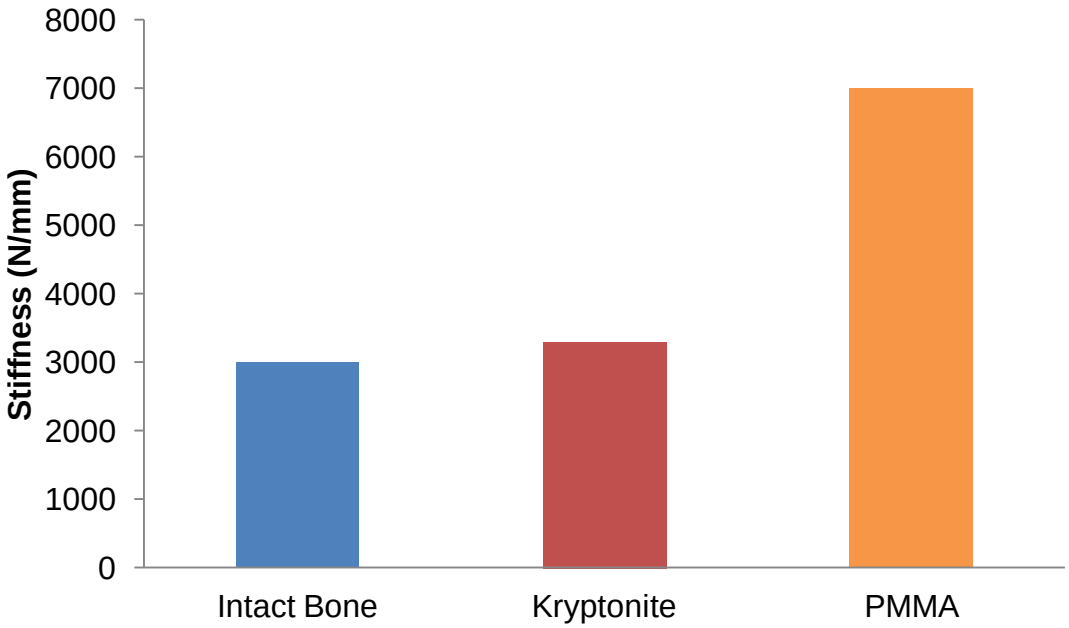

Figure IX. Results of mechanical testing conducted by The Doctors Research Group showing the stiffness of Kryptonite Bone Cement in comparison to intact bone and PMMA (Santanglo et al., 2010).

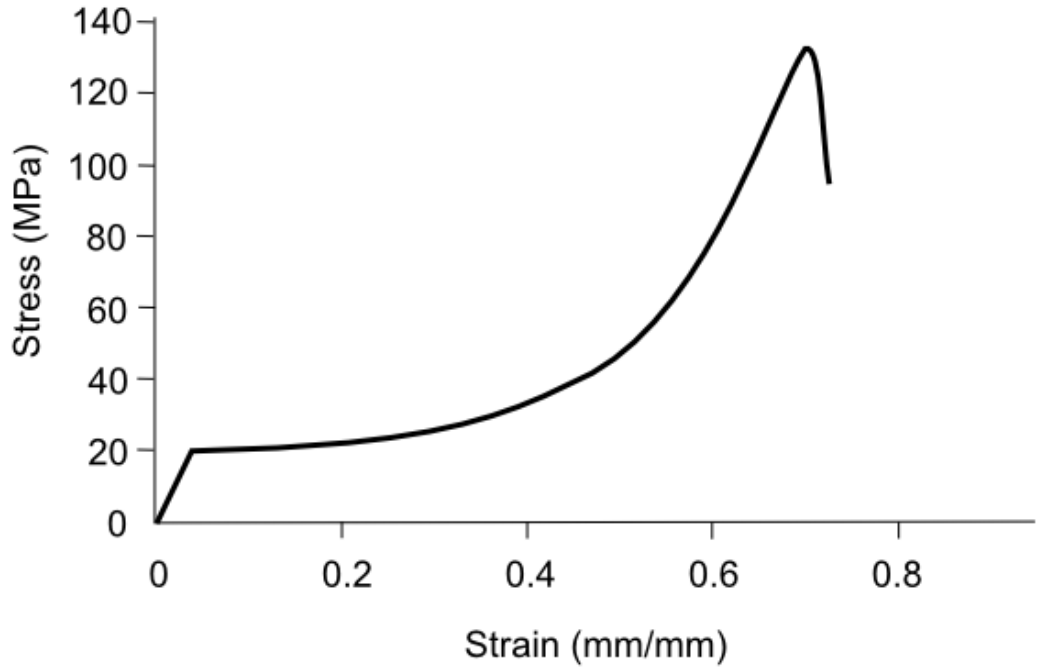

Figure X. Results of mechanical testing of Kryptonite Bone Cement conducted by The Doctors Research Group (Santanglo et al., 2010).

Boxberger et al (Boxberger et al., 2011) studied the material properties of Kryptonite, which he used in repairing radius fractures. Cadaveric radii specimens underwent transverse osteotomies to remove the head of each radius. Specimens were repaired using Kryptonite bone cement, and were treated as a cantilever beam under failure testing. In bending, the tensile elastic modulus due to tension of Kryptonite reached as high as 723 MPa, and the compressive elastic modulus as high as 754 MPa with a reported yield stress was 20.3 MPa.

1.4.3 Kryptonite as an adhesive bone cement

The bone-like properties and adhesive quality of Kyrptonite makes it ideal for use in bone reconstruction. Kyrptonite was used in six patients undergoing cranial

reconstruction surgery following the removal of brain tumors (Nuzzo et al., 2010). For cranial fixation, Kyrptonite was injected at the site of fixation while in its liquid phase in order to secure the bone flap in place. After reaching the adhesive phase, Kryptonite was molded for optimal fixation, and to allow for expansion upon drying. CT scans were conducted one week following surgery, and all patients with Kryptonite fixation showed a perfect alignment of the craniotomical bone, as well was complete filling of the bony defects of surrounding bone. Approximately one year after surgery, additional scans showed that the reconstruction site showed full bioabsorbability.

In another study, Kryptonite was used as a fixation method following midline sternotomy in human cadavers (Fedak et al., 2010). The current method of sternal closure is through the use of wire cerclage. In this study, Kryptonite was used in conjunction with a standard wire cerclage, under the hypothesis that it would prevent pathologic sternal displacement following fixation, and also would improve mechanical strength. Samples using a conventional wire fixation method were subjected to mechanical testing and the results were compared to those seen when using a mix of wire cerclage and Kryptonite. The specimens were cyclically loaded from 10 N to 100 N for 30 cycles, and were increased in 100 N increments following each 30 cycles of loading. Pathologic displacements were measured in the manubrium, midsternum, and xiphoid of the sternum. Significant displacement was noted in the control group, yet displacement in the specimens fixed with Kryptonite did not exceed 1 mm, even at the maximum force of 600 N. Conversely, at maximal loading, displacement reached as high as 4 mm in the control specimen.

In order to validate the previously mentioned study, the same research group conducted clinical trials in which they used Kryptonite as a fixation following midline sternotomy in 8 patients, while 7 patients underwent a routine closure with wire cerclage. The surgical outcome in each of the patients was observed approximately 3 months following surgery, and each fixation showed full biocompatibility with no indication of infection. Additionally, each closure remained stable, with negligible displacement and showed no trace of bony gaps, migration, expansion, or posterior ridge formation of the closure site. In each category of evaluation, the adhesive specimen performed as well as, if not better, than the control specimen. In an additional study, the same experiment was conducted on a larger population of patients (Fedak et al., 2011). The results were in accordance with those previously seen. In addition to measuring the sternal displacement, the osteoconductive properties of Kryptonite were evaluated. At 12 months post-operatively, there was evidence of healing within the fixation site, as well was the formation of new bone in-growth into the porous network of Kryptonite.

In addition to determining the elastic modulus of Kryptonite due to compression and tension, Boxberger et al (Boxberger et al., 2011) subjected the radii specimens to loading in order to determine the load to failure. The load to failure of radii repaired with Kryptonite was compared to those repaired with PMMA cement. Following cantileaver beam loading, the Kryptonite treated group was found to have a load to failure of approximately 318.5 N, while the PMMA group failed at a load of approximately 134.1 N. Furthermore, the Kryptonite treated radii were able to withstand a higher shear stress compared to the PMMA group. Peak shear stresses at the load of failure were found to

be 0.87 MPa and 0.39 MPa in the Kryptonite and PMMA treated specimens, respectively. The amount of bone cement penetration into the surrounding trabecular bone of both materials was evaluated as well. In both treatment groups, approximately the same amount of bone cement was applied to the fracture site. Upon hardening, the expansion of Kryptonite into surrounding trabecular bone spanned at least 10.4 mm, while the expansion of PMMA cement was only 7.0 mm. Similar studies with various types of bone cement have demonstrated that the repair strength is highly correlated with the level of bone cement penetration into the network of surrounding trabecular bone (MacDonald et al., 1993; Mann et al., 1997).

2. AUGMENTATION OF ACETABULAR DEFECT WITH KRYPTONITE BONE CEMENT. AN EXPERIMENTAL STUDY

2.1 Introduction

One of the main goals of the total hip replacement (THR) is to preserve the integrity of the hip kinematics. (Dalstra et al.,1990).

In the case of uncemented total hip replacement implants, one of the most common causes of failure due to dislocation or migration is due to initial instability upon implantation (Pilliar et al., 1986). Although a small amount of migration due to micromotion is present between two surfaces, high values of micromotion can lead to instability over time due to an unstable fixation between the acetabular cup and the surrounding bone (Perona et al., 1992). Over time, this micromotion limits bone growth into the prosthesis coating and can cause complete implant failure (Geesink et al., 1987; Geesink et al., 1995). Aseptic loosening of the acetabular cup component following initial THR can lead to bone loss over time, resulting in either minor or severe bone deficiencies at the hip joint (Haydon et al., 2004; Sporer et al., 2005; Chen et al., 2000; Paprosky et al., 1994; Van der Linde et al., 1994). Often, acetabular defects are seen in patients with severe arthritis or extensive bone loss due to traumatic injury at the hip joint (Ranawat et al., 2009). The occurrence of bony deficiencies can be problematic for the stability of the implant because of reduced stability of the surrounding posterior or anterior acetabular walls (Rees et al., 2011). Approximately 15% of patients undergoing a THR must undergo a second replacement surgery due to eventual failure of the initial component (Blackley et al., 2001). Therefore, in order to provide optimal stability in the presence of acetabular defects, it is especially important

to maintain the anatomical center of the hip while restoring the structural integrity of the cup-bone interface (Howell and Bolland, 2011).

The most efficient and effective method of management stability following bone loss remains controversial among the orthopaedic community (Johanson, et al., 2010). Currently, several different methods of corrective products exist, and are in use. A literature review reveals various techniques that researchers have done to determine the relative micromotion at the bone-implant interface.

2.2 Experimental investigation of acetabular cup stability in uncemented THR

Several researchers have attempted to study and quantify the cup-bone interface following a cementless THR through a number of in vitro experiments (Zivkovic et al., 2010; Perona et al., 1992; Brooker et al., 1984; Won et al., 1995). In vitro experimental studies of the hip joint before and following total hip replacement can be utilized to fully understand the biomechanics of the joint. These studies can shed light not only on the mechanisms of failure, but also the stability of the bone-implant interface and the stresses seen at the joint under a variety of loading conditions.

The initial cup fixation of a press-fit aceatabulr cup was examined using linear variable differential transformers (LVDTs) to register and record the displacement of the acetabular cup during simulated post-operative loading (Zivkovic et al., 2010). The hemi-pelvis of cadaveric specimens was press-fit with an acetabular cup, and the pelvis was then mounted in a polysterene resin to hold the bone in place. The motion of the cup was captured using LVDT sensors positioned around the rim of the acetabular cup while a load which mimicked the forces seen when rising from a low seated position was applied to the cup. The results of this study indicate that for an applied load under

600 N, the average micromotion of the cup remains below 50 microns with an average rotation of less than 0.1 degree.

The micromotion of porous-coated acetabular cups following an uncemented THR was studied (Stiehl et al., 1991). Thirty-three hemi-pelvises were cleaned of all soft tissue and acetabular cups were press-fit implanted at varying degrees of under-reaming and secured with screws. LVDT sensors were used to measure the mechanical stability of the cup over the course of loading. Transducer holders were utilized to place six LVDT sensors perpendicular to the rim of the cup. Specimens were loaded in the vertical plane. Motion was defined as the quantitative amount of recovered cyclic motion during any given applied load. The results of this study indicate that cyclic loading up to 300 kg, the cups demonstrated an average micromotion of 125 microns.

Won et al (Won et al., 1995) evaluated the micromotion seen at the bone-implant interface following THR in human cadaveric pelvic specimens. The micromotion of press-fit and non-press-fit acetabular cups was evaluated in response to cyclic loading up to 1500 N, in both the presence and absence of screw fixation. Each whole pelvic was completely stripped of all soft tissue, and cobalt chromium alloy cups were inserted and secured with varying levels of screw fixation. Motion of the cup was measured using LVDT sensors, which were attached to the periacetabular bone surrounding the bone-implant interface. The load was applied at an angle of 15 degrees medially through a metallic femoral head which articulated with a polyethylene liner. Won found that despite the number of fixation screws, micromotion was greater in the cadavers fit using the non-press-fit technique compared with press-fit. Under a compressive load of 1500 N, sensors surrounding the acetabular cup rim measured a maximal micromotion

value of 52 microns in a non-press-fit specimen with two fixation screws, compared with only 35 microns in the same region of a press-fit cup secured with two screws. Because this study was limited to a total of three LVDT sensors, a 3-dimensional evaluation of the micromotion of the cup was not possible. Additionally, no consideration was made for deformation of the bone over the course of loading, which could result in inaccurately high micromotion readings of the cup.

2.3 Objective

This study aims to examine initial acetabular cup stability during total hip arthroplasty with and without the presence a bony defect of the acetabular wall reinforced with bone screws and augmented with Kryptonite bone cement. The stability was assessed through in-vitro experimental measures in which the acetabular cup was subjected to loading conditions. LVDT sensors were used to determine the special orientation and position of the acetabular cup throughout cyclic loading. Additional biomechanical testing was conducted on cadaveric hip specimens after THA in the presence of a defect along a portion of the acetabular rim in order to determine the efficiency of Kryptonite as bone cement and its ability to stabilize and reduce micromotion of the acetabular cup during acetabular wall reconstruction in the presence of a defect. This chapter details the process by which biomechanical testing was carried out.

2.4 Specimen Preparation

Ten hemi-pelvises were obtained from a total of 5 fresh-frozen cadavers stored at approximately -20 C were obtained (Table 6). In all specimens, no abnormalities or musculoskeletal abnormalities were noted upon visual inspection of the specimens post-implantation.

Table VI. Donor Information.

ID Number	Sex	Age at death	Donor Height	Donor Weight
53862	Female	58	5’10”	170
100284	Male	72	5’9”	160
18331	Male	73	5 8	125
18359	Female	60	5 4	145
2640	Female	85	5 6	125

Five unembalmed adult human cadavers were dissected using a posterolateral approach to expose the acetabular rim. The specimens were stored at -20˚C in sealed plastic bags and were thawed to room temperature before testing. In order to maintain correct anatomical geometry of the hip, the superior portion of the femur was fully preserved. For each cadaveric specimen, one side of the pelvis was used as a control, while the other was subjected to a defect creation to serve as the testing side. The control and defect each had a 50% occurrence on the left and right hemi-pelvis. The defect on the acetabular rim was created to imitate the characteristics of diseased or

eroded rims commonly seen in patients with osteoarthritis. To calculate the defect size on one acetabulum of each hip, the total circumference of the acetabular rim was measured, and 30% of that measurement imposed as the defect arc length (Table 7). The imposed defect depth was 30% of the defect arc length.

Table VII. Specimen Information for Defect Creation.

Sex	Age at Death	Weight [lbs]	Rim Circumference [cm]	Hemi-Pelvis Side	Hemi-Pelvis Side	Defect Length [cm]	Defect Depth [cm]	Cup Diameter [mm]	Room Temp at time of Kryptonite Mixing [°C]
Female	58	170	15.0	Right	Kryptonite	4.5	1.35	54	24
			15.0	Left	Control	--	--	56	24
Male	72	160	14.7	Right	Control	--	--	52	24
			14.7	Left	Kryptonite	4.40	1.30	52	24
Male	73	125	14.0	Right	Kryptonite	4.20	1.26	58	20
			14.0	Left	Control	--	--	58	20
Female	60	145	14.0	Right	Control	--	--	52	20
			14.0	Left	Kryptonite	4.20	1.26	52	20
Female	85	125	13.5	Right	Kryptonite	4.15	1.245	53	20
			13.5	Left	Control	--	--	53	20

A coordinate system was put in place using bony landmarks of the hemi-pelvis to ensure that defect placement remained consistent between specimens. The acetabulum was first divided into a four-quadrant system, as described by Wasielewski

(Wasielewski et al, 1990), where Line 1 begins at the anterior superior iliac spine (ASIS) and extends through the ischial tuberosity (Figure 10). The defect was then created by removing a portion of the acetabular wall beginning on Line 1 in the posterior superior quadrant and extending towards the posterior inferior region (Figure 11). The plane $\overline{\boldsymbol{XY}}$ is created by the plane of the rim of the cup and contains the origin (*o*), which is a projection of the volumetric center of the cup (*o'*) onto the plane (Figure 22). The *y*-axis is created parallel to the projection of Line 1 onto $\overline{\boldsymbol{XY}}$. The *z*-axis was defined as a polar axis perpendicular to $\overline{\boldsymbol{XY}}$ through the origin point. The *x*-axis was defined as the vector cross product of $\vec{\boldsymbol{y}} \times \vec{\boldsymbol{z}}$. The anterior edge of the reconstructed defect was located adjacent to the *y*-axis.

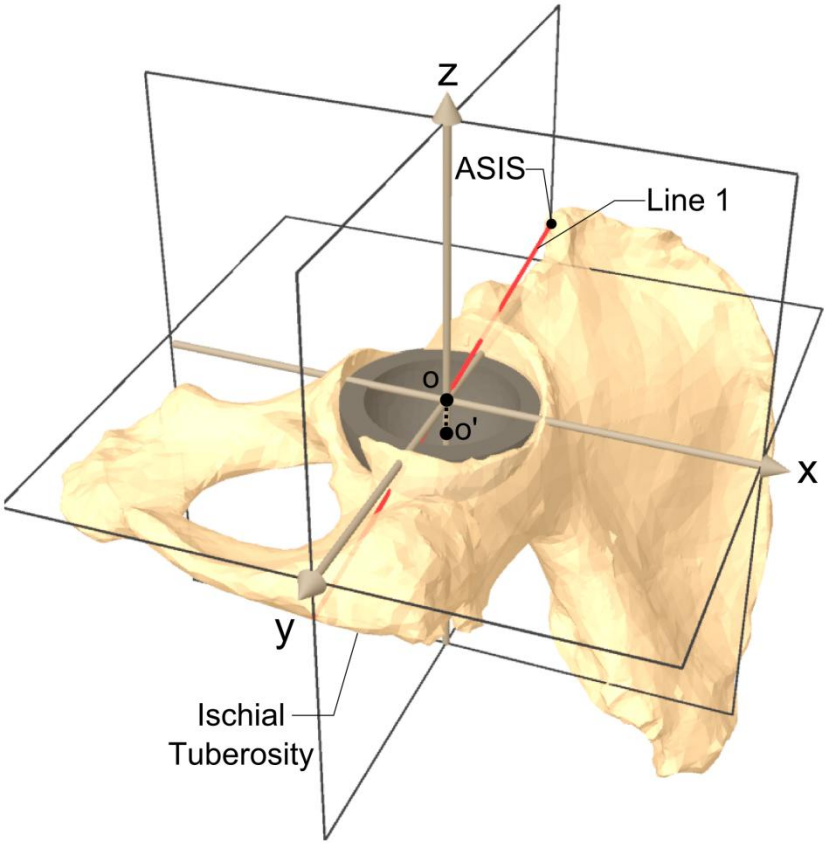

Figure XI. Coordinate system of the hemi-pelvis based on the four-quadrant system.

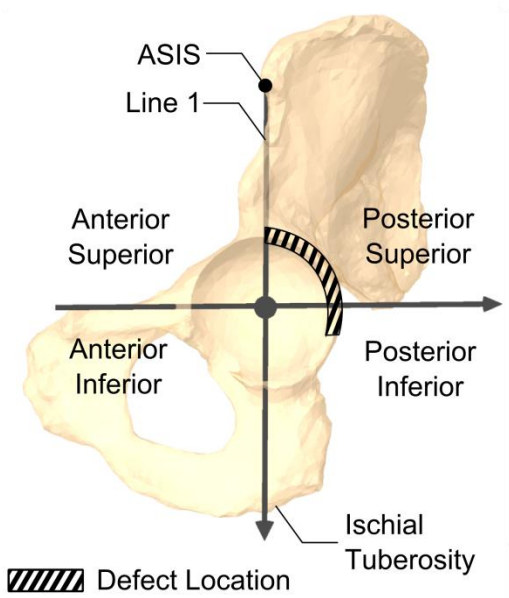

Figure XII. Sectioning of the acetabulum in a lateral view into a four-quadrant system with the ASIS and ischial tuberosity acting as bony landmarks in order to establish consistency for defect creation.

Three separate cortical bone screws (Smith and Nephew, Memphis, TN) were screwed into the trabecular bone, located equidistance from one another within the defect.

The three components of Kryptonite (Doctors Research Group) were mixed according to the manufacturer's instructions. In Step 1, the prepolymer Component A and poylol Component B were added to Component C, which is a calcium carbonate. The mixture was thoroughly mixed so as to remove any lumps for approximately 1 minute. In Step 2, and for the next 8 minutes, the mixture was allowed to set and polymerize as Components A and B react with one another. Once in the moldable putty phase of Step 3 after at least 15 minutes, Kryptonite was applied and molded into the

acetabular wall to serve was a structural support and an adhesive for the cup at the site of the defect creation.

Once solidified, the Kryptonite continued to expand slightly, and once solidified, the acetabulum was reamed with increasing reaming sizes until the reamed diameter was 1 mm less than the diameter of the acetabular cup. Depuy Pinnacle titanium acetabular cups Johnson & Johnson, DePuy, Warsaw, IN) were then press-fit inserted. The cups were coated with a 180 degree fiber-mesh. The remaining side of each hip was used as a control, where the acetabulum was reamed and the cup inserted with no creation of a defect. Following skeletonization of the pelvis, it was divided and each hemi-pelvis was mounted using the polyester resin, Bondo (Bondo Corp., Atlanta, GA) (Figure 12). Despite attempts to minimize the influence of bony deformation surrounding the cup-bone interface, displacement values recorded by LVDT sensors include some amount of deformation by the surrounding bone.

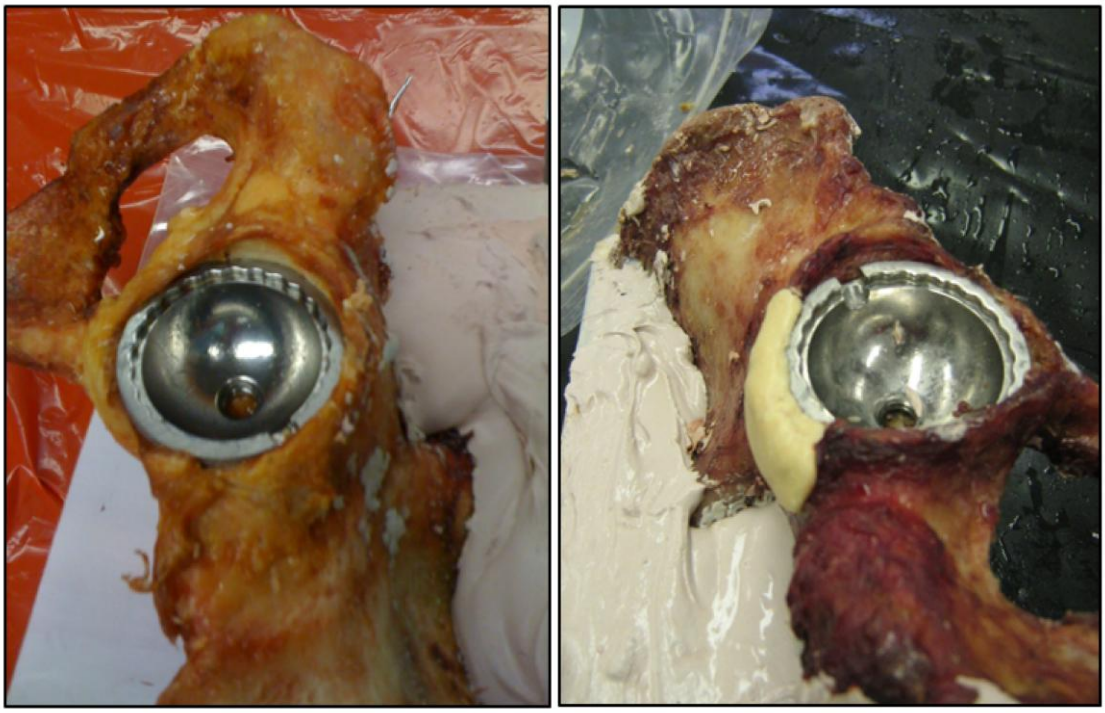

Figure XIII. Control (left) and reconstructed defect augmented with Kryptonite treated specimen (right) following reaming and cup implantation into each hemi-pelvis.

2.5 Testing Apparatus Description

2.5.1 Instron Loading System

Many types of mechanical testing systems are currently in use for the purpose of mechanical and biomechanical testing of a wide variety of materials and systems. Two commonly used types of loading systems are uni-axial and multi-axial devices. In contrast to multi-axial systems, uni-axial systems allow for compressive, tensile, bending, or hardness testing with the use of a single line actuator. In this study, an Instron 5500 Series (Instron Corp., Canton, MA), shown in Figure 13, was used for

biomechanical testing of each hemi-pelvis. A number of Instron components contribute to the biomechanical testing system. These components include a load unit, controllers, and a data management system. The load unit allows for the application of a compressive or tensile load to the testing object. This is done by the use of actuator rods, which contain a linear variable differential transducer in order to transfer information concerning the displacement of the load cell to the controllers. The controllers provide for data output, and can also control the load application rate, as well as the actual magnitude of the applied load. The data management system is composed of a computer connected to the Instron testing machine. The data management system allows for a user interface in which the user can alter study parameters, as well as access data output information. The specific data management system used in this study was Merlin (Instron Corp., MA).

Figure XIV. Instron 5500 Series uni-axial loading system.

2.5.2 Specimen Holding Device

After being potted and secured with Bondo in an aluminum box, each specimen was clamped between the adjustable jaws of the Instron vice, and anchored to the support plate via screws on the vice. The purpose of the holding device is to ensure that the specimen remains stationary during loading, so as to eliminate any movements that could interfere with the motion detection at the bone-implant interface.

2.5.3 LVDT Sensors

In the experimental setup, AC gaging linear variable differential transformers (LVDTs) were used to register and record micromotion movement of the acetabular cup/bone interface. LVDTs use an induced voltage to measure linear displacement, and consist of three coils aligned end to end with a magnetic rod through the center.[15] When an alternating current is applied, the primary coil induces a current in the two secondary coils. As the rod moves, voltage is increased in the secondary coil, while the other decreases. When the conversion between the voltage and displacement is known, the linear displacement can be calculated. The LVDT sensor chosen was a Transtek 333 Miniature AC gauging series (Trans-tek, Ellington, CT), with a linear range of ±.1.27 mm and a sensitivity of 4 mV/V/mil. Design specifications are shown in Table 8.

Table VIII. Design Specifications for Transtek 333 Series LVDT Sensor.

Linear Range	±0.05 in (1.27 mm)
Maximum Non-Linearity	< ±0.20% maximum
Housing Outer Diameter	0.375 inches
Input Impedance	245 ohms
Frequency of Excitation	7 kHz

2.5.4 Sensor Holding Device

In order to account for the differences in bone anatomy for specimens from different cadavers, as well as between the left and right pelvises, a sensor arrangement must be adjustable depending on the exact position of the acetabular cup in relation to the bone post-implantation. The ideal sensor arrangement would be to position recording sensors at four points on the cup, located equidistance from one another. However, differing bone anatomy may interfere with the desired sensor location, making placement difficult and even impossible in some cases. Because bone removal would potentially compromise the integrity of the implant, the sensor holding device must be able to position the sensor in a manner that avoids contact with these locations. Sensors were located around the bone were held in place with a bracket, attached to a holding device attached to a magnetic holding system equipped with swiveling adjustable arms (NOGA 64016, Noga Engineering Ltd.). In order to result in accurate readings, the sensor holding device must be securely attached to the working surface, which was achieved through a magnetic base.

The actual sensor holding device was located at the end of each side arm, and was designed with high precision so that the sensors measuring displacement at one location on the bone are located in the same plane, yet each the central axis of both is orthogonal. The sensor holding device is shown in Figure 14. In total, three sensor holding brackets were placed surrounding the acetabular cup.

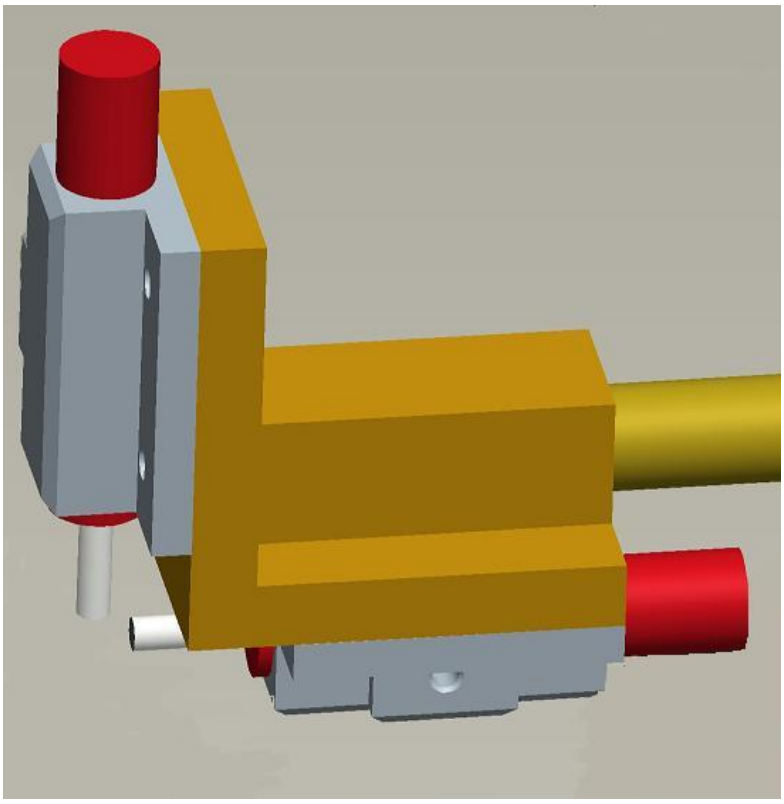

Figure XV. Sensor holding device (Zivkovic, 2006).

Additional sensors were positioned surrounding the loading device. In some cases and due to bone abnormalities, the sensor holding device was unable to be placed in a manner so that the sensors were able to reach the rim of the cup. The solution to this problem was to remove the sensors from the cup rim, and to place them elsewhere. Because the loading device is securely screwed into the center of the acetabular cup, the two items can be considered one rigid body. As such, motion can be recorded on one position of the rigid body (i.e. the loader), and through calculations, computed to represent the motion elsewhere (i.e. the cup rim). In order to provide for a defined location for sensor placement on the loader, a cruciform structure was securely

attached to the loader via screws located on each side. Three sensors were located on the arms of the structure, with each sensor measuring displacement along a different, but orthogonal axis. A sensor holding place, located parallel to, and several centimeters above the rim of the cup, was utilized to ensure that the sensors surrounding the cruciform were securely mounted. Sensors measuring displacement along the vertical axis were held in place with brackets welding to the sensor holding plate, shown in Figure 15, while horizontal sensors were located on the underside of the plate. The placement of sensors, located both around the acetabular cup rim allowed for insight into the migration of the cup during compressive cyclic loading.

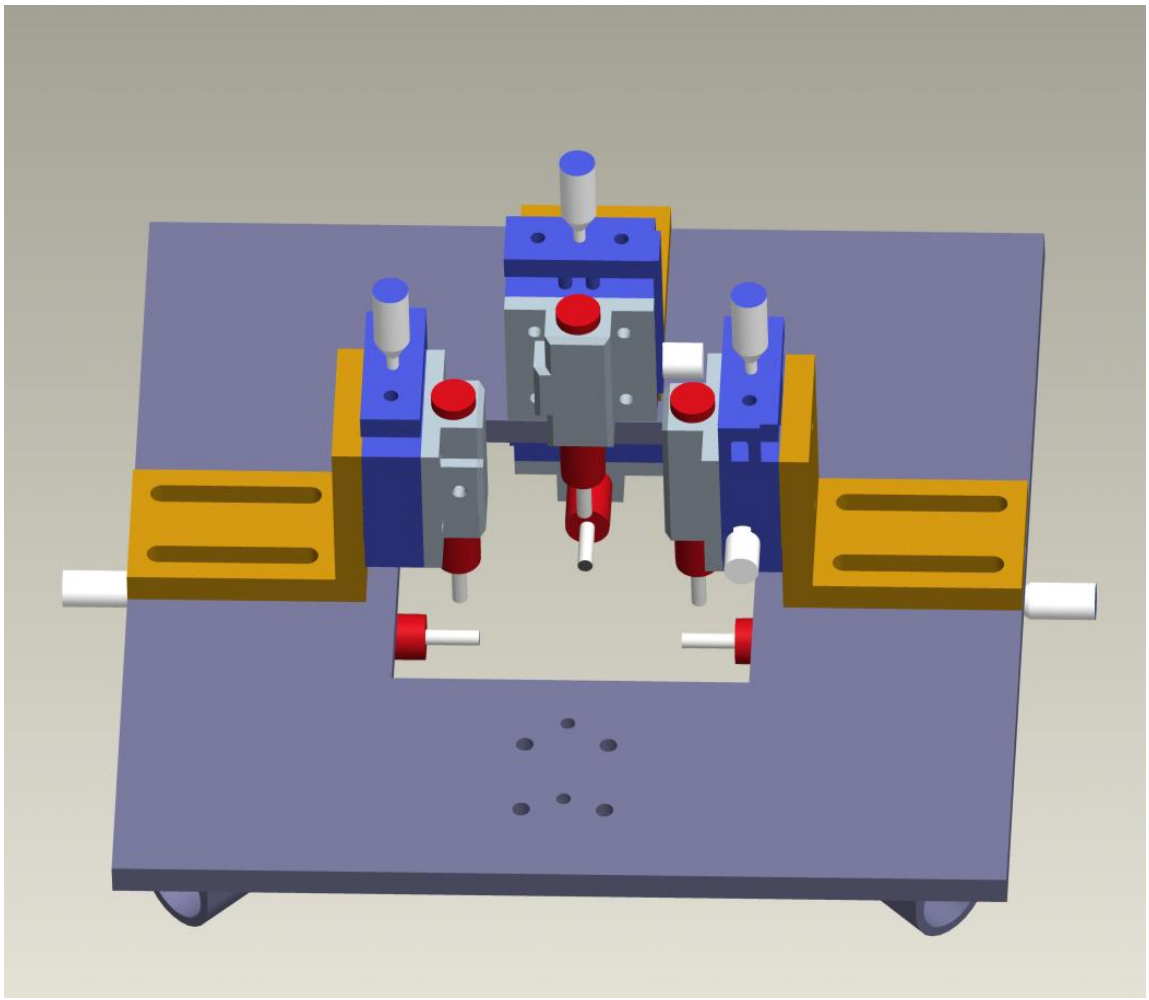

Figure XVI. Sensor holding plate with brackets for optimal sensor placement around the cruciform located on the loader (Zivkovic, 2006).

3.6 Testing and Data Acquisition

3.6.1 Sensor Placement

In order to ensure that each specimen would be testing under the same conditions, a strict procedure was adapted for specimen and sensor placement. First, the potted specimen was positioned in the specimen holding device and was securely

positioned in place with the clamp. Next, the load cell was coupled with a moment arm and a shaft connected to the prosthetic acetabular cup through a threaded stud located at the bottom of the shaft. The moment arm was first connected to the vertical shaft loading rod and the load cell was driven in a downward direction until it engaged the loader. While driving the load cell downward, care was given so as to not apply any significant initial load into the cup. Once in place, the moment arm was measured. The square sensor holding plate was secured in a position so that the loading arm would not come into contact with the sensor calibrator. The testing device configuration is shown in Figure 16.

Figure XVII. Experimental Setup for mechanical testing.

Finally, the LVDT sensors were secured in place surrounding the cup, as shown in Figure 17, so as to effectively capture the relative motion of the acetabular cup. Each sensor was manually calibrated through compression of the sensor (while it was in contact with the implant/cross) in order to 'zero' the sensor displacement. Sensors 1, 2, 10, and 11 were placed at the two points were the *x*-axis crossed the rim of the acetabular cup. Sensors 1 and 10 measured displacement along the *x*-axis, while sensors 2 and 11 recorded displacement in the direction of the *z*-axis. Sensors 3 and 9 were placed at the intersection of the *y*-axis and the rim of the acetabular cup on the side of the ischial tuberosity. Sensors 3 and 9 recorded displacement along the *y*- and *z*-axis, respectively.

In order to apply a compressive load to the cup/bone interface of the specimen, a loading electromechanical system (Instron Model 5569, Instron Corp., Canton, MA) was used. The loading parameters were set and adjusted using the data management system, Merlin. The load cell was set to apply a compressive load along the *z*-axis with the moment arm of 30 mm along the *x*-axis of the desired force for a total of 5 cycles, ranging from zero to the maximum force at that setup, and back to zero. Forces ranging from 100N to 1500N, in increments of 100 N, were applied in a cycle of 5 repetitions for each loading cycle. Speed was set to 8 mm/sec.

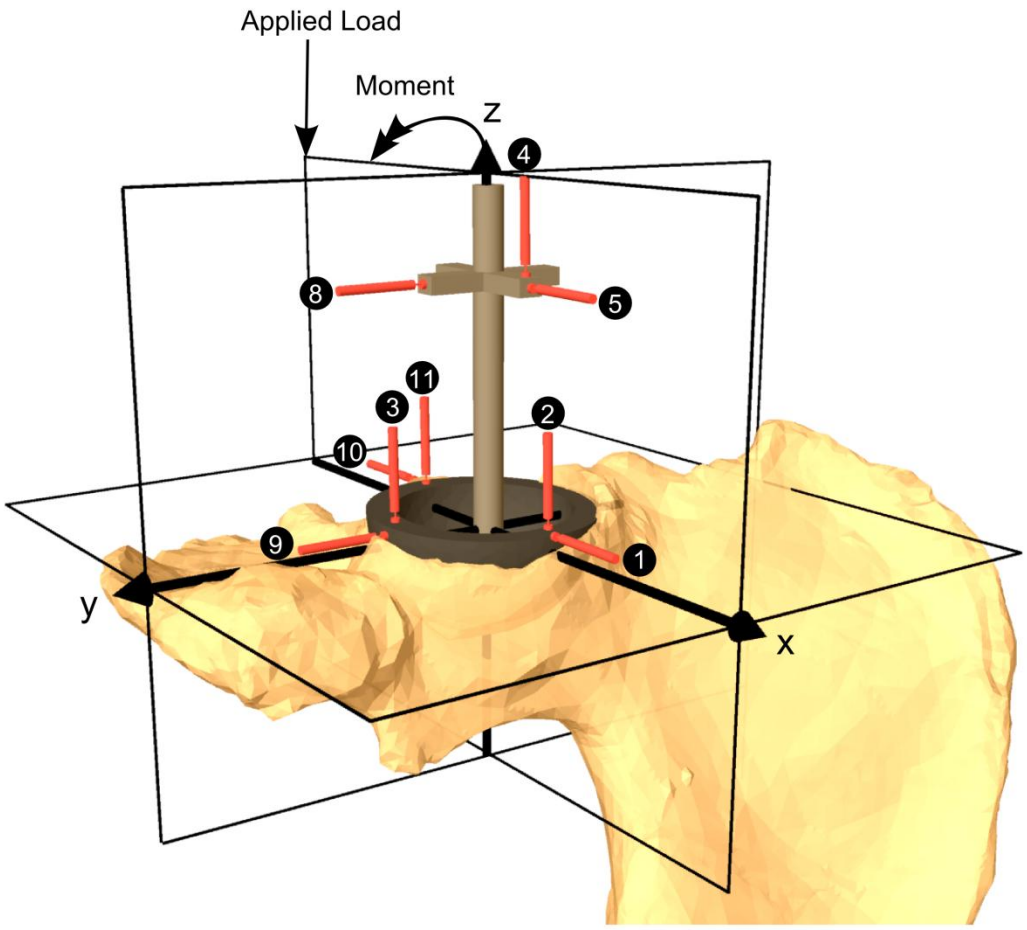

Figure XVIII. Schematic of sensor placement

3.6.2 Data Acquisition

Data was collected using an NI DAQCard-AI-16E-4 (National Instruments) and a testing and data acquisition system was designed in LabVIEW Virtual Instrument (VI) to register and record the voltage difference between the secondary coils of the LVDT sensors in real time.

The data acquisition process can be divided into five main steps, which are to configure analog input, start acquisition, read data, process data, and stop acquisition.

2.7 In-Vitro Experimental Results

2.7.1 Data Analysis

A program was then created to graphically represent the changes in displacement through force loading for each specimen. Finally, a program was developed to track the location of the center of the acetabular cup using the principles of rigid body mechanics and three points located around the acetabular cup rim. Using these three points, it was possible to track migration of the cup over loading and in relation to the location of the reconstructed defect. Taking note of the plane contained by the $\overline{\boldsymbol{XY}}$ plane and displacement recorded along the *z*-axis allowed for an understanding of the rotation of the cup about an Euler axis. The results of each cadaveric in-vitro testing are shown as follows in Tables 9-18.

2.7.2. In-Vitro Results of Press-fit Control Specimens

Table IX. Specimen 1: 2640 (left).

Specimen Characteristics

Gender:	Female
Cup Size:	52 cm
Comments:	The cup still appears stable, but has been noticeably displaced into the bone.

Figure XIX. First control specimen tested. Depuy PINNACLE acetabular cups were press-fit implanted.

Table X. Specimen 3: 18359 (right).

Specimen Characteristics	
Gender:	Female
Cup Size:	52 cm
Comments:	The cup appears stable.

Figure XX. Third control specimen tested. Depuy PINNACLE acetabular cups were press-fit implanted.

Table XI. Specimen 5: 18331 (left).

Specimen Characteristics	
Gender:	Male
Cup Size:	58 cm
Comments:	The cup is noticeably loosened within the acetabulum, with an approximate displacement of 4.0 mm.

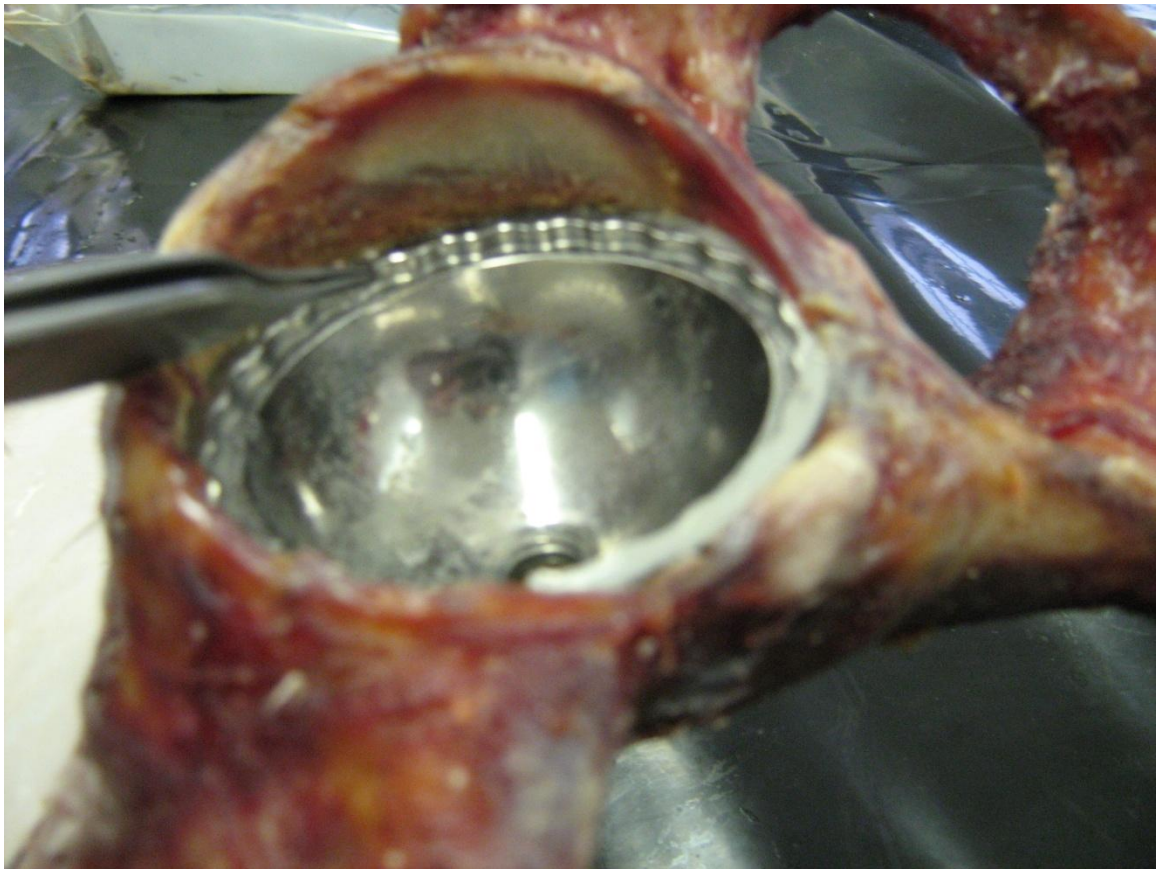

Figure XXI. Second control specimen tested. Depuy PINNACLE acetabular cups were press-fit implanted.

Table XII. Specimen 7: 100284 (left).

Specimen Characteristics	
Gender:	Male
Cup Size:	52 cm
Comments:	The cup appears stable.

Table XIII. Specimen 9: 53862 (right).

Specimen Characteristics	
Gender:	Male
Cup Size:	56 cm
Comments:	The cup appears stable.

2.7.2. In-Vitro Results of Specimens with Reconstructed Wall Augmented with Kryptonite

Table XIV. Specimen 2: 2640 (right).

Specimen Characteristics

Gender:	Female
Cup Size:	52 cm
Comments:	The cup appears stable.

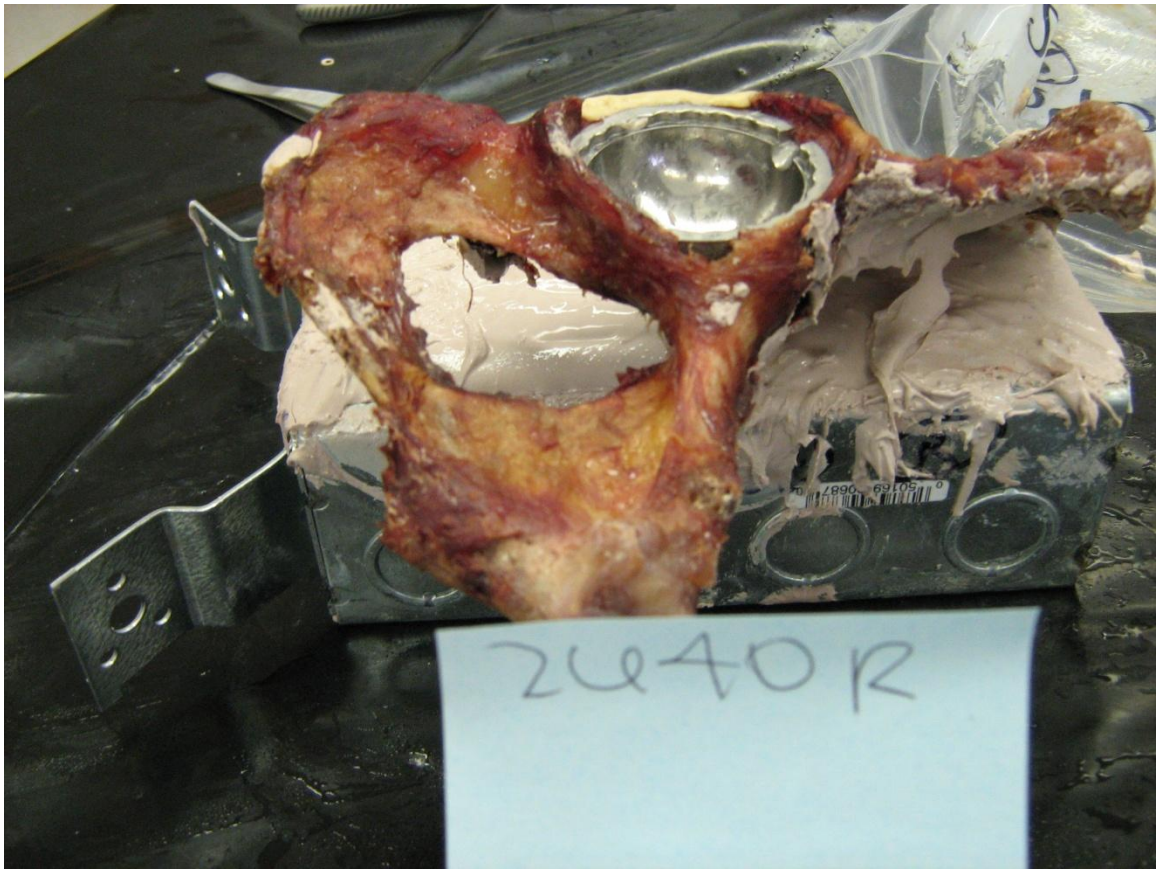

Figure XXII. First specimen with reconstructed wall augmented with Kryptonite bone cement Depuy PINNACLE acetabular cups were press-fit implanted.

Table XV. Specimen 4: 18359 (left).

Specimen Characteristics	
Gender:	Female
Cup Size:	52 cm
Comments:	The cup is noticeably loosened and is able to move freely. Removal of the cup showed cracking near the site of kryptonite reinforcement.

Figure XXIII.Third specimen with reconstructed wall augmented with Kryptonite bone cement Depuy PINNACLE acetabular cups were press-fit implanted.

Table XVI. Specimen 6: 18331 (right).

Specimen Characteristics

Gender:	Male
Cup Size:	58 cm
Comments:	The cup appears stable.

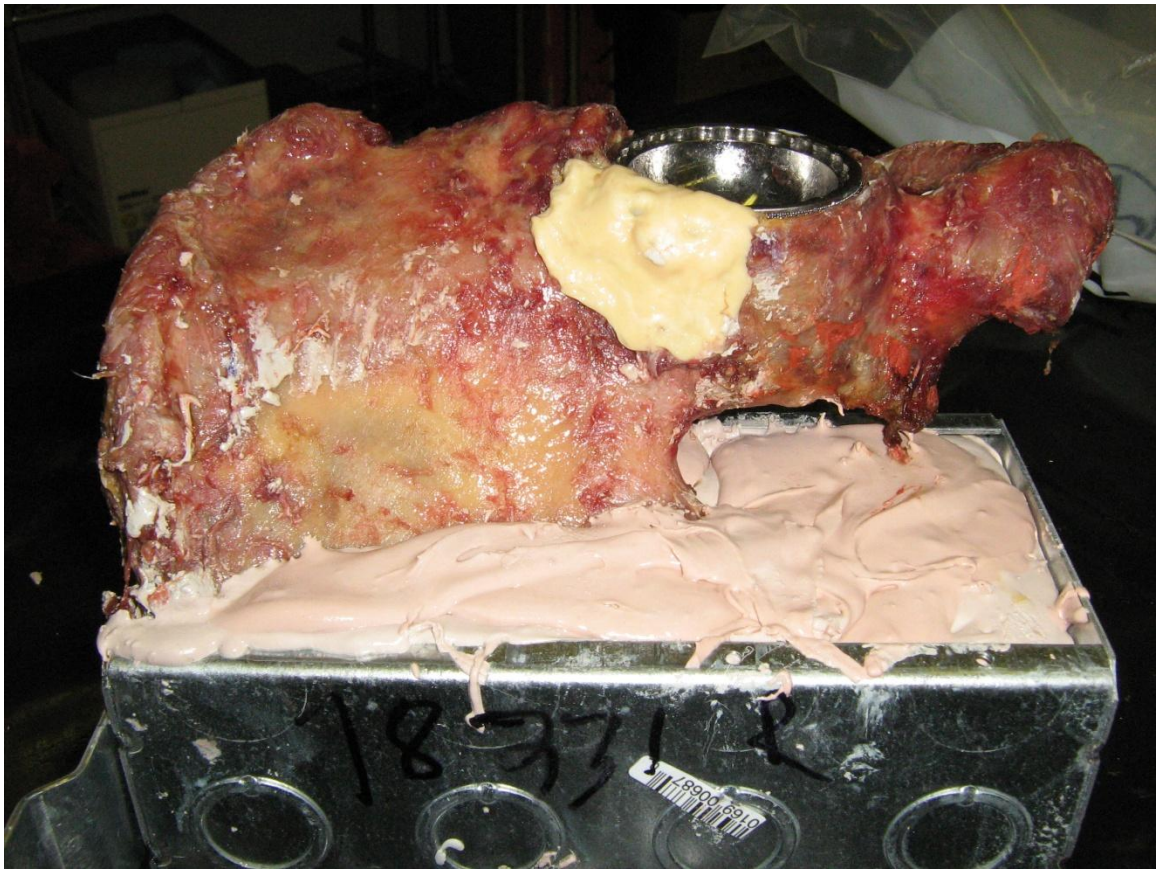

Figure XXIV. Second specimen with reconstructed wall augmented with Kryptonite bone cement Depuy PINNACLE acetabular cups were press-fit implanted.

Table XVII. Specimen 8: 100284 (right).

Specimen Characteristics	
Gender:	Male
Cup Size:	52 cm
Comments:	The cup appears stable.

Table XVIII. Specimen 10: 53862 (left).

Specimen Characteristics	
Gender:	Male
Cup Size:	54 cm
Comments:	The cup appears stable.

2.7.3. Migration of the Acetabular Cup as a result of Loading

The position of the center of the acetabular cup in each specimen was tracked over the course of loading (Figures 24-34). Testing was aborted in one specimen with reconstructed defect after loading at 700 N due to fracture of the acetabular wall near the site of the defect. According to the principles of rigid body mechanics, the rigid body motion of the acetabular cup can be explained in terms of translation about the *x*-,*y*-, and *z*-axis by $\boldsymbol{T_x}$, $\boldsymbol{y}$, and $\boldsymbol{T_z}$. Translation was defined according to the reference system previously described.

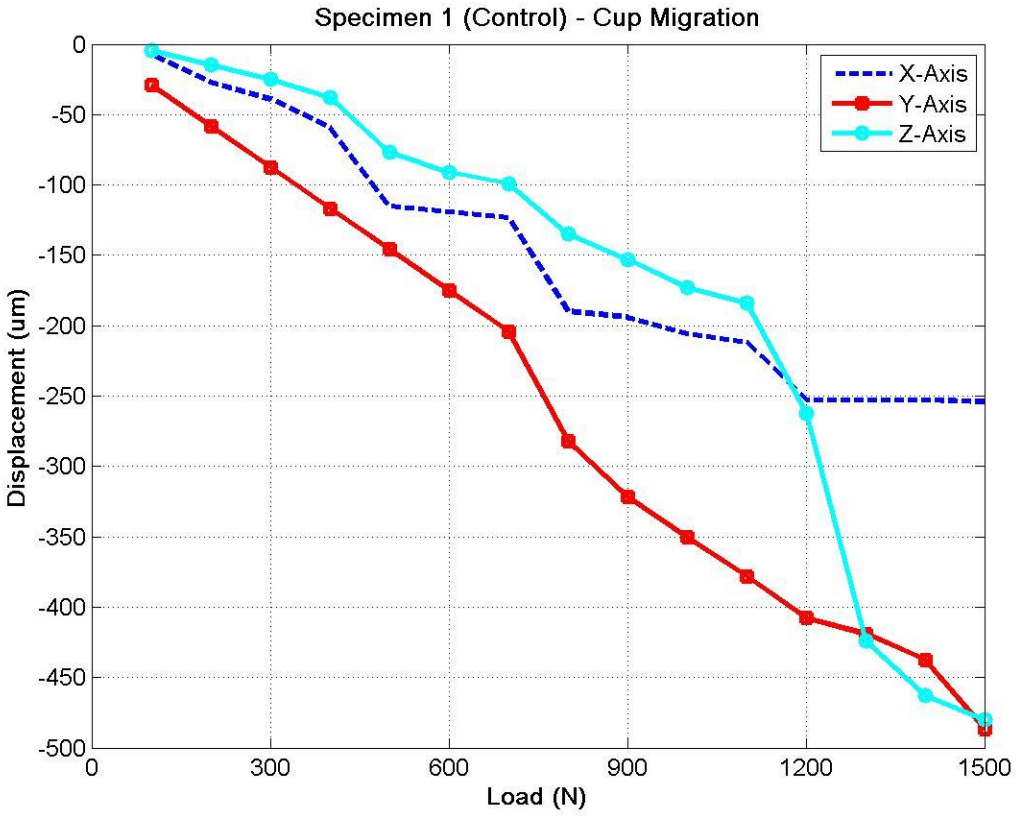

Figure XXV. Translation along the x-,y-, and z-axis for Specimen 1, where no defect was present .

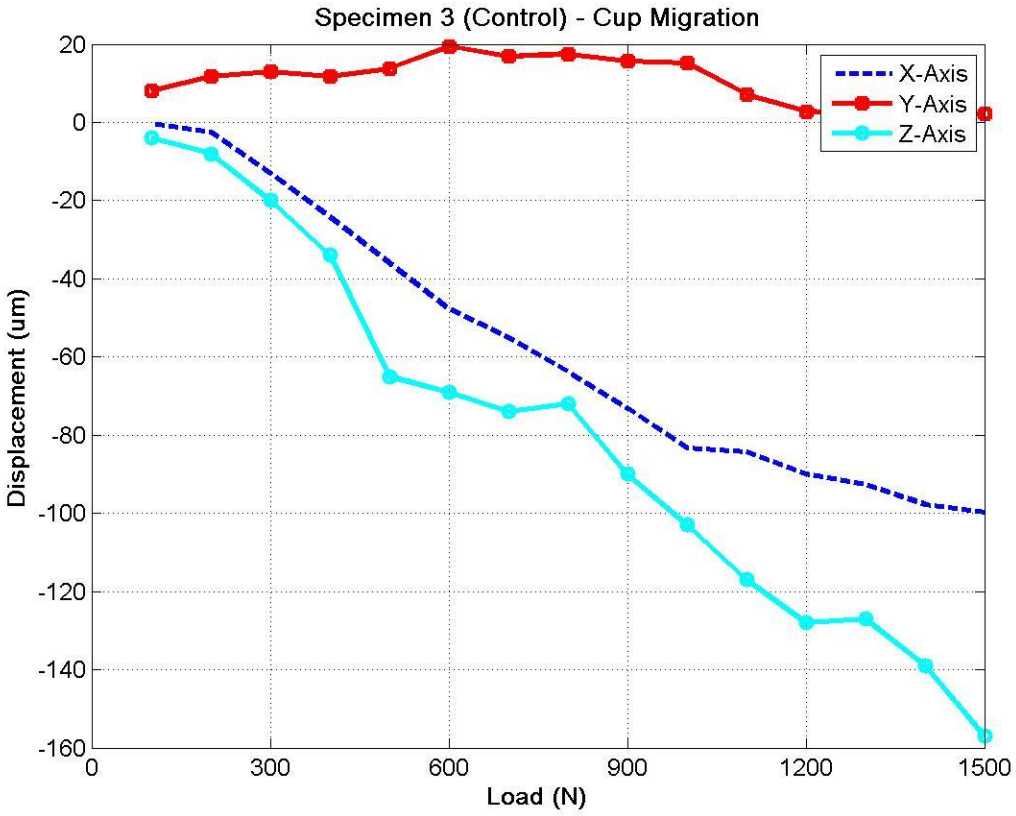

Figure XXVI. Translation along the x-,y-, and z-axis for Specimen 3, where no defect was present .

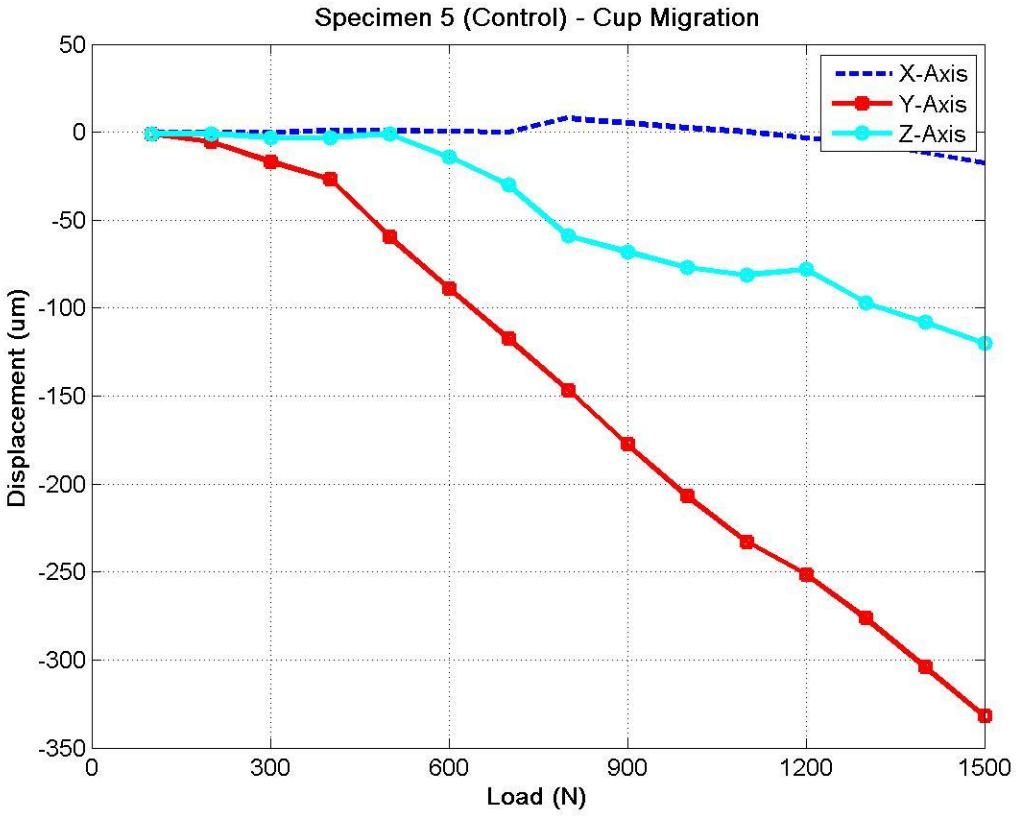

Figure XXVII. Translation along the x-,y-, and z-axis for Specimen 5, where no defect was present .

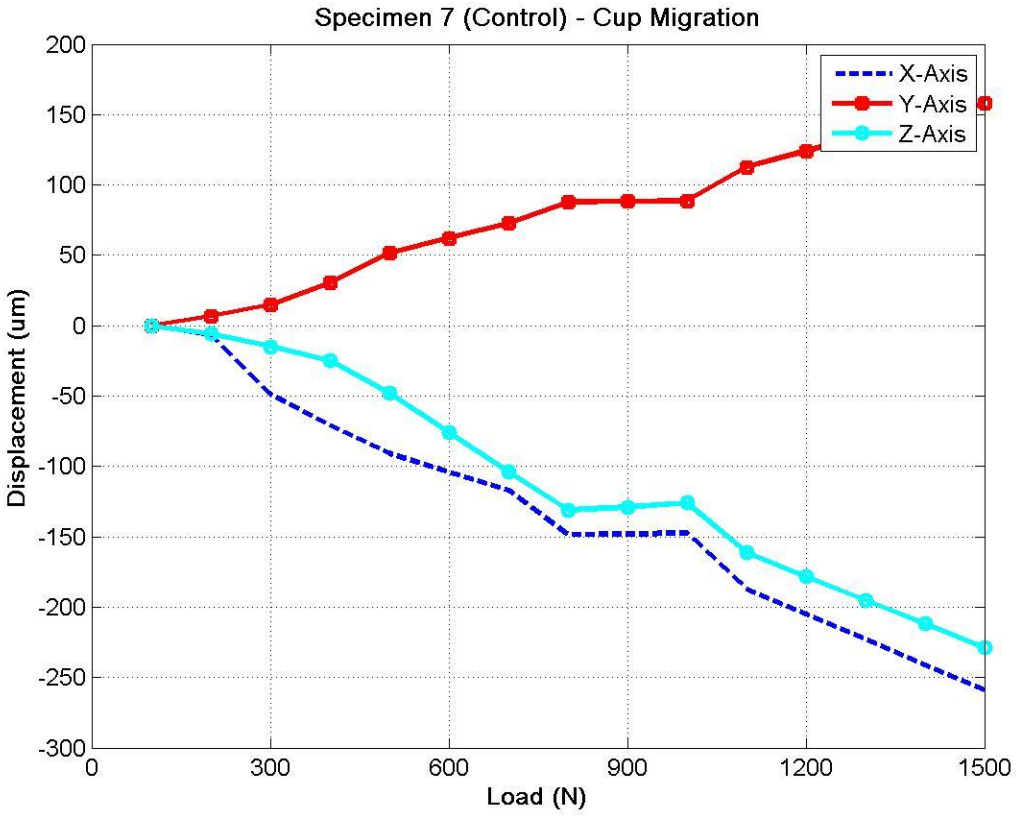

Figure XXVIII. Translation along the x-,y-, and z-axis for Specimen 7, where no defect was present .

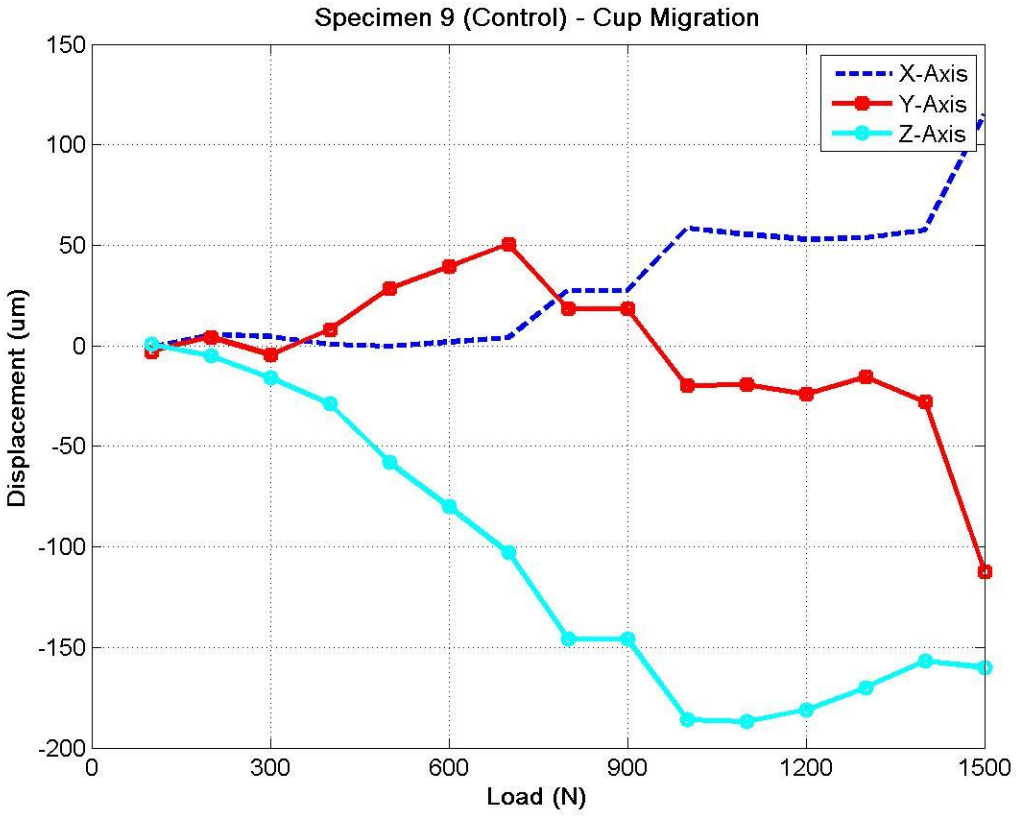

Figure XXIX.Translation along the x-,y-, and z-axis for Specimen 79 where no defect was present.

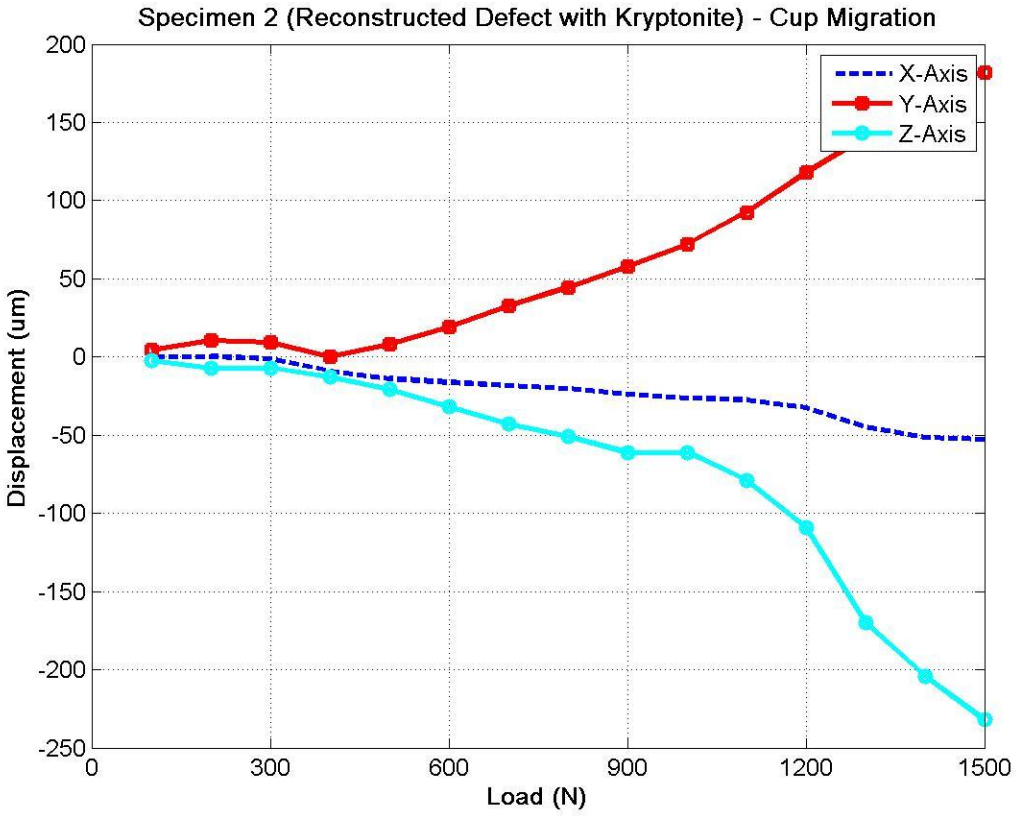

Figure XXX. Translation along the x-,y-, and z-axis for Specimen 2, with reconstructed defect.

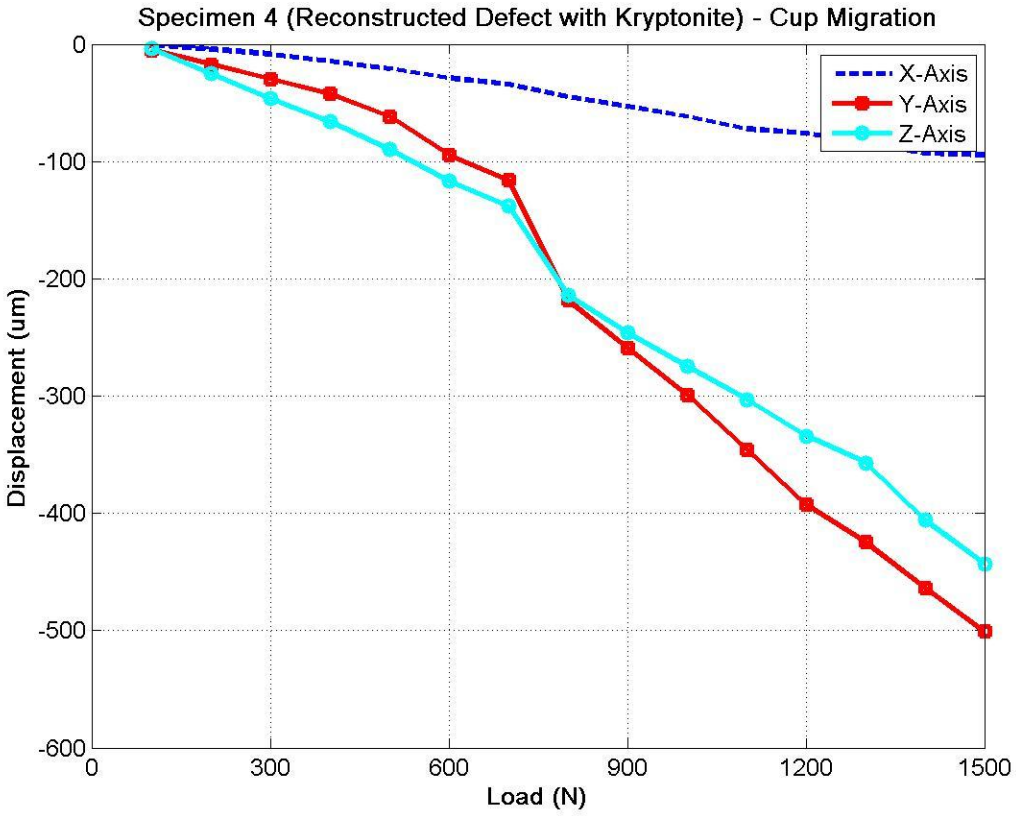

Figure XXXI. Translation along the x-,y-, and z-axis for Specimen 4, with reconstructed defect.

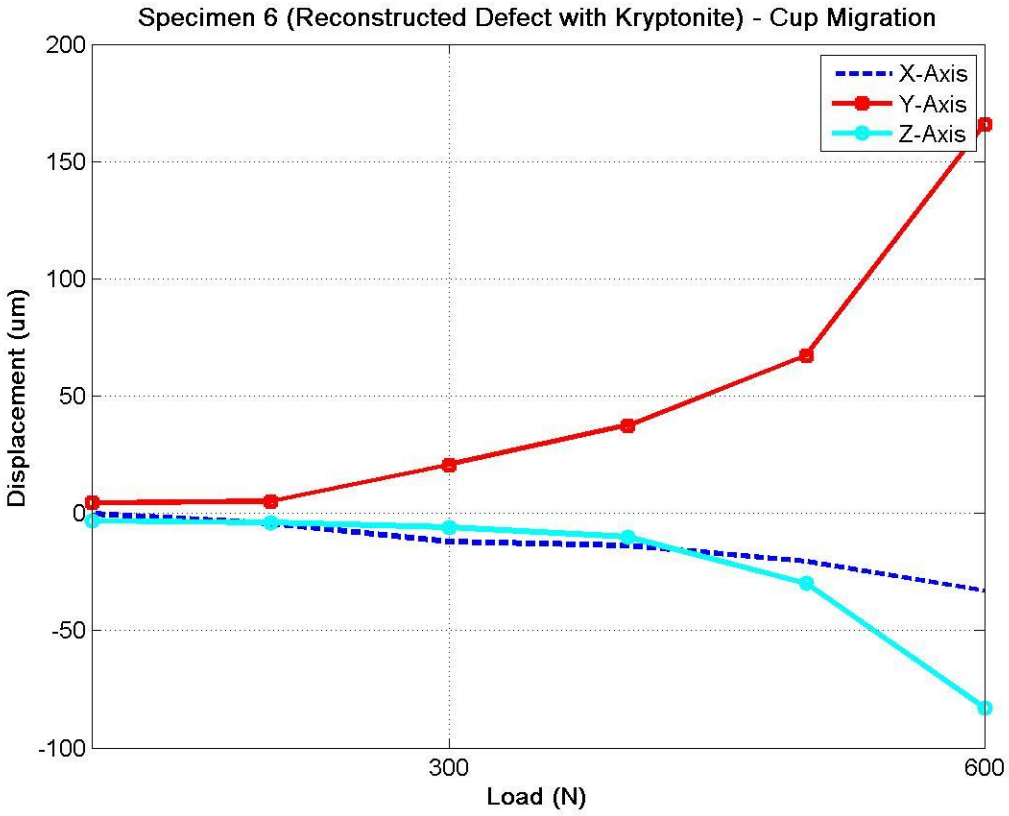

Figure XXXII. Translation along the x-,y-, and z-axis for Specimen 6, with reconstructed defect.

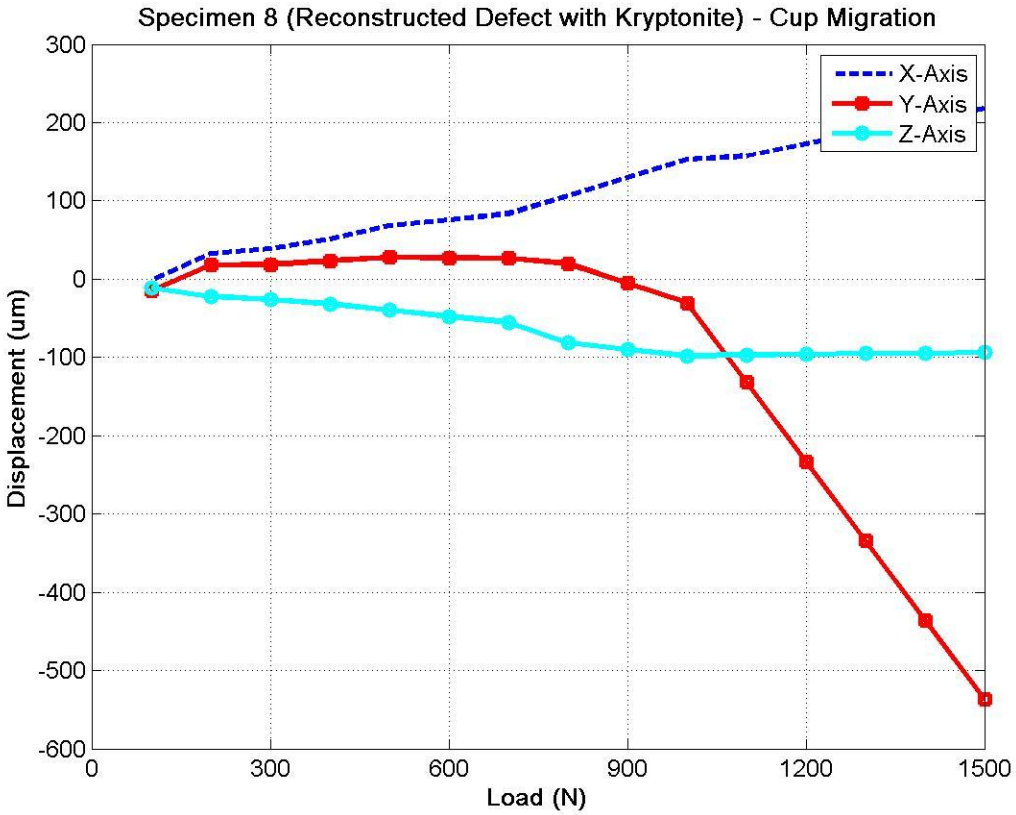

Figure XXXIII. Translation along the x-,y-, and z-axis for Specimen 8, with reconstructed defect.

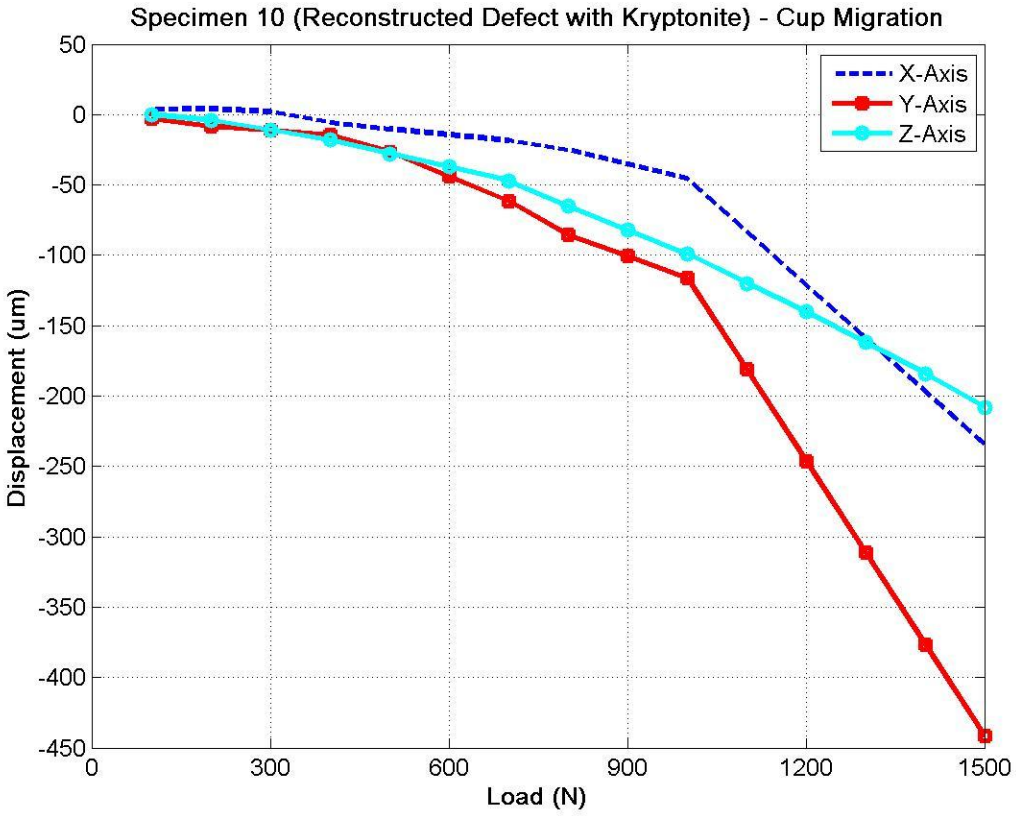

Figure XXXIV. Translation along the x-,y-, and z-axis for Specimen 10, with reconstructed defect.

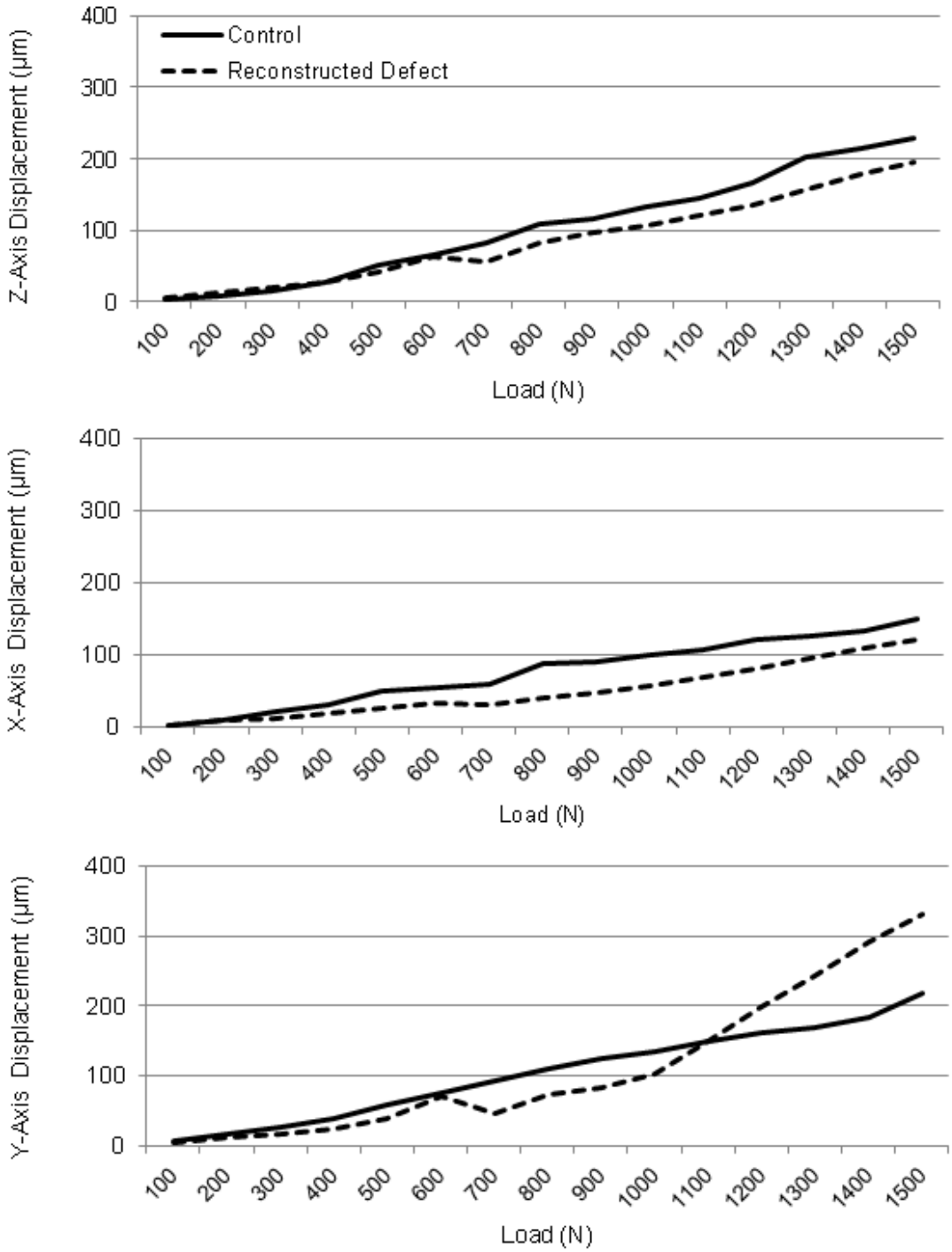

Figure XXXV. Average displacement of the center of the acetabular cup along the z-, x-, and y-axis in the control and reconstructed defect groups.

Up to loading at 600 N, the average displacement of the cup along the *z*-axis in both the control and reconstructed defect groups remained below 50 microns. Displacement exceeded 100 microns at loading greater than 800 N. At applied loads of greater than 600 N, average recorded displacements differed by about 20% between the two groups, with greater displacement seen in the control specimen.

Average displacement along the *x*-axis measured 132.81 microns in the direction of the anterior superior region in the control specimen at an applied load of 1000 N, and 106.68 microns in the same direction of the reconstructed defect. The difference in recorded migration continued to decrease as a function of increasing applied load, with just 22% greater amount of motion in the control specimen at 1500 N. Average displacement along the *y*-axis was 136.14 and 103.48 microns for the control and reconstructed groups, respectively, in the direction of the anterior inferior region at 1000 N (Figure 35). At applied loads of greater than 1000 N, a significant shift was seen in migration along the *y*-axis. While displacement of the acetabular cup in the presence of the reconstructed wall remained below that of the control specimen under 1000 N, migration continued to increase linearly above this loading case, and at 1500 N, displacement was almost 50% greater than in the intact specimen.

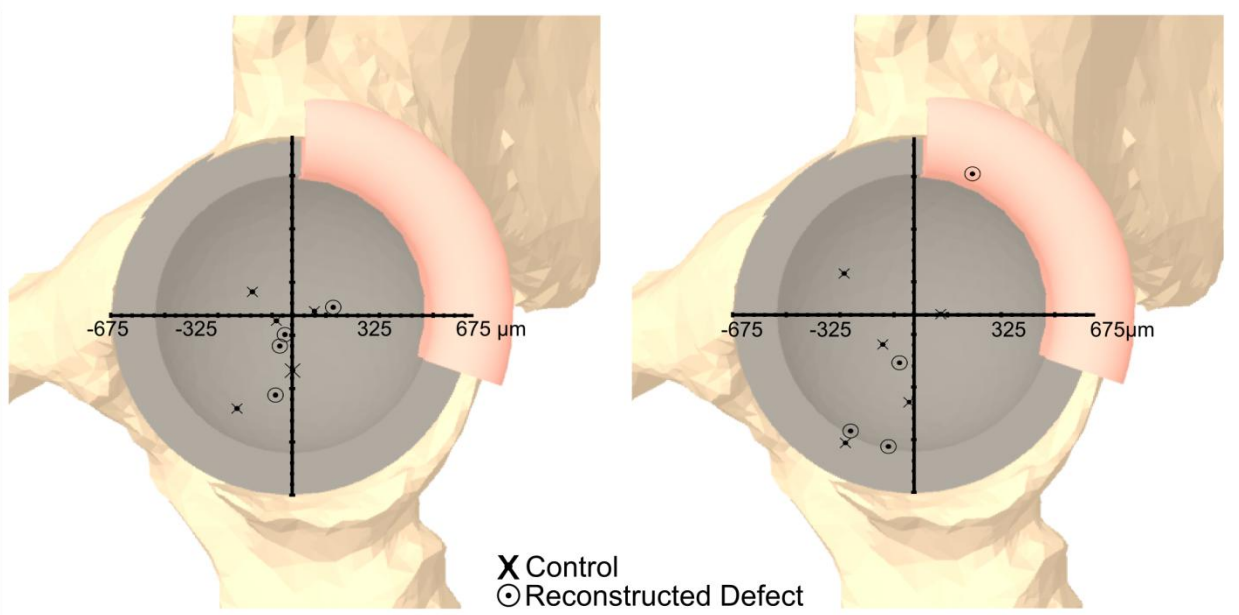

Figure XXXVI. Migration of the center of the acetabular cup center in relation the x- and y-axis at (A) 1000 N and (B) 1500 N. Displacement values have been magnified 40 times for viewing purposes.

2.7.4. Rotation of the Acetabular Cup as a result of Loading

The rotation of the acetabular cup was calculated using the principles of rigid body kinematics in the form of Euler angle and Euler parameter calculations (Amirouche, 2006). Using the displacement calculated at the three previously mentioned points surrounding the rim of the acetabular cup the final location of a rotating frame of a rigid body allows us to express that rotating frame in relation to a fixed frame by three successive rotations, $\boldsymbol{\theta_x}$, $\boldsymbol{\theta_y}$, and $\boldsymbol{\theta_z}$, in the direction cosine matrix, $\boldsymbol{S^{sr}}$. These rotations are deteremined by the following equation, where $\boldsymbol{S^{sr}}$is the obtained using the dot product of two dextral sets of unit vectors, given in Equations 2.1 and 2.2.

$$[\boldsymbol{S^{sr}}] = \{\overline{\boldsymbol{n}}^{\boldsymbol{s}}\} \cdot \{\overline{\boldsymbol{n}}^{\boldsymbol{r}}\} \quad 2.1$$

$$[\boldsymbol{S^{sr}}] = \begin{bmatrix} \boldsymbol{S_{11}} & \boldsymbol{S_{12}} & \boldsymbol{S_{13}} \\ \boldsymbol{S_{21}} & \boldsymbol{S_{22}} & \boldsymbol{S_{23}} \\ \boldsymbol{S_{31}} & \boldsymbol{S_{32}} & \boldsymbol{S_{33}} \end{bmatrix} \quad 2.2$$

These successive rotations can be expressed as a single rotation, $\boldsymbol{\theta}$, about a unit vector, $\boldsymbol{\lambda}$, along the line of rotation, $\boldsymbol{L}$, where $\boldsymbol{\theta}$ is calculated using the Euler parameters, $\boldsymbol{e_1}$, $\boldsymbol{e}$, $\boldsymbol{e_3}$, and $\boldsymbol{e_4}$ in Equations 2.3-2.6.

$$\boldsymbol{e} = \begin{bmatrix} \boldsymbol{e_1} \\ \boldsymbol{e_2} \\ \boldsymbol{e_3} \end{bmatrix} = \boldsymbol{\lambda_1 \sin}\left(\frac{\boldsymbol{1}}{\boldsymbol{2}}\boldsymbol{\theta}\right) \quad 2.3$$

$$\boldsymbol{e_4} = \boldsymbol{\cos}\left(\frac{\boldsymbol{1}}{\boldsymbol{2}}\boldsymbol{\theta}\right) \quad 2.4$$

$$\boldsymbol{e_1}^{\boldsymbol{2}} + \boldsymbol{e_2}^{\boldsymbol{2}} + \boldsymbol{e_3}^{\boldsymbol{2}} + \boldsymbol{e_4}^{\boldsymbol{2}} = \boldsymbol{1} \quad 2.5$$

$$\boldsymbol{\lambda_1}^{\boldsymbol{2}} + \boldsymbol{\lambda_2}^{\boldsymbol{2}} + \boldsymbol{\lambda_3}^{\boldsymbol{2}} = \boldsymbol{1} \quad 2.6$$

The Euler parameters can be related to the rotation about each axis using Equations 2.7-2.11.

$$\boldsymbol{e_1} = \boldsymbol{cos}\left[\frac{\boldsymbol{1}}{\boldsymbol{2}}\left(\boldsymbol{\theta_x} - \boldsymbol{\theta_y}\right)\right]\boldsymbol{sin}\left(\frac{\boldsymbol{1}}{\boldsymbol{2}}\boldsymbol{\theta_z}\right) \quad 2.7$$

$$\boldsymbol{e_2} = \boldsymbol{sin}\left[\frac{\boldsymbol{1}}{\boldsymbol{2}}\left(\boldsymbol{\theta_x} - \boldsymbol{\theta_y}\right)\right]\boldsymbol{sin}\left(\frac{\boldsymbol{1}}{\boldsymbol{2}}\boldsymbol{\theta_z}\right) \quad 2.8$$

$$\boldsymbol{e_3} = \boldsymbol{sin}\left[\frac{\boldsymbol{1}}{\boldsymbol{2}}\left(\boldsymbol{\theta_x} + \boldsymbol{\theta_y}\right)\right]\boldsymbol{cos}\left(\frac{1}{2}\theta_z\right) \quad 2.9$$

$$e_4 = cos\left[\frac{1}{2}\left(\theta_x + \theta_y\right)\right]cos\left(\frac{1}{2}\theta_z\right) \quad 2.10$$

$$\cos(\theta) = 2{e_4}^2 - 1 = {e_4}^2 - {e_1}^2 - {e_2}^2 - {e_3}^2 \quad 2.11$$

Using the displacement calculated at the three previously mentioned points surrounding the rim of the acetabular cup the final location of a rotating frame of a rigid body allows us to calculate rotation about the *x*-,*y*- and *z*-axis. These three successive

rotations, indicated by θ_x, θ_y, and θ_z, were expressed as a single rotation about the Euler axis for both the control and reconstructed defect specimens (Figures 36-37).

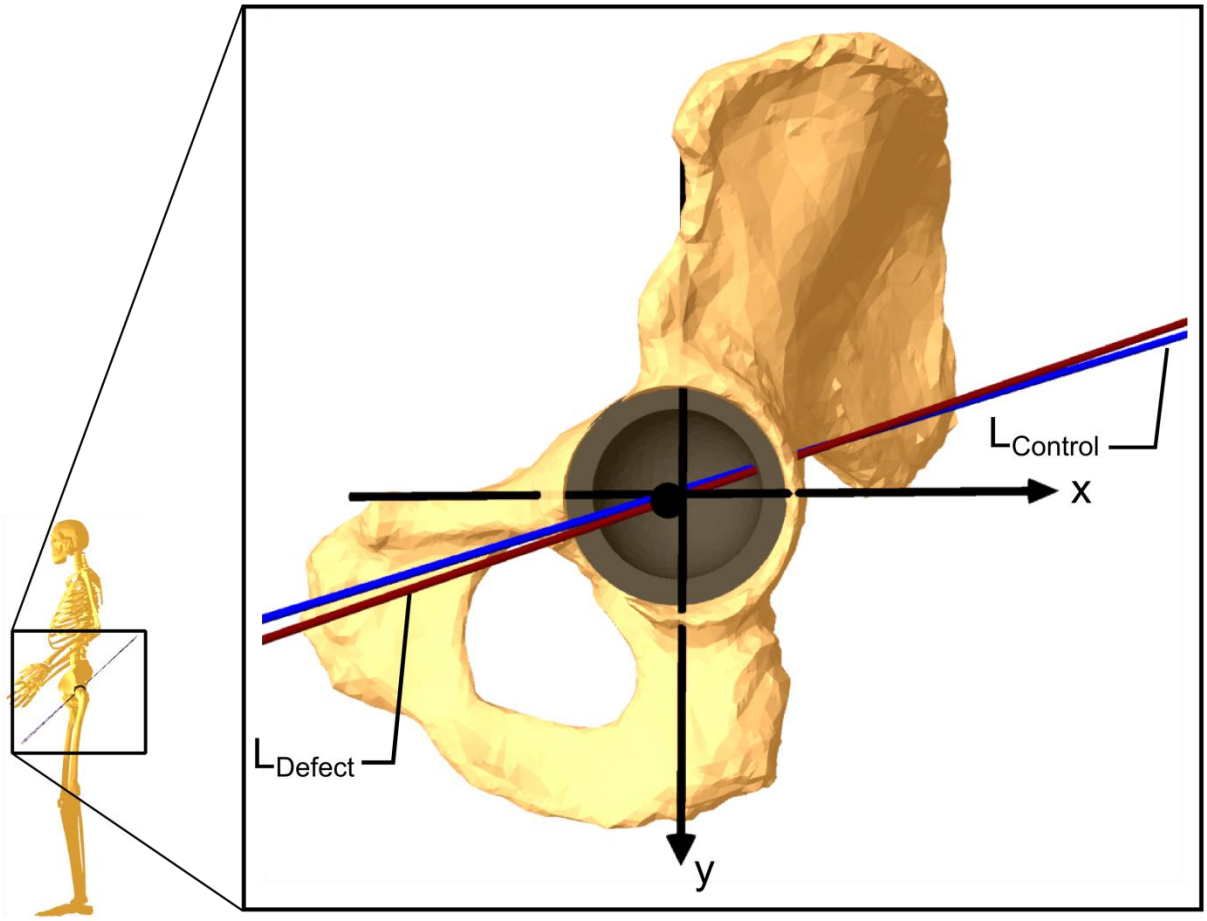

Figure XXXVII. Lateral view of the pelvis showing the average Euler axis for the control (LControl) and reconstructed defect (LDefect) at 1500 N.

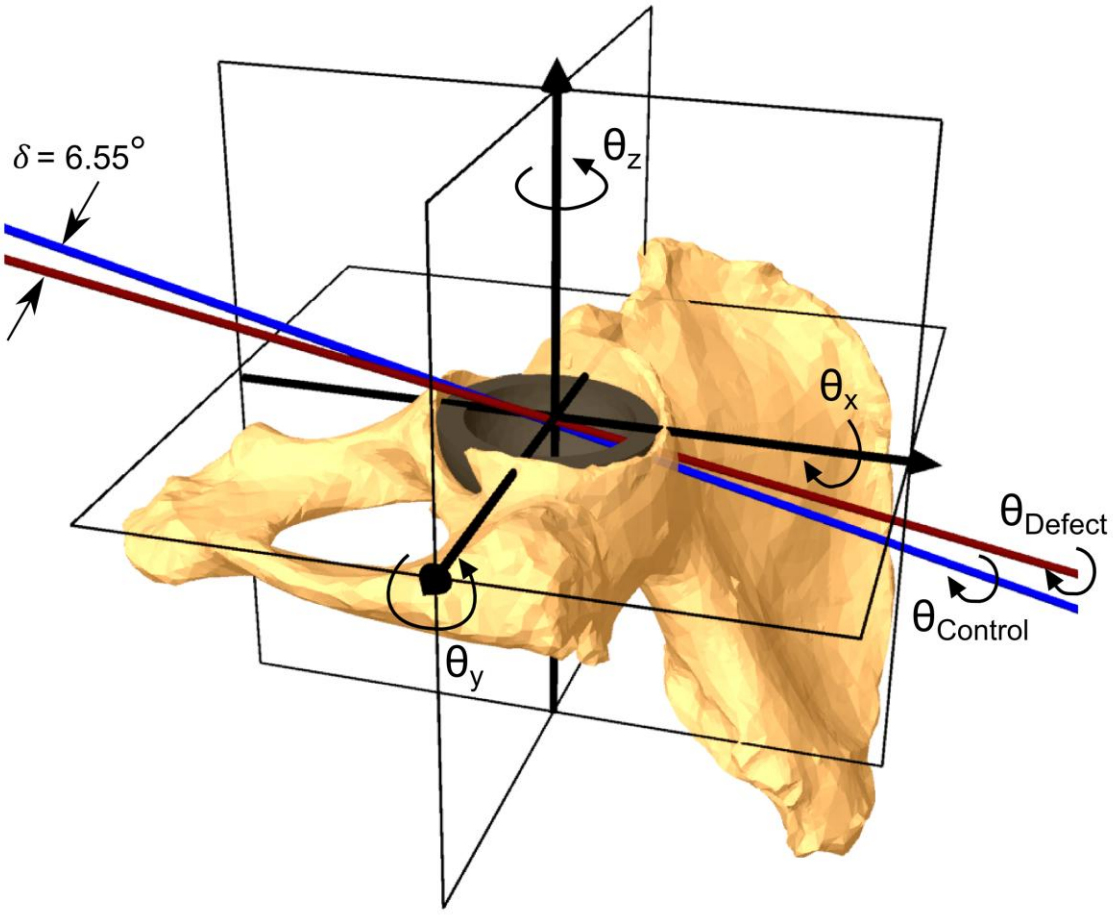

Figure XXXVIII. Rotation of the acetabular cup in 3D space about the reference system and rotation about the Euler axis for the control (Θ Control) and reconstructed defect (Θ Defect) where the directional variation (δ) at 1500 N was 6.55˚.

The results show that the directional variation between the average Euler axis of rotation for the control and reconstructed defect group is 6.55˚ at 1500 N. A closer look at the average Euler angles of rotation of the cup about the cup-bone interface revealed that on average, the control specimen underwent a greater amount of rotation up to 1400 N, at which point a small increase in rotation was seen in specimens with a

reconstructed defect of the acetabular wall (Figure 38). Due to early fracture of the acetabular wall in one specimen with reconstructed defect, an isolated peak in rotation occurs at 700 N.

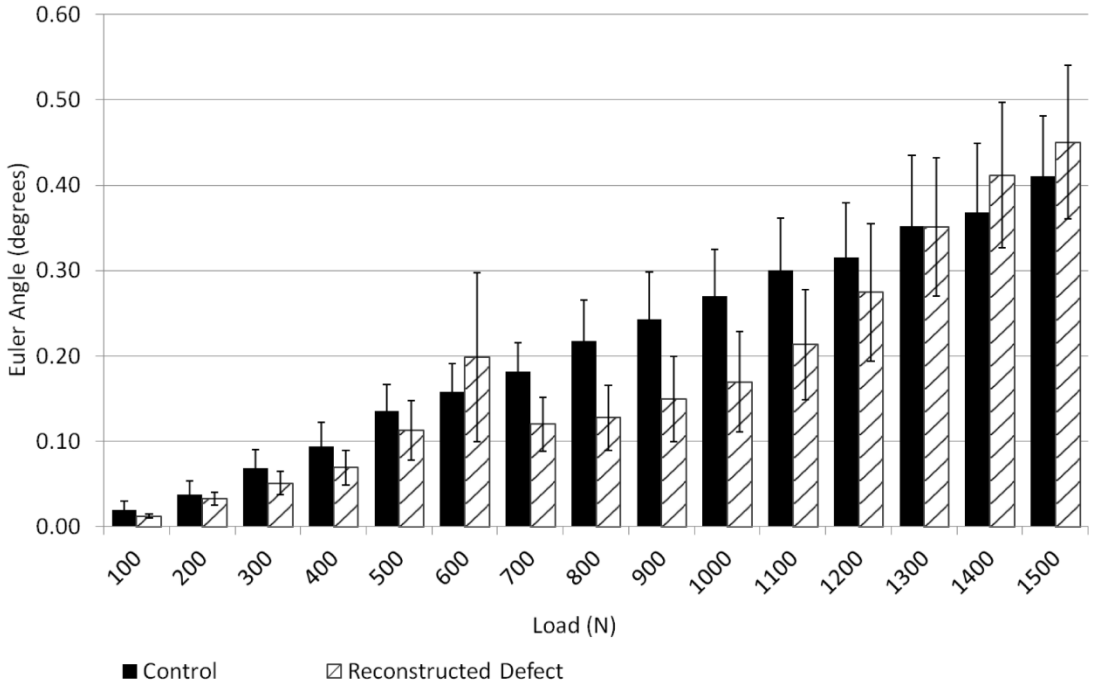

Figure XXXIX. Comparison of recorded Euler's angles (degrees) for control and Kryptonite treated defect about the Euler axis.

2.7.5 Clinical evaluation of acetabulum following loading

Following mechanical testing, the acetabular cup was removed from each specimen to have an understanding of the structural integrity of the cup-bone interface

after post-operative loading. The structural integrity of the bone was maintained in all but one specimen. In one specimen with reconstructed defect, a fracture was seen in the bone at the site of the bone-screw interface of the reconstructed defect (Figure 39).

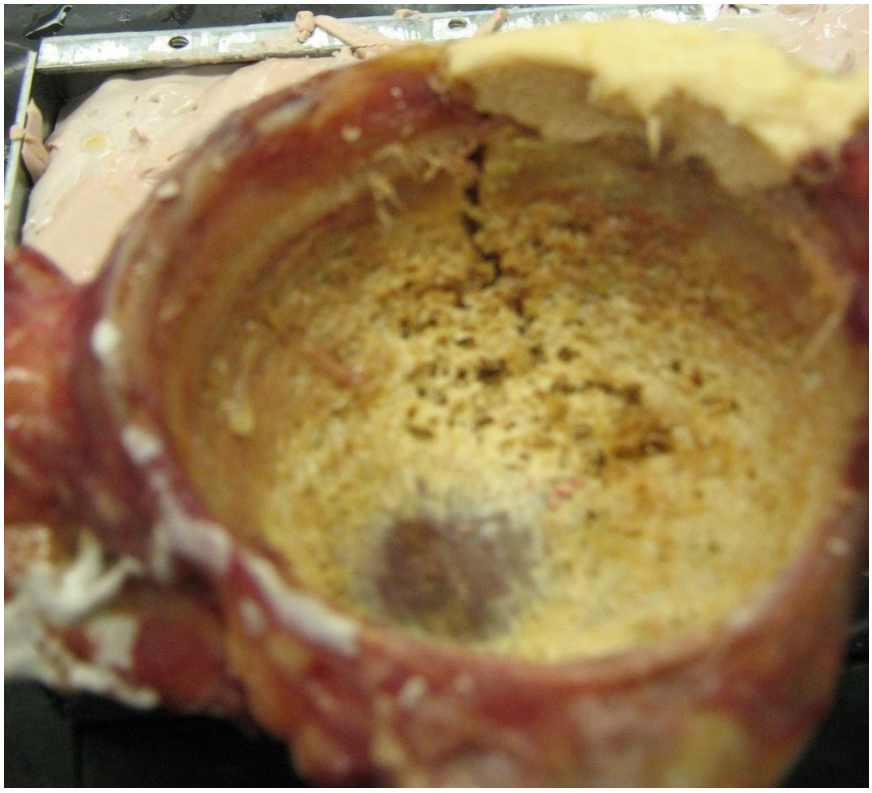

Figure XL. Bony fracture of the acetabulum in one specimen near the bone-screw interface with reconstructed defect.

2.8 Discussion

Acetabular defects were created in the acetabular walls of cadaveric specimens and following wall reconstruction with cortical bone screws and Kryptonite bone cement, the acetabula were reamed and press-fit inserted with acetabular cups. The non-continuity and general non-uniformity of the acetabulum at the site of the cup-bone interface can have a direct affect on the stability and fixation of the acetabular cup, which is estimated by measurements of cup migration or angular rotation about an Euler axis. As the force applied to the compressive load was increased, in both groups, sensors registered increased positional displacement which indicates migration of the acetabular cup at the cup-bone interface.

Micromotion of the cup between the first and second compressive loading cycles were measured along each axis for loads between 100N – 1500N in both the control and Kryptonite treated acetabulum. Displacement along the *z*-axis measured the amount of penetration into the acetabular cavity due to loading. A closer look at the displacement at each load indicates findings about the stability over the range of forces. While displacements of both the control and reconstructed defect groups remained below 50 microns at 600 N, forces above this load caused notable changes in the displacements of cups implanted in both. Because a greater displacement from original location suggests a more dramatic migration, one can conclude that the untreated, control acetabulum underwent a greater deformation and positional shift along the *x*- and *y*-axis, particularly below 1000 N of loading. In general, sensors registered migration of the center of the acetabular cup towards the anterior superior and anterior inferior regions of the acetabular wall. This phenomenon was most notable in the

reconstructed specimen, particularly above 1000 N, where an increase in displacement was noted along the *y*-axis. It is interesting to note that the direction of migration is similar in both groups, despite the presence of a reconstructed defect, which might suggest that the presence of Kryptonite inhibited motion towards the defect. The results suggest that the presence of Kryptonite at the site of the acetabular defect allowed for a successful reconstruction of the acetabular wall. Therefore, it can be assumed that Kryptonite effectively acted as a protective agent at the site of the defect when used to complement acetabular wall reconstruction reinforced with bone screws, resisting micromotion towards the superior posterior region, as increasing forces were applied.

The Euler axis can be used to provide further insight into the stability and fixation of the cup when comparing different pathologies at the interface. The results indicate that between 700 to 1400 N, treatment at the defect site with Kryptonite has a strong reduction in rotation about the Euler axis. The amount of rotation about the axis at the site of the reconstructed defect remained below the rotation observed in the control specimen below 1400 N. The results indicate that the behavior of the cup in the presence of a reconstructed defect is dependent on loading conditions. The increase in rotation can be observed in the directional variation of the Euler axis, which gives additional evidence of the relation between Kryptonite behavior and load. The difference of 6 degrees in direction of the Euler axis between the two groups at 1500 N is likely due to a strong change in displacement in the reconstructed defect specimen that was observed along the *y*-axis after 1000 N. Considering that the movement is related to the amount of load at the hip joint, the use of Kryptonite and the dimensions of the reconstructed defect wall must be patient-specific in order to provide a stable interface.

Having a clinical understanding of where fracture occurred during post-operative loading can provide further insight into the displacement and rotation results of the acetabular cup in this study. Incidentally, fracture occurred in the same specimen (number 6) in which excessive displacement occurred between 600-700N, after which point testing was aborted. The high values in rotation and displacement, as well as the large standard deviation in the average rotation at 600 N can be attributed to the occurrence of this fracture.

Several limitations exist in the current study. Essentially, the outcome of the experiment was that Kryptonite does, in fact, serve as an effective protective agent in the presence of acetabular defect and increases the stability of the acetabulum during immediate post-operative loading in the setting described and below a certain compressive load. Because of the occurrence of bony in-growth over time could affect the fixation, it is unknown whether Kryptonite will behave in the same manner in-vivo. More accurate data could be obtained through additional experiments on a larger number of cadaveric specimens where average displacements for additional cyclic loading could be imposed to study the stability at several weeks following surgery.

3. DEVELOPMENT AND VALIDATION OF FINITE ELEMENT MODEL OF THE CUP-BONE INTERFACE FOLLOWING THR

3.1 Introduction

Basic finite element methods were first introduced in the late 1950s and 1960s. Finite Element Analysis (FEA) gained popularity in the 1970s and 1980s and now it is becoming a vital critical tool in all design analysis applications including biomechanics. has gained a widespread popularity among engineers and researchers who wish to computationally evaluate the effect of a various applied loads, material properties, and stress or strain distributions on a given structure. Often, the geometry of structures evaluated with FEA is too complex to be solved through analytical methods. Hence, FEA allows for the solution of extremely complex problems because it allows for even the s used to handle components, called elements. Each material or structural property of a given material is defined within that mesh. Essentially, FEA is composed of three main parts – pre-processing, meshing and analysis, and post-processing. In the pre-processing stage, the user constructs a computer aided design (CAD) model representative of the object to be analyzed. The model is then meshed and then the appropriate boundary conditions and loading are applied to determine the model behavior and response to various conditions. Finally, the post-processing stage allows the user to graphically view the results of the preformed analysis.

3.2 Modeling of the Hip Joint and THR

Several studies have used finite element analysis techniques to study the effect of material properties, interface conditions, and loading characteristics on micromotion of the acetabular cup at the bone-implant interface following total hip replacement

(Dalstra et al., 1993; Dalstra et al., 1995; Heijink et al., 2008; Abdullah et al., 2010; Vicentonti et al., 2000; Mann et al., 1995). Through the use of computer modeling, the stresses and micromotion of the acetabular cup seen at the hip joint can be quite easily predicted. Furthermore, the use of segmented bone geometry through scanning techniques allows for detailed modeling of geometric parameters from individual patients or specimens. Using finite element analysis, that geometry can be subjected to a number of loading conditions in order to determine the resulting stress and displacement, as well as other parameters.

3.2.1 Modeling Material Properties

When conducting finite element analysis, the proper material properties must be considered in order to obtain accurate results. In modeling the pelvis following THR, the implanted acetabular cup is most commonly modeled as a linear, homogenous and isotropic material with an elastic modulus of 110 MPa and a Poisson ratio of 0.3 (Heijink et al., 2008; Abdullah et al., 2010).

Daltra et al (Dalstra et al., 1993; Dalstra et al., 1995) used CT image data to develop two separate finite element models of the pelvis, both of which modeled the trabecular bone of the pelvis as an 8-node parametric brick mess. In modeling the cortical bone, a cortical shell of 1 mm was created to represent the thin layer of cortical bone surrounding the sponge bone, under the assumption that the cortical bone would be subjected to only in-plane loading. In total, the model consisted of approximately 2,602 elements connected by 1862 nodes. Material properties were assigned based on measurements from CT scans of the obtained pelvis. In the first of the two finite element models, the trabecular bone of the pelvis was modeled as an isotropic material with a

Poisson's ratio of 0.2. Based on values seen in literature, the cortical shell was modeled with a Young's modulus of $E = 17\ GPa$ and a Poisson's ratio of $\upsilon = 0.3$. In the second finite element model, the material properties for both the trabecular and cortical bone were assumed to be uniform and homogenous. In this model, it was assumed that the cortical and trabecular bone Young's modulus is $E = 70\ GPa$ and $E = 17\ GPa$ respectively. Poisson's ratio remained the same as had been assumed in the first model.

In an effort to validate the work done by Dalstra, and to determine the effect of various resurfacing techniques on stresses seen in the pelvis, Thompson et al developed a finite element model of the pelvic bone from the CT scan of an 89 year old male. Young's modulus of the trabecular bone was defined as a function of apparent density, which resulted in a Young's modulus varying between $E = 0.0013\ GPa$ and $E = 1.6\ GPa$, and a Poisson's ratio $\upsilon = 0.2$. The cortical bone thickness was determined to vary between 0.96 and 2.06 mm, and Young's modulus and Poisson's ratio of $E = 17\ GPa$ and $\upsilon = 0.3$ were assigned, respectively.

To determine the effect of screw insertion in stabilizing the acetabular cup at the cup-bone interface and to validate the previously mentioned in vitro work by Kwong et al., Hsu et al. utilized a finite element analysis model of the pelvis (Hsu et al., 2007). The pelvic model was constructed using a 10-node tetrahedral model, which consisted of the cortical and trabecular bone of the pelvis, as well as the femoral head, polyethylene liner and the titanium acetabular cup. In this model, the acetabular cup was constructed to model an exact fit condition with the acetabulum. In other words, no under-reaming or over-reaming was done. The cortical bone was modeled as a shell

element with a thickness of 0.9 mm with $E = 5600\,MPa$ and $\upsilon = 0.3$. Trabecular bone was modeled with $E = 500\,MPa$ and $\upsilon = 0.3$. The screws were modeled as cylinders, and the screw-bone interface was regarded as a bonded contact.

3.2.2 Modeling of the Bone-Implant Interface and Contact

Many different approaches exist to modeling the interface between the bony acetabulum and the implanted acetabular cup. Because the elements of these two objects are not connected together by any nodes, a contact model is needed in order to effectively achieve a load transfer across the interface and between the two objects. This interface is especially important when modeling an uncemented total hip replacement because the two objects are not homogenously bonded throughout the interface. Finite element software commonly allows the user to create a contact set between two bodies, in which the proper parameters can be set to as to effectively model the behavior of in-vivo conditions. The parameters include the contact element type, which can be surface to surface, surface to node, or node to node. Studies have shown that in models which can involve some sliding between the bodies of the interface, such as in an uncemented THR, both surface to node and surface to surface are quite accurate. (Vicentonti et al., 2000; Mann et al., 1995). Additional parameters of the contact set include convergence tolerance, contact algorithm, coefficient of friction, and contact stiffness. In particular, the coefficient of friction has a significant role in the fixation stability of the interface. The frictional properties at the bone-implant interface between both porous and smooth surfaces have been previously measured and recorded over the course of cyclic loading (Dammak et al., 1997). It was determined that coefficient of friction was independent of the normal contact pressure, the rate of

displacement, and also the site of cancellous bone. However, the surface coating of the implant was found to have a significant influence of the friction at the interface, with that of the porous surface being significantly greater than the smooth surface.

Thompson modeled three conditions of the bone-implant interface in order to determine the effect of resurfacing techniques and amount of bone in-growth on stability. The interface was modeled as a fully bonded unit, assuming that bony in-growth had fully occurred, as a unbonded interface with a coefficient of friction of $\mu = 0.5$, and also an unbonded interface with $\mu = 0.1$.

Hsu et al modeled the contact of the cup-bone interface as a surface to surface contact with a coefficient of friction of 0.5. Prior to loading, the nodes of the model were constrained in all degrees of freedom on the sacroiliac joint, as well as the pubic symphysis. The model tested during a course of 26 different loading conditions to mimic the loading seen on the hip joint over the course of daily activity. In addition to the applied force, a torque was applied in the lateral direction so that stability under torsional loading might be evaluated. In this model, the bone was not loaded with any muscle forces, as the pelvis was considered a “stand-alone” structure in which only the micromotion at the interface was evaluated.

3.2.3 Determination of Stress Seen at the Bone-Implant Interface

In a realistic pelvic model constructed from CT image data, Daltra (Dalstra et al., 1995) used finite element analysis to compute cortical bone stress and compared that data to stresses determined experimentally. To validate the FE model, Daltra placed strain gauges on a cadaveric pelvis to measure the strain seen in cortical bone. FE predictions of von Mises stress in the cortical bone of the pelvis under a load of 600 N

were approximately 5 MPa, compared to a maximal von Mises stress of nearly 7 MPa which was computed during experimental testing. In mechanical testing, the regions showing high stresses were the area beneath the acetabular dome, as well as on the superior acetabular rim. Dalstra was able to conclude that the realistic FE model accurately predicted the regions of high stress, although no statistical analysis was done to quantify the accuracy of comparison.

In order to determine the von Mises stress seen at the bone-implant interface, Thompson compared peak stresses seen for three interface conditions in both the cortical and trabecular bone surrounding the implant. Peak von Mises stresses ranging from 7.3 to 11.1 MPa were seen in the trabecular bone. It was determined that in the cases of unbonded contact, the amount of friction at the interface had a large influence on the failure rate of trabecular bone, with the lower coefficient of friction resulting in a much higher rate of failure. In cortical bone, a peak stress of 71 MPa was seen, with the greatest amount of stress being seen in the region of the anterior superior iliac spine. In contrast, low stresses were seen near the sciatic notch and the pubic bone. Unlike stresses seen in the trabecular bone, the amount of friction at the interface had little influence on the stresses experienced by the cortical bone.

3.2.4 Determination of Implant Micromotion following THR

Recently, advances in image processing have made the characterization and study of such models much more accurate. With these more accurate models, it is possible to use CT image data to generate and study a realistic 3D model of the human pelvis which include both cortical and trabecular bone (Simonian et al., 1997). Because finite element analysis is able to solve problems with complex geometries with a great

accuracy, it is well suited to determine study the effect that different loading conditions have on the micromotion of an acetabular cup used in total hip replacement after implantation.

For example, Hsu et al. effectively used finite element analysis to study the resulting micromotion at the cup-bone interface following screw fixation of the cup. Surface normal displacements were calculated in the polar and peripheral regions of the cup, and were compared to the in vitro data collected from Kwong. Hsu found that micromotion of the acetabular cup is reduced as the number of stabilization screws is increased. Additionally, it was concluded that the micromotion calculated at the peripheral region of the cup were larger than that found in the polar region. Peak micromotion values were found under the loading conditions which mimicked downstairs climbing, and in some cases, reached as high as 221.7 microns. Such studies have allowed for various loading conditions and coefficients of friction to be subjected upon the model in order to determine at which conditions minimal motion occurs (Hsu et al., 2007).

3.3 Patient specific or CT-based finite element model development

The process by which the finite element model was created is outlined and detailed in the flowchart shown in Figure 40.

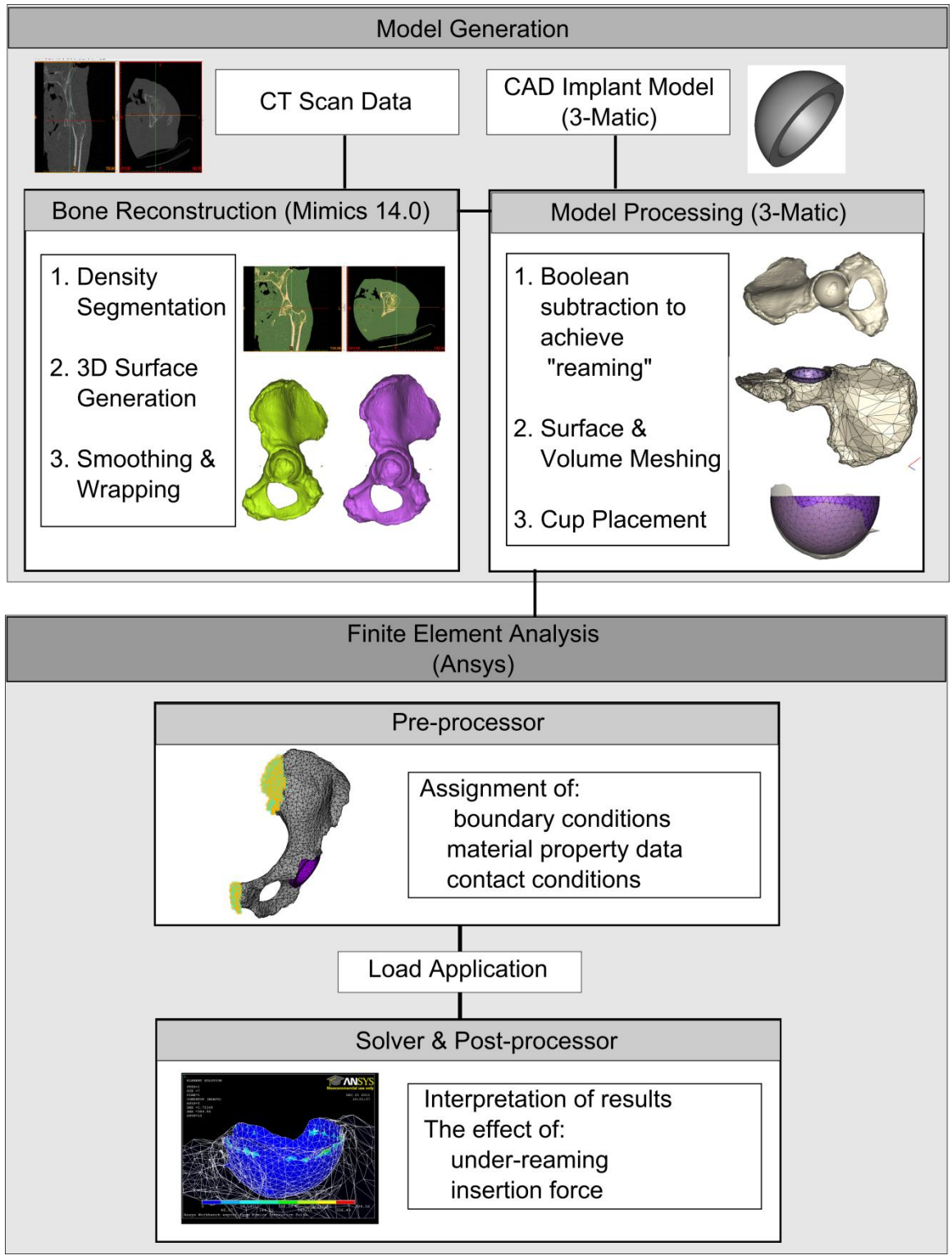

Figure XLI. Development of a patient specific three dimensional finite element model.

In order to construct a finite element model of the hip joint following THR, the geometry of the pelvis and acetabulum were required. Additional factors that must be considered include the material properties of the bone as well as the implant, refinement of the constructed mesh, an accurate definition of the bone-cup interface, and the application of contact or loading forces.

3.3.1. Acetabular Cup Design

Mimics was used to generate a CAD (computer aided design) three-dimensional model of the acetabular cup using actual cup dimensions supplied for the Depuy PINNACLE acetabular cup component, as shown in Figure 41. While acetabular cup components are available in a variety of shapes and sizes, the cup modeled for the purposes of this study represents the geometry of the specific cup used in the biomechanical testing. The cup used in this experiment was a hole-less cup which was hemispherical in shape. While the model represents the geometry of the real acetabular cup, minor details such as the surface roughness have been omitted in order to simplify the model without compromising the surface integrity.

DePuy PINNACLE Cup CAD Reconstruction of Acetabular Cup

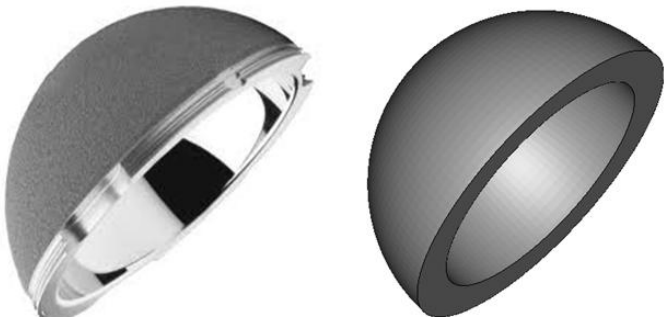

Figure XLII. DePuy PINNACLE acetabular cup and CAD reconstruction.

3.3.2. 3D Pelvis Computer Model Generation

Computed Tomography (CT) scans were conducted on the hip joint in order to obtain images in the Digital Imaging and Communications Medicine (DICOM) format. In the medical field, DICOM is regarded as the standard for handling, storing, printing, and transferring information obtained through medical imaging. DICOM format dictates that patient information, including name and patient ID is embedded into the data sets. This eliminates the potential for error that could arise if the image were separated from the patient information. DICOM data sets also include image pixel data, which corresponds to a single image. However, this attribute may allow for storage of multi-frame data, so that the image may be seen in multiple views. Together, these 2D images stack together to make up the 3D image of the object. The DICOM images are composed of pixels with varying shades of gray intensity, which correspond to different structures, including tendons, soft tissue, cortical and trabecular bone, and cartilage.

The three-dimensional patient-specific reconstruction was developed from CT scans to further explain the results of biomechanical testing and to create a full reconstruction of the intact hemi-pelvis, a reconstruction of the reaming process, as well as the initial and final positions of the implant cup, CT scans were taken prior to and after biomechanical testing of the cup inserted during THR of a single cadaveric specimen.

Diagnostic images attained through a CT scan using a BrightSpeed (GE Medical Systems) scanner (slice thickness of 0.625 mm, pixel size of 0.422 mm, field view of 216 mm) were taken of the complete hemi-pelvis from an 85 year old female prior to cup implantation in order to develop a 3D reconstruction of the intact hemi-pelvis

geometry unaltered by the presence of the titanium acetabular cup. An additional CT scan conducted after biomechanical testing was used to create a 3D reconstruction of the final geometry of the bone and cup.

Using the software Mimics Innovation Suite (Materialise Mimics, Belgium), thresholding as utilized to effectively separate the components of the CT scan based on their local bone mineral densities in order to construct the masks needed for the 3D reconstruction of the hemi-pelvis. Thresholding was based on Hounsfield units to effectively separate both the cortical and trabecular bone from any surrounding tissue, and in the case of the tested specimen, the acetabular cup as well. Masks consisting of the cortical and trabecular bone were selecting using the ranges of 500-3071 HU (Lim et al., 2012; Hoiseth et al., 1990) and 100-499 HU (Hoiseth et al., 1990), respectively. Further manual thresholding was done to reduce residual noise within the two bone interfaces. Lastly, the cavity fill tool was used to eliminate voids between pixels within the mask space. The final density segmentation for the intact hemi-pelvis and the tested hemi-pelvis with the cup in the final position after testing are shown in Figure 42 and 43 respectively.

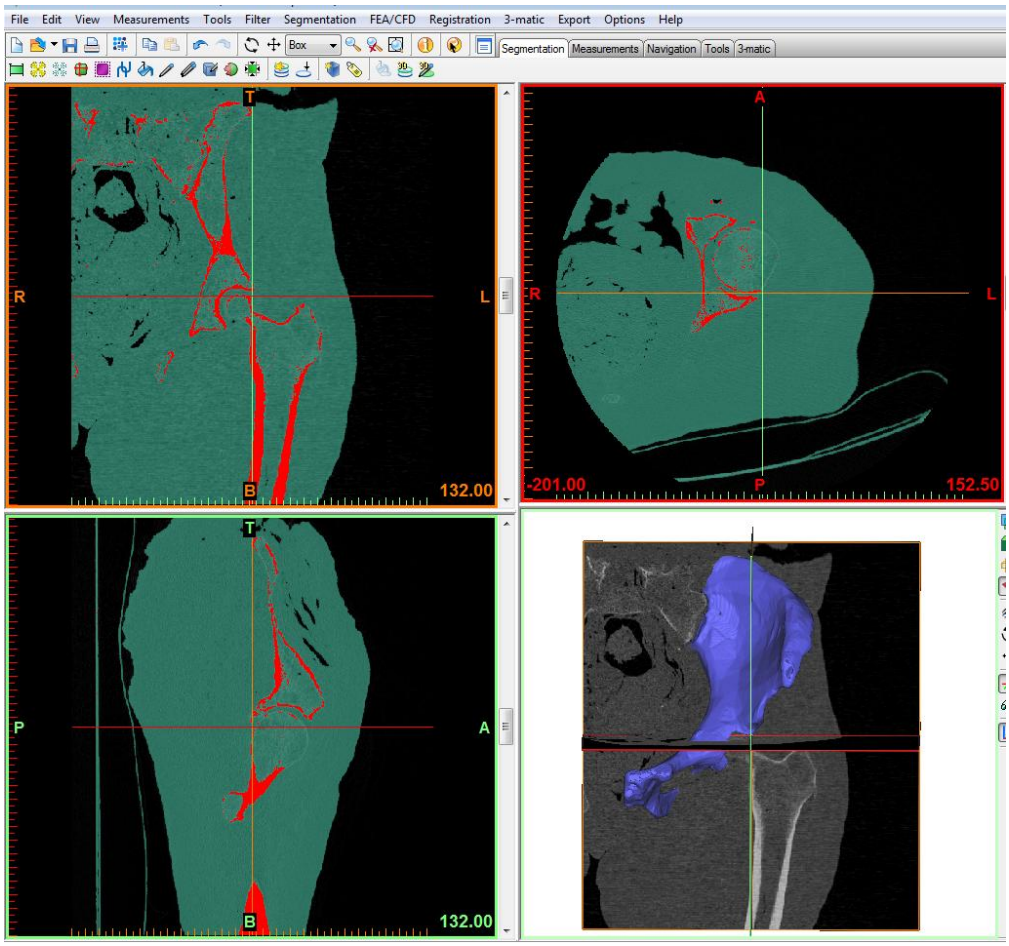

Figure XLIII. High resolution CT scan of the intact hemi-pelvis. Cortical and cancellous bone mask surfaces are automatically generated using density segmentation in Mimics.

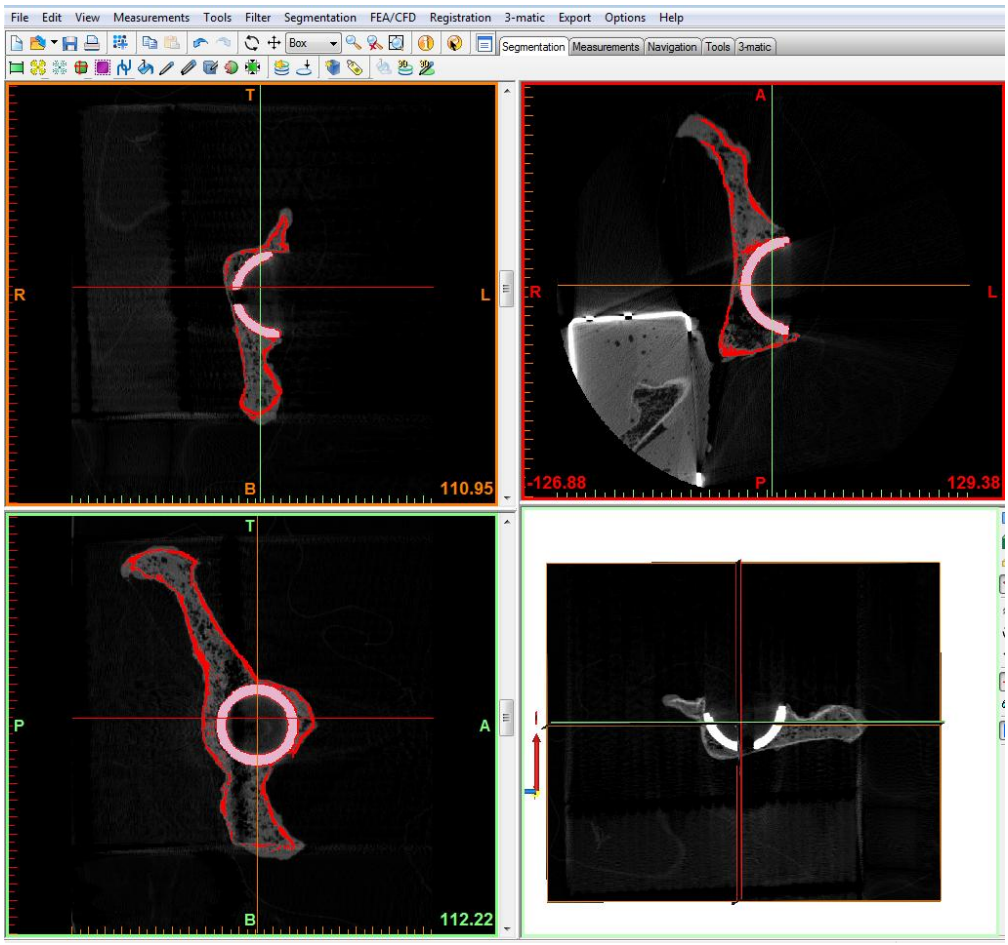

Figure XLIV. High resolution CT scan of the hemi-pelvis following acetabular cup implantation and mechanical testing. Cortical bone and acetabular cup mask surfaces are automatically generated using density segmentation in Mimics.

Each mask was then used to generate a separate 3D reconstruction for both the intact bone, as well as the tested bone with the cup in the final position. The wrap function in Mimics with a closing gap distance of 1.03 mm was used in order to close any remaining small holes or inclusions within the object. The smoothing function was also used to further smooth the surface of the object. The smooth factor was set to 0.4 and 1.0 iteration in order for a suitable model to result. Surface modification can be

through wrapping and smoothing functions is detailed in Figure 44. Finally, the wrapped and smoothed cortical bone reconstruction was exported to 3-Matic (Materialise Mimics, Belgium) for further refinement and the creation of a tetrahedral volume mesh.

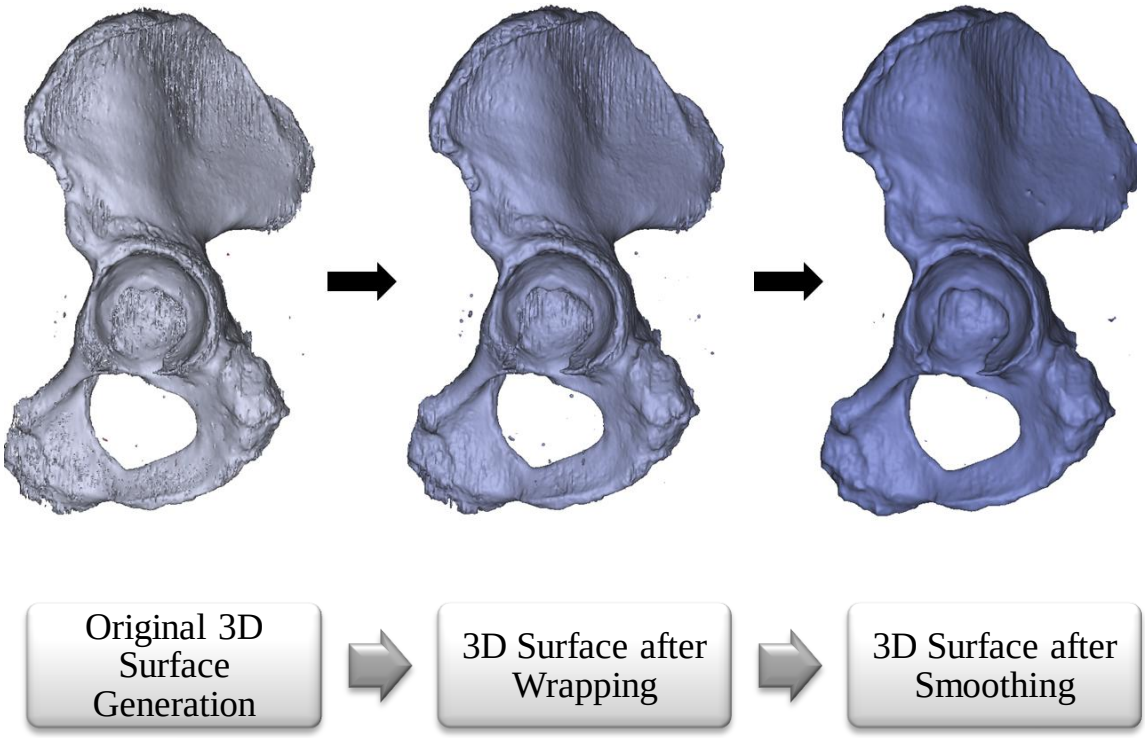

Figure XLV.3D Surface generation of the intact hemi-pelvis.

The 3D surfaces of both the intact hemi-pelvis and the tested hemi-pelvis with the acetabular cup were imported into 3-matic 6.0. The 3D reconstruction from the tested CT scan was used to have an understanding of the position of the cup after testing. The relative position of the cup prior to testing and after cup implantation in

relation to the unaltered reconstruction was obtained by relocating the cup to a position dictated through values obtained from the LVDT sensors, taking into account the permanent deformation recorded at the end of the experiment. Using the established reference system, care was taken to accurately choose nodes representing the location of the LVDT sensors used during the experiment. The position of the cup at this stage represents the location of the cup in the in-vitro experiment after cup insertion but before any post-operative load has been applied. The polar gap distance between the apex of the cup and the floor of the reamed acetabulum was measured on the reconstruction and determined to be 0.681 mm (Figure 45).

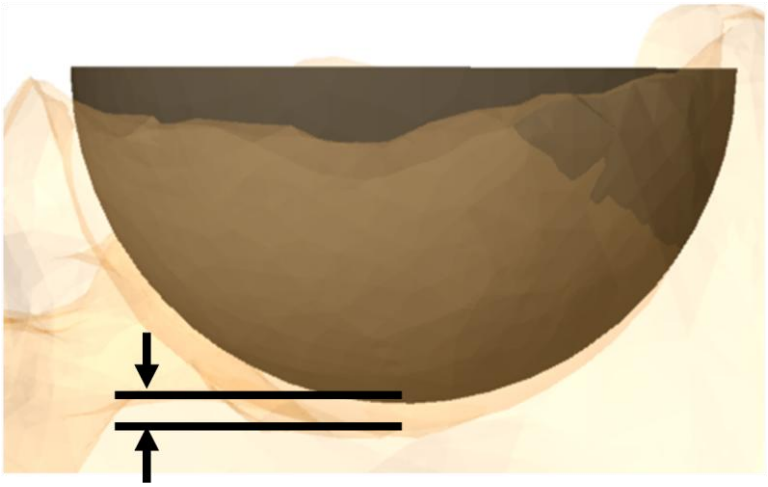

Figure XLVI. Polar Gap Distance between the apex of the acetabular cup and the floor of the acetabulum following cup insertion.

Assuming that the acetabular floor of the model reconstructed from the tested specimen was unaltered by cup insertion, a best fit sphere was created using points located in this region, and used to ream the acetabulum of the intact bone, shown in Figure 46.

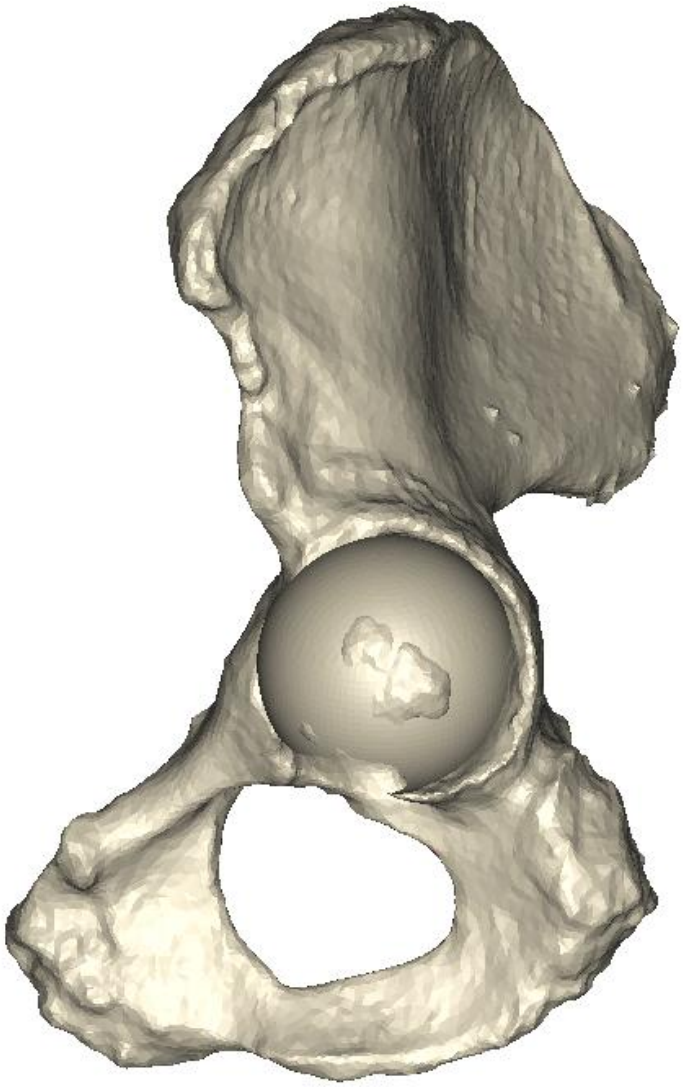

Figure XLVII. 3D Reconstruction of the intact model following reaming.

3.2.3 Meshing and Cup Insertion

As part of the Materialize Mimics Innovation Suite, 3-matic allows for complex computer aided design of 3D anatomical data. An initial triangular mesh was created following importation of the 3D model into 3-matic. Following triangle reduction, which was used to reduce the number of the mesh elements, the Auto Remesh tool was used to remesh the model using a triangle edge length of 4 mm and a maximal geometrical error of 0.15. This tool is useful because triangles with a lower height/base ratio are considered low quality and result in a less accurate model. Therefore, a finer mesh was used at the interface surface near the acetabular cup, while a less refined mesh was utilized in distant areas of bone. A surface consisting of a large number of elements is considered optimal because it results in the most accurate surface mesh. Once the optimal surface mesh was achieved, a tetrahedral volume mesh of the model was created using the surface mesh. The final mesh is shown in Figure 47.

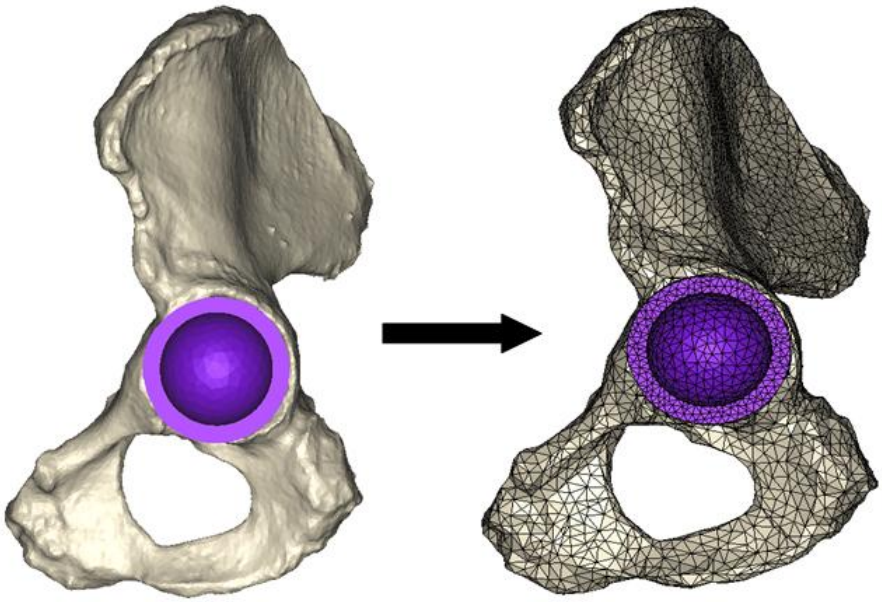

Figure XLVIII. 3D reconstruction before and after meshing of the reamed and intact hemi-pelvis with cup in the equilibrium position.

Finally, in order to achieve a possible hammering/implantation distance, an initial displacement was imposed on the cup using the tangency method between the cup and reamed bone in the 3D reconstruction. The initial position of the cup was obtained moving the cup along a line of action perpendicular to the plane of the cup rim until minimal contact was achieved between the cup and acetabular wall. As such, the initial polar gap distance before implantation between the apex of the cup and the floor of the reamed acetabulum was 1.606 mm (Figure 48).

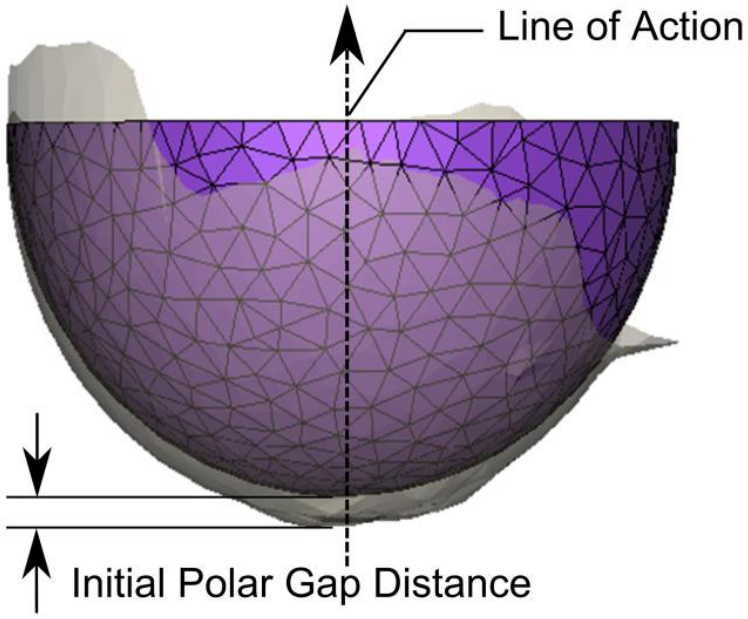

Figure XLIX. A close-up image of the cup bone interface showing the initial polar gap distance between the apex of the cup and the floor of the reamed acetabulum before cup insertion.

3.4 Finite Element Analysis using Ansys

3.4.1 Geometrical Description of Model and Material Properties

The 10,940 element (3,466 node) model of the hemi-pelvis, along with the 3,466 element (865 node) model of the acetabular cup was imported into Ansys. All materials were assumed to be linear elastic and with material properties shown in Table 19. Separately, the cortical and cancellous bone were assumed to be isotropic materials. The elements of the hemi-pelvis as well as the acetabular cup were modeled as Solid72 element types.

Table XIX. Finite Element Model Properties.

Component	Young's Modulus (MPa)	Poisson's ratio
Cortical Bone	17[1]	0.3[1]
Cancellous Bone	.07[1]	0.31[1]
Subchondral Bone	2[2]	0.3[2]
Acetabular Cup	110[2]	0.3[2]

[1] (Barreto and Folgado, 2010)
[2] (Cilinger et al., 2007)

3.4.2 Definition of Element Types

Three different element types were used in the creation of this finite element model: Solid52, Conta174, and Target170. A brief description follows.

The Solid72 element type is a 3D 4 node tetrahedral structural solid, and is commonly used for irregular meshes. This element type allows for a total of 6 degrees of freedom, with translation, as well as rotation in x, y, and z. The input data for this element type include the nodal locations, material properties, and loading information. Additionally, not used in this model, pressures may be applied as a surface element load and temperatures may be input as body loads located at the nodes.

The Conta174 element is used as the contact surface of the deformable surface between two 3D surfaces in contact. This element type is meant to represent the actual contact and sliding between the two surfaces, and is located on the surface of a 3D solid or shell element. This element type takes on the same geometric characteristics of

the element type to which is it connected. Additionally, Conta174 allows for both isotropic and orthotropic friction between the two surfaces in contact. Both the target and contact surfaces are identified with a shared real contact set between the two surfaces. Triangular elements are defined with corner nodes I, J, and K, with duplicate nodes L and O for prism elements. Nodes M, N, and P are created at the midpoints between connecting nodes. Three degrees of freedom are allowed at each node, with translation in the x, y and z directions.

The element type Target170 is used to represent the surface in contact with a given contact element. For 3D surface segments represented by a target element, triangle and quadrilateral segment types are orders in such a way that right hand rule defines the outward normal to the target surface. The corner nodes are represented by I, J, and K.

3.4.3 Bone-Implant Contact Interface

In order to model the interface between the acetabulum and the implant cup, a contact set was implemented so that load could effectively be transferred between the two bodies. In doing so, certain parameters were considered. The contact method chosen was a nonlinear, asymmetric, frictional, surface-to-surface contact model. In general, there are three approaches to modeling the contact detection. The method chosen in this case was the Gauss Integration point system. In this method, one of the two bodies in contact is considered the contact surface, which is usually a deformable solid, while the other is the rigid body target surface, as shown in Figure 49. Additionally, the contact algorithm chosen is the augmented Lagrange method, which utilizes an iterative method in order to determine the exact Lagrange multipliers. The

integration points, or contact detection points, are located on either nodal points or Gauss points. The contact elements on the target surface are constrained to resist penetration at the integration points, thereby making it a rigid solid.

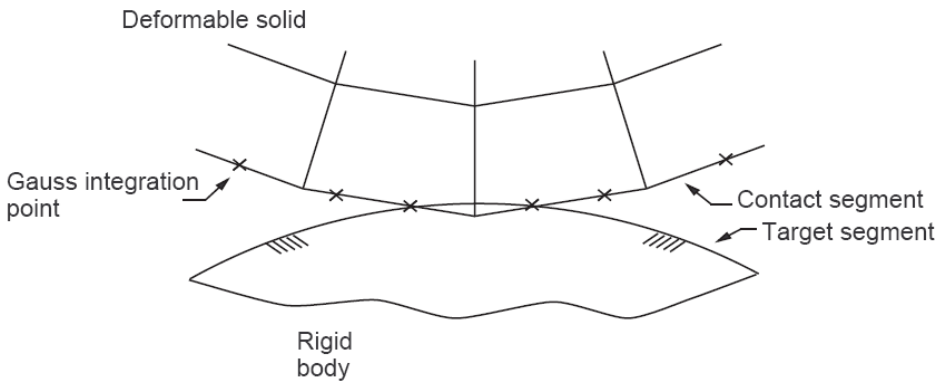

Figure L. Gauss Integration Contact Method (Stolarski et al., 2006).

The contact model constructed for this study consists of the titanium acetabular cup as the rigid target surface (Targe170) and the surrounding bone as the flexible contact body (Conta172). The cup can be considered rigid because the high elastic modulus that it exhibits makes it considerably stronger in comparison to the surrounding bone, regardless of loading magnitude. In comparison, the viscoelastic nature of the bone makes it a suitable contact surface because under extremely high loads, the surrounding bone may deform considerably. The coefficient of friction between the target and contact surfaces was 0.5 to represent the interface between the

Hydroxyapatite coated titanium acetabular cup and the reamed acetabulum in the absence of lubrication.

3.4.4 Boundary Conditions

In order to mimic the conditions of the mechanical testing conducted on each hemi-pelvis, the iliac crest and a portion of the ilium, as well as the ischium were constrained in all directions (UX=UY=UZ=0) to avoid translational movement of the bone, and to mimic the setup of the biomechanical testing, as shown in Figure 50.

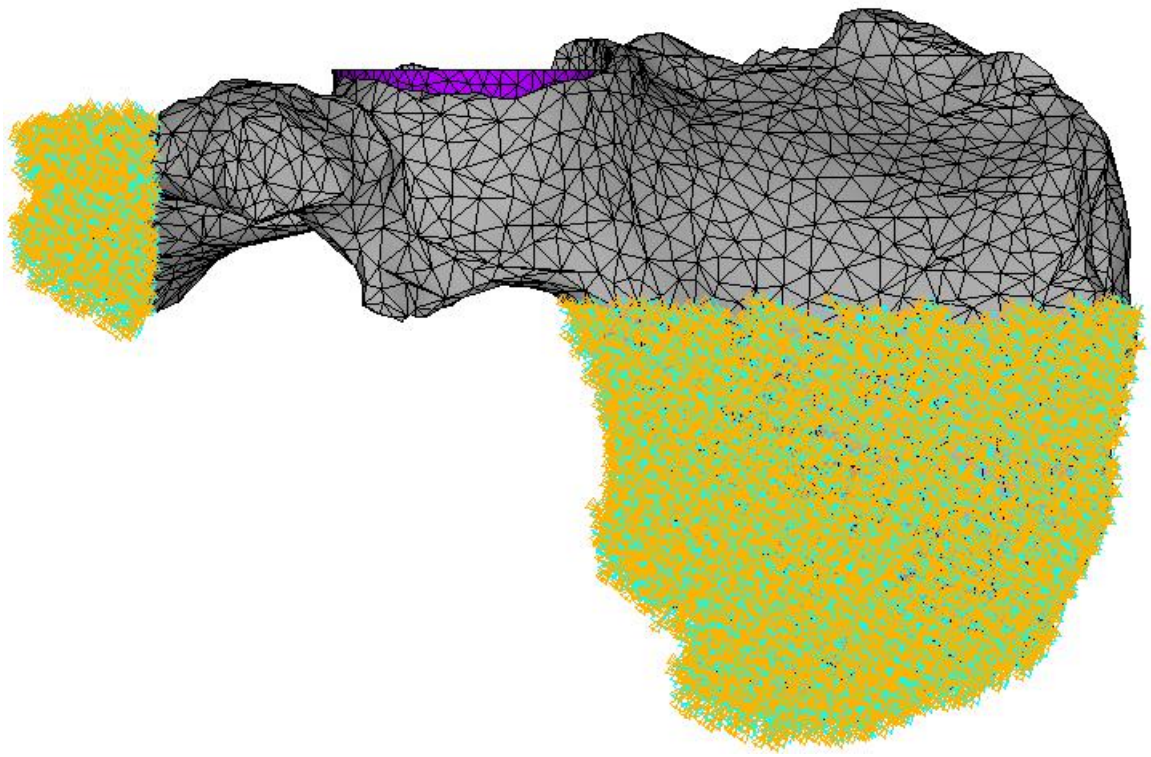

Figure LI. Boundary constraints of the hemi-pelvis with the ilium and a portion of the ischium fully constrained.

3.5 Parameter Fitting Characterization and Model Validation

A parameter fitting method was utilized to optimize the imposed hammering distance during insertion for the model such that it accurately represented the in-vitro experiment. The entire process for model parameter fitting and validation is shown in Figure 51.

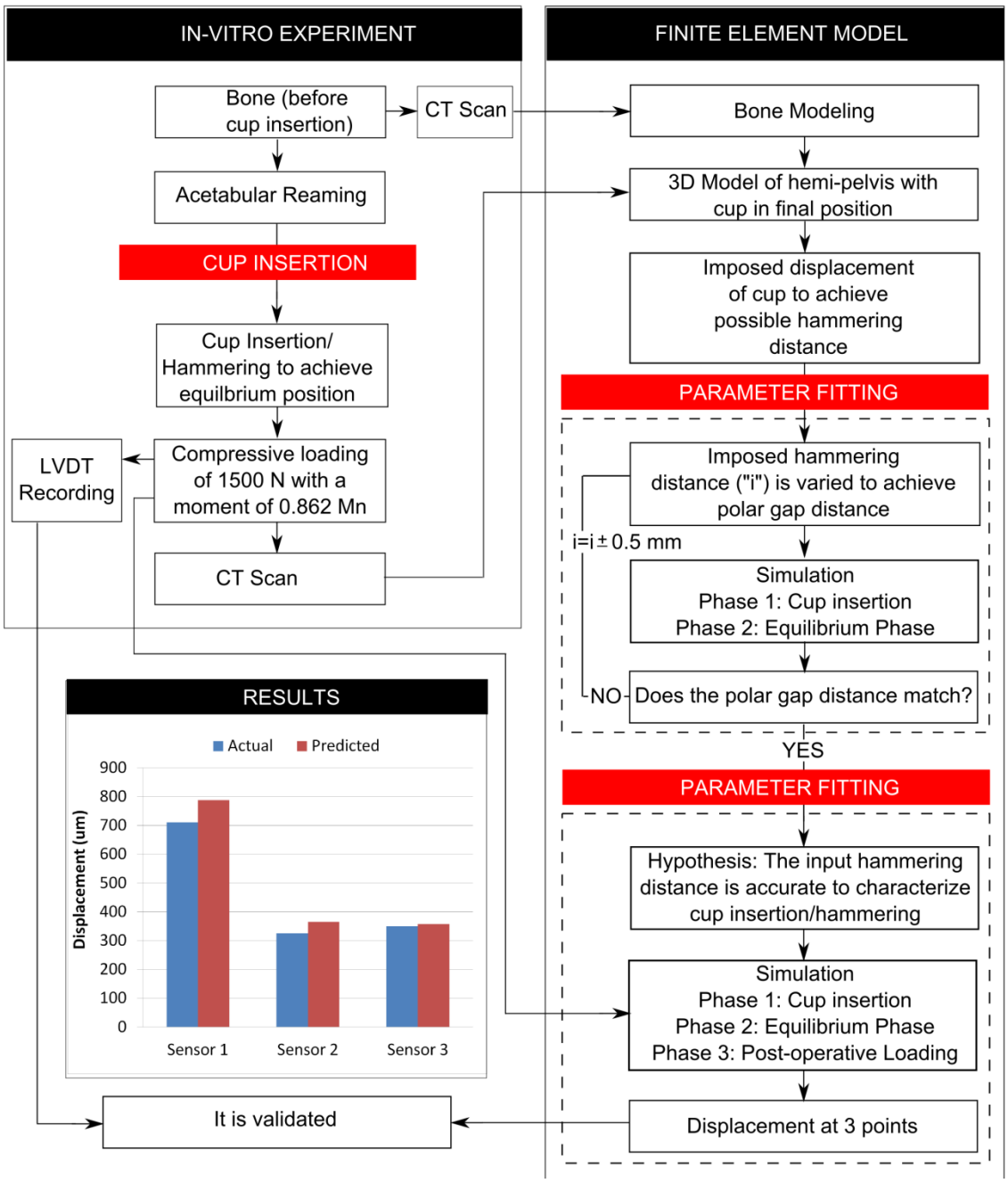

Figure LII. Algorithm for the process of parameter fitting and model validation.

3.5.1 Simulation of Cup Insertion

In reality, the press-fit insertion of acetabular cups requires multiple blows to an impactor through a mallet until the cup is fully inserted into the acetabular cavity. Few studies have been conducted on the peak forces seen during cup insertion or the duration of each blow by the mallet. One study showed that the average impaction force was needed to fully seat a press-fit acetaulbar cup into artificial bone was 7.5 kN when inserted with a surgical hammer, and as high was 7.9 kN when the same experiement was carried out with a dynamic testing machine which applied increased loadings in a cylic motion (Fritsche et al., 2010). In another study, over-sized cups were press-fit inserted using a pre-programmed loading sequence which applied mutliple cyclic laods at sequentially increasing magnitudes up to 3 kN until the cup was determiend to be fullly implanted (Kim et al., 1995). Achieving a fully accurate representation of cup insertion based on the impaction force, duration of each blow, and the number of blows would be difficult in this study. Rather, the press-fit insertion of the cup into the acetabular cavity was modeled in two phases.

Input values of imposed hammering distances to the cup were sequentially varied to achieve the polar gap distance from the in-vitro experiment. The iliac crest and a portion of the ilium were constrained in all directions to mimic the conditions of the mechanical testing and to avoid translational movement of the bone. The simulation was done in two load step phases, the first of which mimicked cup insertion/hammering due to imposed hammering distance. The boundary conditions on the cup were such that it was allowed freedom of movement in only the direction it was to be displaced. In the second phase, all boundary conditions were removed from the cup, at which point

the cup was able to rebound and adjust to an optimal conformity, finding the equilibrium position. The location of the cup at the end of the second load step was regarded as the equilibrium position of the cup following press-fit implantation.

The mathematical model was run, varying the imposed hammering distance until the predicted polar gap distance matched the polar gap distance from the in-vitro experiment with less than 2.0% error. The chosen imposed displacement to achieve near the measured polar gap distance was 1.55 mm, which achieved a polar gap distance of 0.691 mm (Table 20).

Table XX. Actual and predicted gap distances for parameter fitting of model.

Imposed Hammering Distance (mm)	Actual Gap Distance (mm)	Predicted Gap Distance (mm)	Percent Error
1.5	0.681	0.43326	36%
1.55	0.681	0.69114	1%
1.6	0.681	0.7135	5%
1.65	0.681	0.60743	11%

3.5.2 Simulation of Cup Loading

Following parameter fitting of the imposed hammering distance to accurately predict the equilibrium polar gap distance, the model was validated using the micromotion values of three nodes located in the same position as Sensors 1, 2, and 3 from the in-vitro experiment. Care was taken to select nodes located in the same position as the sensors using the reference system that was previously described.

Validation was conducted in three load step phases. The first two load steps mimicked the insertion and equilibrium phases, respectively. In the third and final load step, a compressive load from 0 N to1500 N along the z-axis and a moment arm of 30.38 mm was placed on the cup, as in the in-vitro experiment.

3.5.3 Validation of the Pelvis-Cup Finite Element Model

Displacement values were calculated at three nodes located in the same location as LVDT sensors from the experiment. Using the reference system eastlibahsed in Chapter 4, care was taken to accurately select three nodes located in the same position as the sensors from in in-vitro experiment. These values were compared to the displacement values of the biomechanical testing in order to validate the finite element model for loading from 0 to 1500 N. The final values of cup displacement at 1500 N of the three nodal points representing sensors 1, 2 and 3 were predicted with a percent error of 11%, 12%, and 2%, respectively (Table 21).Throughout loading, the predicted values of micromotion matched the actual values with about 20% error or less (Figure 52).

Table XXI. Comparison of actual and predicted values of displacement for loading from 0 to 1500 N for model validation.

Sensor	Predicted	Actual	Percent Error
Sensor 1	788.445	710.13	11%
Sensor 2	279.73	325.56	14%
Sensor 3	375.66	350.12	7%

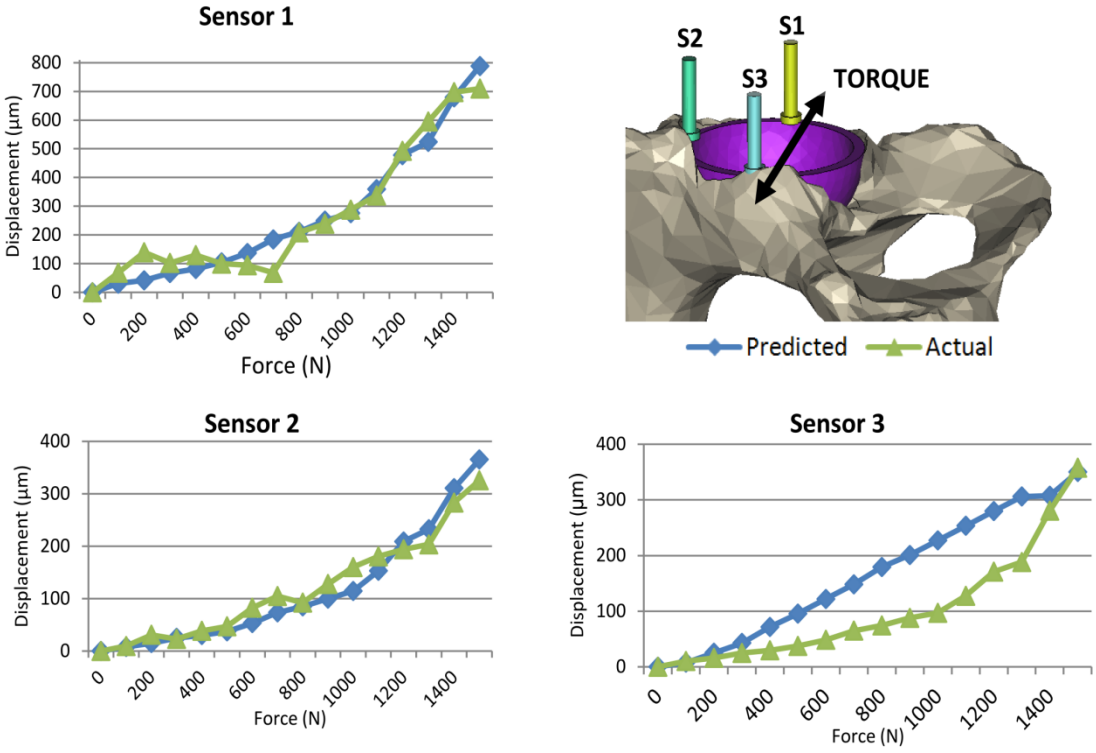

Figure LIII. Comparison of predicted and actual values from 0 to 1500 N of loading for model validation.

3.6 Factors Influencing Initial Cup Stability in Total Hip Arthroplasty

3.6.1 Objective

In THR, the permanent fixation and final position of the cup is a function of several parameters: the amount of under-reaming, offset impact force to insert the cup and allowable micro-motion due to post-operative loads within the first weeks following surgery. This study aims to quantify the effect of each parameter on the contact at the bone-implant interface, as well as the correlation to implant stability. This chapter

details the process by which the complete geometry of the hip joint, as well as the acetabular cup implanting during THR, and how the influencing factors affect this procedure.

3.6.2 Sensitivity Analysis of the Finite Element Model

The 3D finite element model construction was previously described in this chapter. Following model validation, the influence of varying input parameters and the effect each has on stresses, surface conformity, polar gap distance, and micromotion at the interface was evaluated. Three load steps were used to mimic the press-fit insertion, equilibrium, and loading phases. The nodes at the pubic symphysis and the sacro-iliac joint were constrained in all degrees of freedom to simulate in-vivo conditions at each step (Figure 53). Various configurations were run as the first load step to account for 1 and 2 mm of under-reaming for press-fit insertion with varying hammering distance depths in order to achieve different amounts of contact at the cup-bone interface. During the second load step, constraints were removed from the cup to allow for equilibrium, and during the third load step, a force of 1500 N was applied to the cup to mimic post-operative loading.

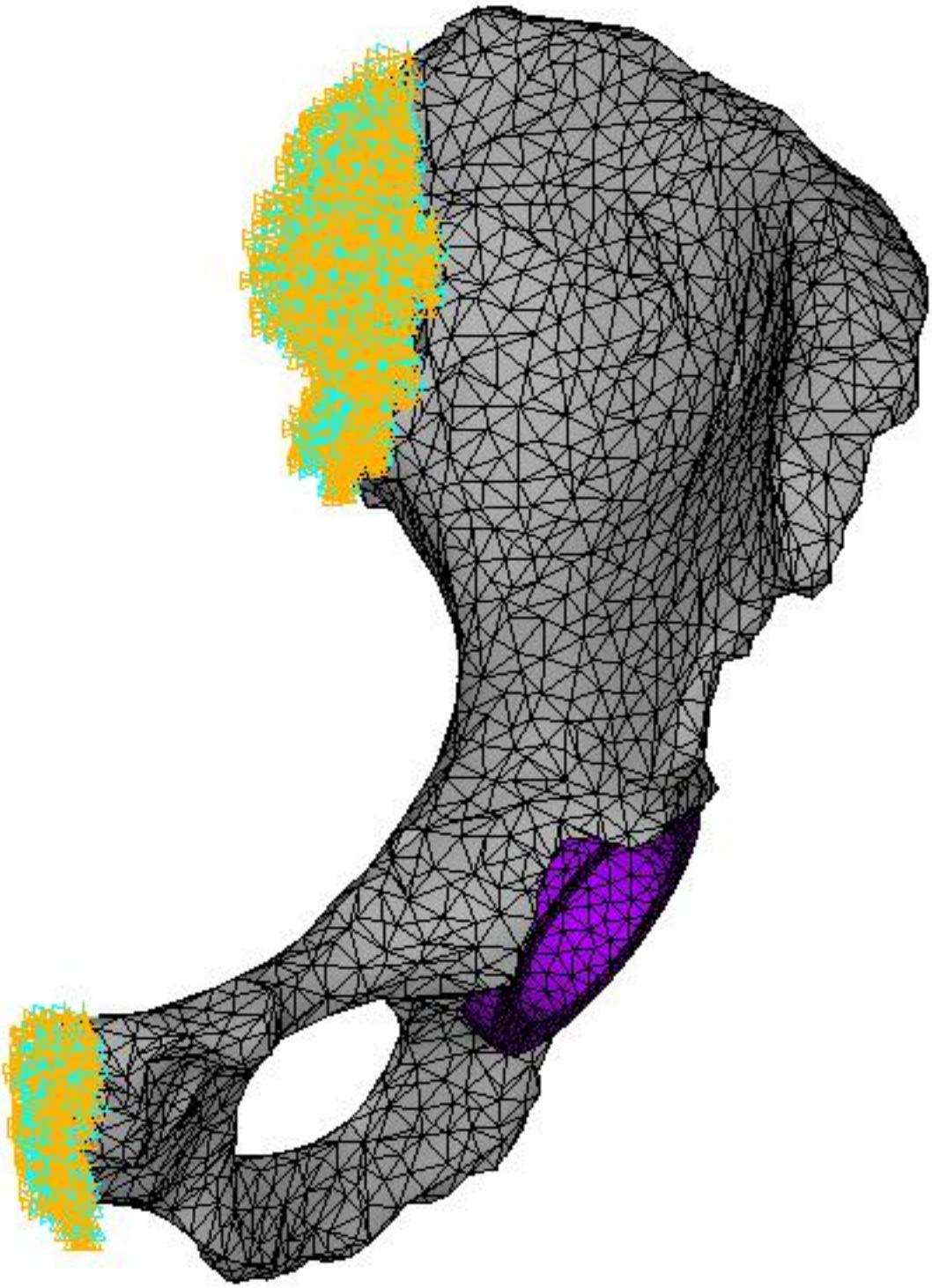

Figure LIV. Finite element model of the hemi-pelvis with constraints at the pubic symphysis and the sacro-iliac

3.6.3 Results

3.6.3.1 Analysis of the Cup Insertion Force During THR

Following the first phase of cup insertion, the reaction force of the cup due to inertion was evaulated in order to eventually determine the influence of the force needed to insert under-reamed cups set to varying target locations, as specified by the hammering distance imposed on each cup. The aim is to determine which configuration a minaml force can be used to eastablish a stable contact at the cup-bone interface. The results show that reaction force increases as a function of the amount of under-reaming, as well as increasing target insertion distances (Figure 54). The average insertion force was approximately 10.4 kN±3.9kN, which is on the same order of magnitude as seen in literature. Considering the fact that this study assumes the cup to be in place following just one pulse of force application, while the others assumed full cup insertion following multiple pulses of increasing force, the forces needed to insert the cup predicted in this study within the same range of magnitude.

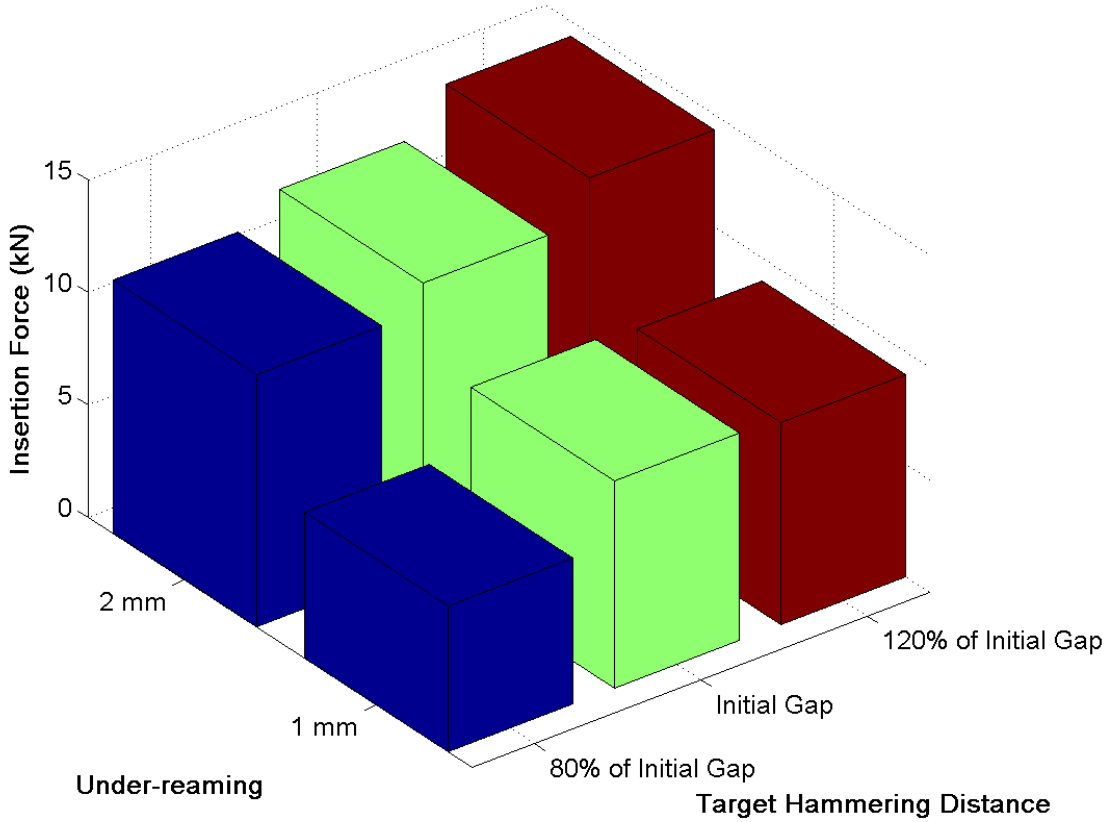

Figure LV. Insertion force as a function of under-reaming and the target hammering distance for cup insertion.

3.6.3.2 Interface Stresses as a Result of Under-reaming and Hammering Force

The distribution of total stress on the acetabulum at the cup-bone interface immediately following cup insertion is presented for various amounts of hammering force used to press-fit insert the cup (Figure 55). Total stress is a measure of the sum of the contact pressure and the contact sliding stress at the interface. The distribution of total stress of the bone at the contact interface with the acetabular cup was calculated as a percentage based on the total number of elements at the interface. For each

configuration, higher stresses were present on the bone around the peripheral rim of the acetabular cup, with the highest stresses noted at the superior region of the acetabular wall. In the cases presented with 1 mm of under-reaming, 95% of elements at the interface experienced a stress less than 20 MPa, with no elements exceeding a stress of 220 MPa. Under-reaming by 2 mm resulted in 92% of elements predicted stress less than 20 MPa, with just 0.17% of elements predicting a small region of peak stress greater than 220 MPa, which approached the upper range of yield strength for bone, which is 167-210 MPa.[33] Because a stress ranging from 0 to 55 MPa was predicted by greater than 95% of elements at the interface, we are able to conclude that the contact at the interface is nearly homogenous.

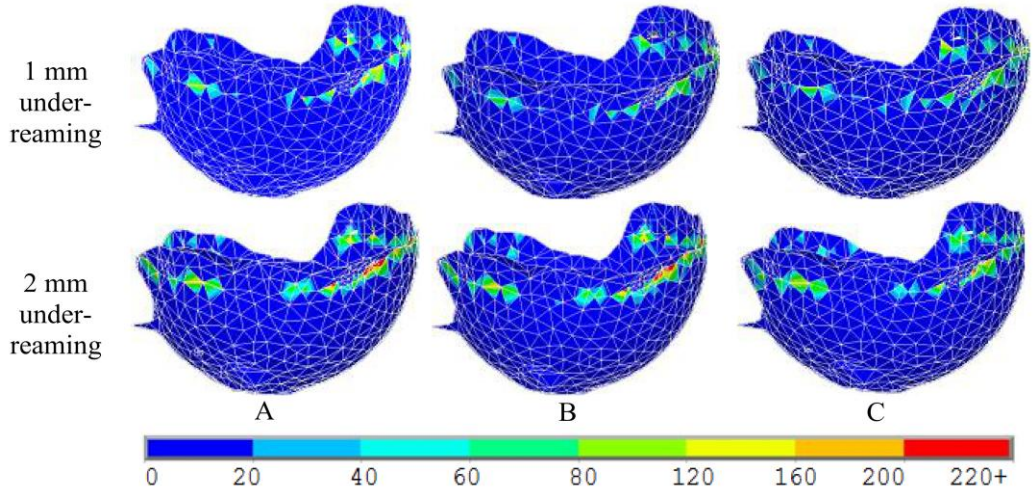

Figure LVI. Total stress (MPa) on the acetabular wall at the cup-bone interface for 1 and 2 mm of under-reaming during (a) cup insertion (b) cup equilibrium, and (c) loading.

3.6.3.3 von Mises Stresses as a Result of Under-reaming and Hammering Force

The distribution of von Mises stress at the aceabulum as well as the entire hemi-pelvis was predicted following press-fit insertion of the cup for various configuriations. High streses were predicted in the superior region of the acetabular wall, as well as a portion of the ischium. For press-fit insertion with 2 mm of under-reaming, high von Mises stress values were predicted compared with 1 mm of under-reaming, but with the same general distribution around the acetabular wall. The results suggest that because the greater than 90% of elements predicted a stress ranging from 0 to 55 MPa, with just a small region of higher predicted stress exceeding the elastic range of bone, fracture of the acetaublar wall will not occur during cup insertion or loading.

3.6.3.4 Surface Conformity at the Cup-Bone Interface

In order to evaluate the surface conformity at the cup-bone interface, the percentage of nodes with a contact penetration depth of less than 0.1E-6 at the interface was calculated at the end of each load step. It is interesting to note that despite the degree of under-reaming, the hammering distance - and therefore the impaction force - needed to press-fit the cup had a greater influence on the amount of surface conformity at the interface. Increasing the hammering force by just 2500 N resulted in approximately a 10% increase in the surface in contact at the interface for 1 mm of under-reaming. Under-reaming by 2 mm achieve only a slight increase in good surface conformity immediately following cup insertion.

An adjustment of the conformity of the peripheral bone of the acetabular wall due to over-sized cup insertion was observed. It was assumed that the bone at the floor of the reamed acetaubulum reamined largely unaffected by cup insertion. Therefore, the

acetabular cavity became more ovular in shape. Gap distances at the apex of the cup and the nearest point of the floor of the reamed acetabulum were also compared and are representative of the results of clinical cases, in which polar gap distances of 0.5 mm were reported following the implantation of press-fit cups. A comparison between percent of surface contact, polar gap distance and hammering distance is shown in Figure 56.

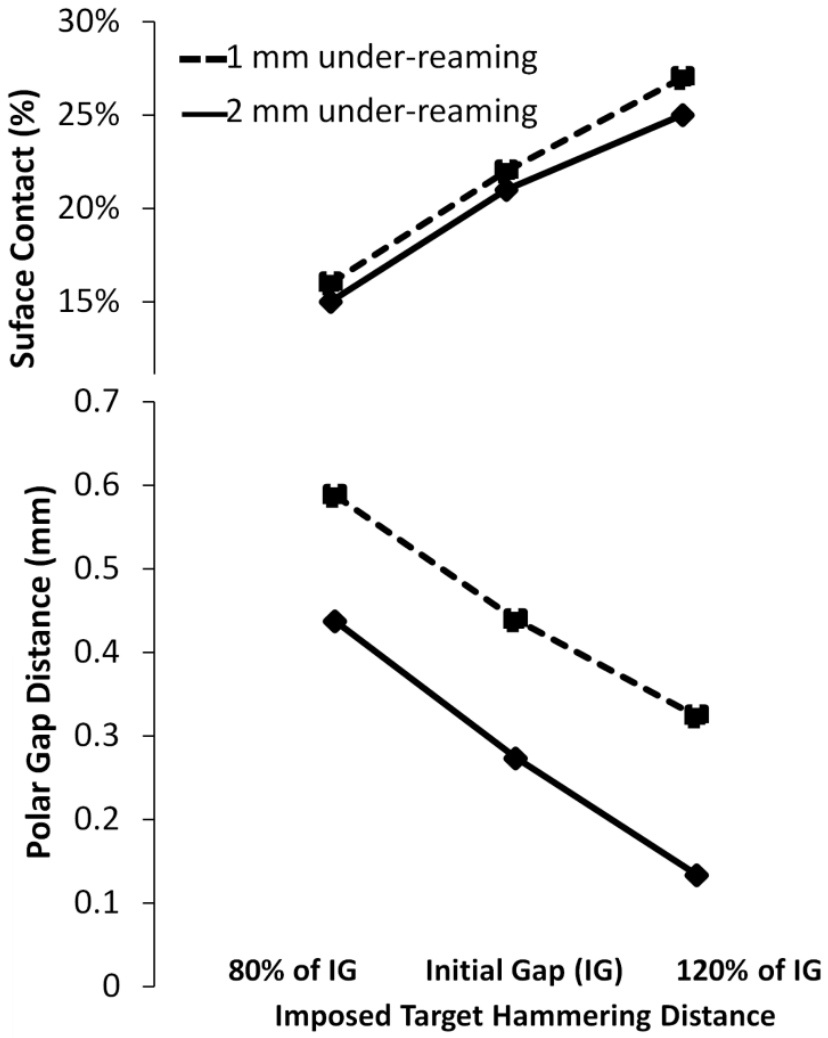

Figure LVII. Percent of contact surface at cup-bone interface during cup insertion and polar gap distance between apex of cup and floor of reamed acetabulum during cup insertion as a function of hammering distance due to input target penetration depth.

During the second phase, the cup was allowed to relax into an equilibrium position, at which point a more uniform percentage of surface contact that the interface was achieved, despite the hammering force used to insertion the cup (Table 22). For 1 mm of under-reaming, the difference between the surfaces in contact at the itnerface for

two extremes of cup insertion differed by only 6%, rather than the 10% difference seen immediately following cup insertion. Between the first and second phases of cup insertion, the percentage of surface in contact decreased by an average of 3%. In addition to a decease in surface confmirty during the equilibrium phase, the gap distance at the apex of the cup almost doubled, despite hammering force or amount of under-reaming. Following cup loading up to 1500 N, a slight decrease in the percentage of surface contact and increase in gap distance at the apex of the cup was observed. However, during cup loading, the percentage of surface in contact at the interface decreased by an average of just 1%, indicating that the cup and bone maintained a stable fixation during loading.

Table XXII. Percentage of Surface Contact at the cup-bone interface for cup insertion, cup equilibrium, and loading for 1 mm and 2 mm of under-reaming at varying target penetration depths.

Imposed Hammering Distance	Cup Insertion		Cup Equilibrium		Loading at 1500 N	
	1 mm under reaming	2 mm under reaming	1 mm under reaming	2 mm under reaming	1 mm under reaming	2 mm under reaming
80% of Initial Gap	15%	16%	14%	16%	13%	16%
Initial Gap	21%	22%	18%	19%	16%	18%
120% of Initial Gap	25%	27%	20%	20%	18%	19%

3.6.3.5 Micromotion of the acetabular cup during loading

The criterion for surface conformity at the interface was evalualted as a function of the percentage of surface contact at the interface, as well as the displacement of the

cup due to loading. The results indicate that force needed to insert the acetabular cup increases as a function of increasing percentage of surface in contact, as well as a greater amount of under-reaming (Figure 58). Conversely, displacement of the cup decreases as a function of increasing surface contact and a greater amount of under-reaming. While the movement of the cup remains relatively stable for 1 mm of under-reaming, ranging from 430 to 455 μm, a sharp decrease in displacement occurs for only a small increase in the amount of surface contact but with 2 mm of under-reaming.

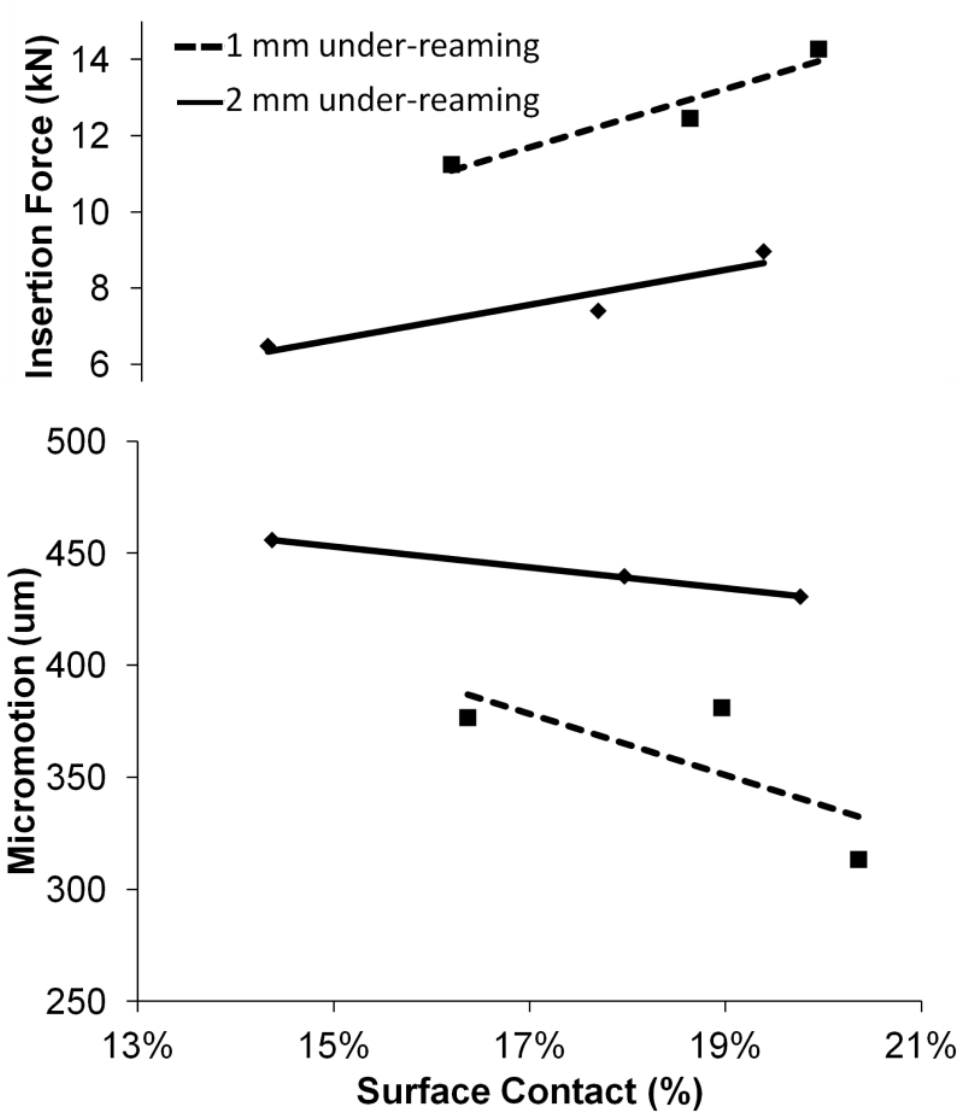

Figure LVIII. Relation between insertion force, displacement, and percentage of surface contact at 1500 N of loading for 1 and 2 mm of under-reaming.

3.6.4 Discussion

A finite element model suitable for patient specific analysis was created and validated in order to understand the behavior at the cup-bone interface following total

hip replacement. In particular, the roles of various parameters on the behavior and stability of the cup were varied and evaluated. Each clearly has a strong influence on the stability and conformity of the cup-bone interface following cup insertion and loading.

The force used to insert the acetabular cup for various imposed hammering distances was determined for two different degrees of bone under-reaming. The average insertion force was approximately 10.4 kN±3.9kN, which is on the same order of magnitude as seen in literature.

The degree of under-reaming and impaction force used for cup placement plays a significant role in the amount of surface contact and micromotion of the cup at the interface. Increased surface contact, measured by evaluating the number of nodes in contact at the interface, shows a positive correlation with increasing levels of under-reaming, as well as increasing force needed for cup insertion.

This phenomenon is visible throughout loading, and is more pronounced in the case of 2 mm of under-reaming, which shows a sharper decrease in micromotion with increasing impact force. However, it is interesting to note that approximately the same percent of surface contact can be achieved with 1 mm of under-reaming and less insertion force. For example, under-reaming by 2 mm requires an impact force 22.5% greater than the force needed to seat a cup with 1 mm under-reaming, but achieves only a 13% reduction in micromotion with nearly the same surface contact. An analysis of the polar gap observed following cup insertion can also provide important clinical relevance. The occurrence of such gaps is difficult to observe in practice, but can be easily investigated with the tools of finite element analysis. While a greater impact force

used during cup insertion results in a slightly greater amount of surface conformity at the interface, a polar gap is still present for both cases of under-reaming despite insertion force used. Furthermore, because a very high impact force would be needed to achieve full surface conformity, the stresses on the bone are likely to increase as well, which may result in fracture of the acetabular wall.

The data shows a significant correlation between the degree of under-reaming and the resulting total stress at the cup-bone interface, as well as the distribution of von Mises stress throughout the entire bone. However, while increased under-reaming results in higher stresses, especially at the interface, it is clear that greater under-reaming also results in a more rigid fixation between the cup and bone. The results suggest that because greater than 90% of elements predicted a stress ranging from 0 to 55 MPa, with just a small region of higher predicted stress exceeding the elastic range of bone, fracture of the acetabular wall will not likely occur during cup insertion or loading. It is important to note that because the stresses seen for 2 mm of under-reaming approach the yield strength for bone in some regions, caution should be taken during cup insertion to avoid fracture of the acetabular wall, especially for increased under-reaming.

4. INITIAL CUP STABILITY FOLLOWING AUGMENTATION OF ACETABULAR DEFECT WITH KRYPTONITE BONE CEMENT IN THR

4.1 Introduction

Understanding initial cup stability is especially important in a total hip replacement done in the presence of defects on the acetabular. The stability and fixation can be compromised due to deficiencies on the posterior or anterior acetabular walls (Rees et al., 2011). A number of corrective methods for stabilizing the wall prior to cup implantation are currently in use, such as bone grafting (Goldberg, 2000) or screw fixation (Moskal et al., 2004), as discussed in Chapter 2. While the method of reconstruction is often dependant on the size of the defect, a specific set of guidelines for ideal treatment is lacking (Pprosky et al., 2002; Paprosky et al., 1999) as surgeons typically rely on experience in determining the course of reconstruction (Gross et al., 2004). Furthermore, augmentation of acetabular defects with bone grafting or screw fixation may often result in a lack of fixation at the cup-bone interface due to uneven contact at the interface (Stiehl et al., 2004).

Mechanical studies detailed in Chapter 2 demonstrate that the presence of Kryptonite at the site of the acetabular defect allowed for a successful reconstruction of the acetabular wall. The results also showed that the resulting micromotion of the cup at the interface is dependent on the amount of load at the hip joint, suggesting that the dimensions of the reconstructed defect should be patient-specific in order to provide the most stable fixation.

4.2 Objective

The aim of this research is to develop a model of the pelvis with an acetabular defect reconstruction following THR which can be used to have an understanding of initial cup stability under various geometrical and structural conditions.

4.3 Development of a Finite Element Model

Using the methodology employed in Chapter 3 to create the validated model of a healthy hemi-pelvis following THR, an additional model was constructed using CT scans taken before and after augmentation of acetabular defect from the opposite side of the hemi-pelvis of the same patient. To remain consistent with the mask segmentation for cortical and trabecular bone used in the healthy bone discussed in Chapter 3, mask segmentation was conducted using the same range of Hounsfield values.

A defect of the acetabular wall was created to mimic the acetabular defect which was imposed on the cadaveric specimen during in-vitro testing. A defect of the superior acetabular wall was created using CAD so that it was possible to simulate THR in the presence of a reconstructed acetabuar wall defect. The reconstruction system consists of three bone screws inserted into the trabecular bone at the site of the defect with a Kryptonite bone cement wall reconstructed over the screws and surrounding bone to create a reinforcement wall. Three dimensional CAD models of the bone screws and Kryptonite component were created in 3-Matic.

4.3.1 Modeling the acetabular wall reconstruction

An observation of the peak stresses seen on the validated model from Chapters 3 and 4 revealed that no significant stress was seen on any portion of the bone greater

than 25 mm from the acetabulum. As such, this reconstruction was cut to exclude portions outside of this range to simplify the model and thereby reduce processing time. The size of the acetabular wall defect was created according to the patient-specific dimensions described in Chapter 2, and the bone was removed using a Boolean subtraction of an entity of that size (Figure 59).

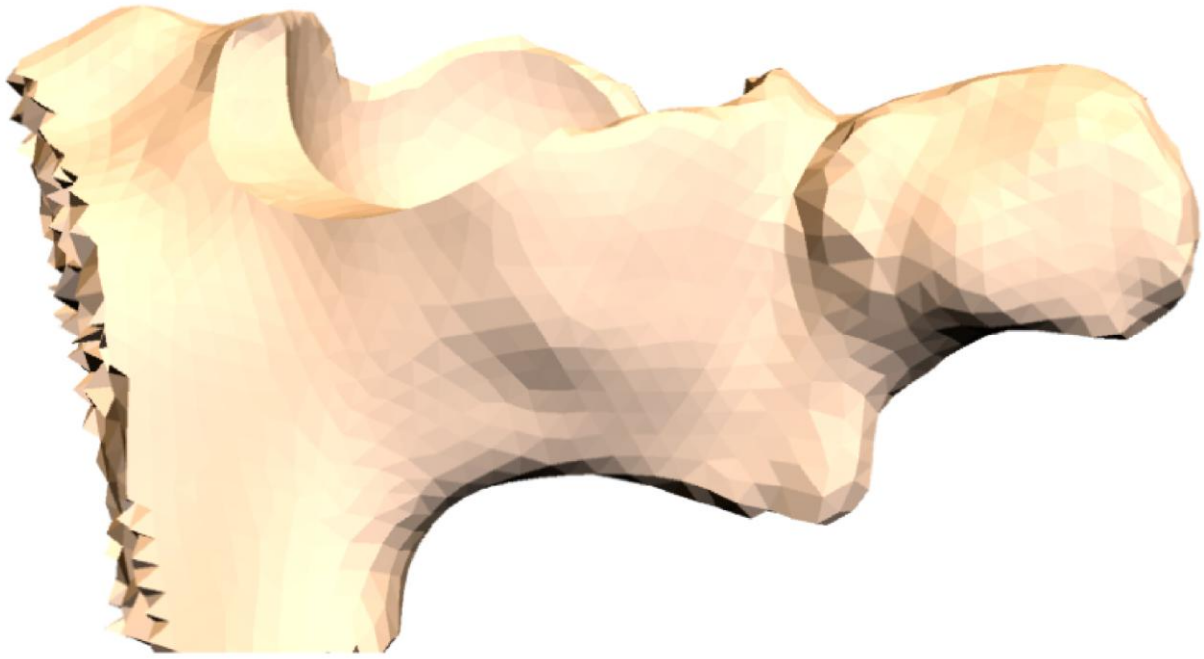

Figure LIX. View of the simplified hemi-pelvis model following bone removal for detect creation.

The three bone screws were modeled as cylinders with a uniform diameter equal to the average diameter of the bone screws used during in-vitro testing. The dimensions

of the screws were obtained through hand instruments. Screw placement was determined according to the position seen within the CT scan, with screws located equidistant from one another within the defect (Figure 60).

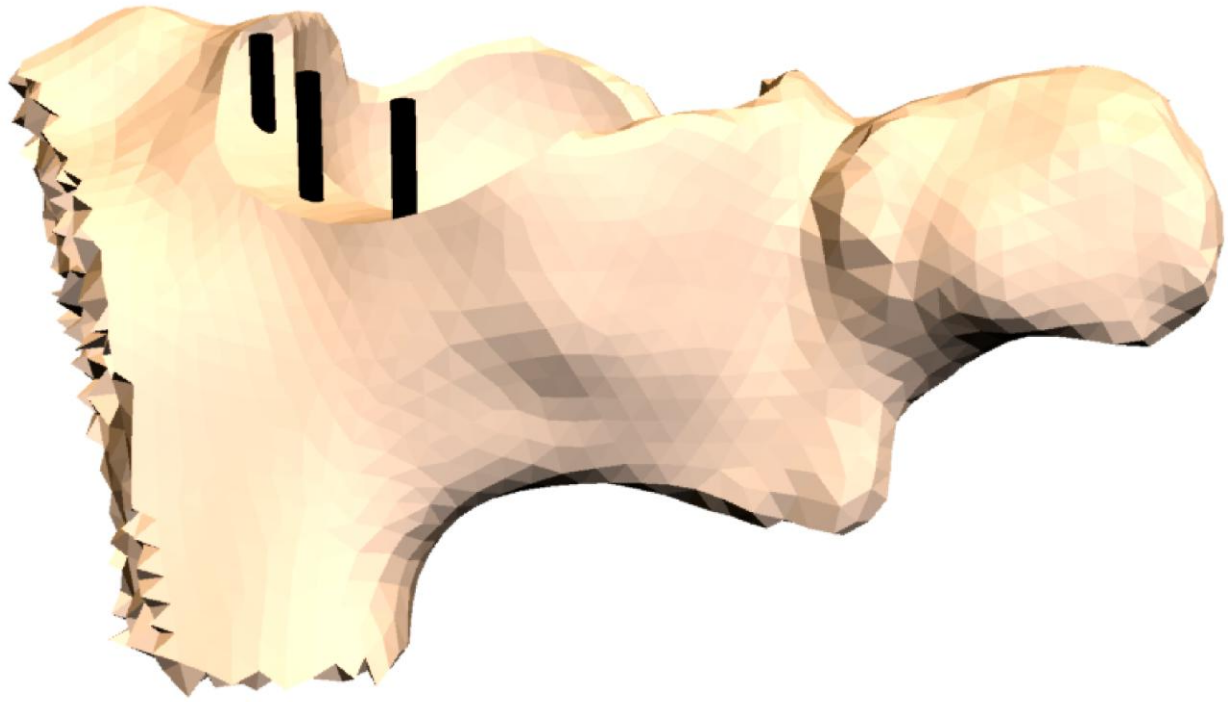

Figure LX. View of the hemi-pelvis model with screws located equidistance from one another within the defect.

A CAD model of the Kryptonite bone cement was manually created in 3-Matic to mimic the conditions of the in-vitro experiment (Figure 61). The acetabulum and Kryptonite were reamed using the same method described in Chapter 3. The initial

location of the acetabular cup component was determined using the same method described in Chapter 3. The complete model is shown in Figure 62.

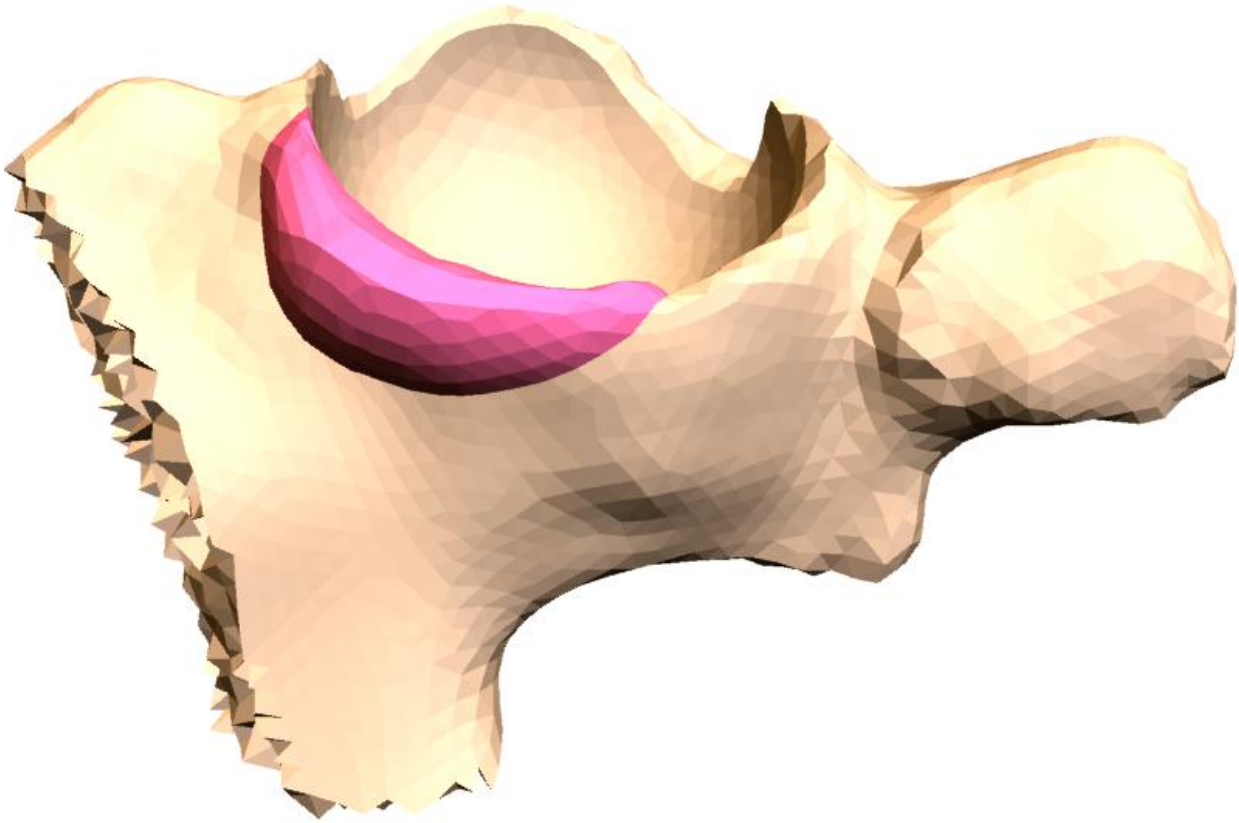

Figure LXI. View of the acetabulum and Kryptonite bone cement following reaming.

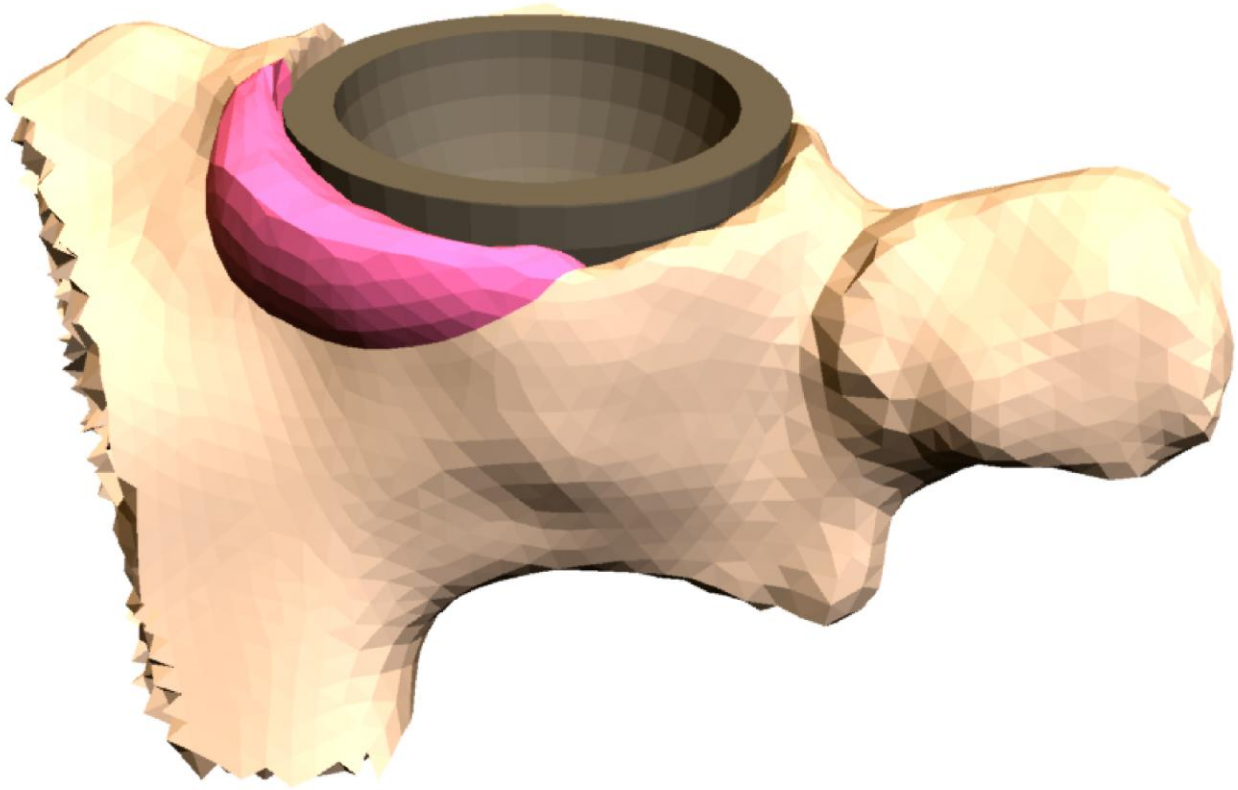

Figure LXII. View of the hemi-pelvis model with acetabular cup and reconstructed acetabular wall defect.

4.3.2 Geometrical Description of the FEA Model and Material Properties

In 3-Matic, Auto Remesh tool was used to create a surface mesh on the model with a maximum edge length of approximately 2.5. Following surface and volume meshing of the model, it was imported into Ansys for finite element analysis. The element and nodal information is detailed in Table 23.

Table XXIII. Geometrical Information of Model.

	Elements	Nodes
Hemi-Pelvis	28648	8753
Acetabular Cup	864	1730
Screws (3 total)	828	345
Kryptonite	2596	639

As in the previous analysis, bone was assumed to be isotropic and elastic. To remain consistent with the material properties of the healthy bone model from Chapters 3 and 4, the same elastic modulus for cortical and trabecular bone was assumed for the healthy bone with augmented defect. Mechanical testing of the trabecular bone of the femoral neck in one study revealed that the percent difference of apparent density between healthy bone and one affected with OP was approximately 35% (Li et al., 1997). Another study found that the average apparent density of a healthy trabecular pelvic bone is 0.248 g/cm^3 with values ranging from 0.109-0.9590.248 g/cm^3 (Dalstra et al., 1993). According to another study, the apparent density of cortical bone may range from 1.5 g/cm^3 to 2 g/cm^3 for OP and healthy bone, respectively (Wirtz et al., 2000).

Several studies have investigated the relation between elastic modulus of bone and apparent density (Helgason et al., 2008; Lotz et al., 1991; Ciarelli et al., 1991). The elastic modulus of bone can be functionally related to the apparent density. The elastic modulus-apparent density relation for cortical (Wirtz et al., 2000) and cancellous bone (Dalstra et al., 1993) are given by Equations 4.1 and 4.2, respectively.

$$E = 1904\rho_{app}^{1.64} \quad \text{Equation 4.1}$$

$$E = 20173\rho_{app}^{2.46} \quad \text{Equation 4.2}$$

According to these equations, the previously used elastic modulus for trabecular and cortical bone resulted in apparent densities within the range of healthy bone. Due to a lack of literature on the influence of OP on pelvic bone, the difference ratio computed from the femoral neck was used for the purposes of this study. Using the given equations, the following material properties were calculated for bone (Table 24). A Poisson's ratio of 0.3 was used for all cases of bone deficiency.

Table XXIV. Bone material properties for osteoporosis, healthy, and osteoarthritis.

Type of Bone	Young's Modulus (GPa)		
	Osteoporosis	Moderate OA	Healthy
Cortical Bone	5.89	10.59	17.00
Cancellous Bone	0.024	0.044	0.07

The material information for the acetabular cup, bone screws, and Kryptonite bone cement is shown in Table 25. In order to simplify the model, the Young's modulus of Kryptonite was approximated using the linear portion of the stress-strain curve, and calculated to be 800 MPa, which is in accordance with values in reported literature (Boxberger et al., 2011).

Table XXV. Finite Element Model Properties.

	Young's Modulus (GPa)	Poisson's ratio
Acetabular Cup	110 (Clinger et al., 2007)	0.3 (Clinger et al., 2007)
Bone Screws	105 (Gefen, 2002)	0.35 (Gefen, 2002)
Kryptonite Bone Cement	0.8	0.3

4.3.3 Cup-Bone Contact Definition

The parameters of the contact interface were modeled as previously described in Chapter 3. The acetabular cup was selected as the target surface, while the contact surface consisted of both bone and Kryptonite bone cement. Because of the bony-like characteristics of Kryptonite, a uniform coefficient of friction of 0.5 was used.

Because of the known adhesive properties of Kryptonite and in order to reduce the amount of computational time needed to run the model, the bone-screw, bone-Kryptonite, and Kryptonite-screw interfaces were regarded as a bonded contact during all stages of loading.

4.3.4 Boundary Conditions

During cup insertion, the cup is fully constrained along the x- and y-axis, with an input displacement along the z-axis. During the equilibrium and loading phases, the cup is fully unconstrained. During all phases, the bone is fully constrained to simulate in-vivo conditions (Figure 63).

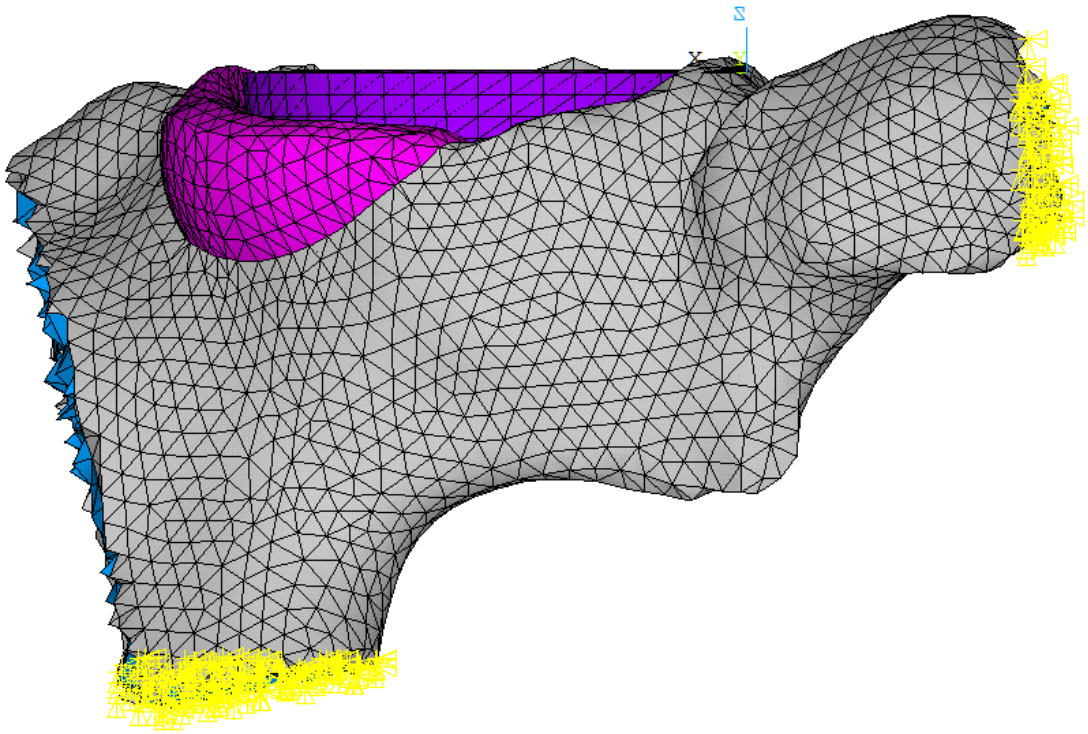

Figure LXIII. Finite element model of the hemi-pelvis with constraints to mimic in-vivo conditions.

4.4 Results

The reaction force on the acetabular cup was measured in order to have an idea of the force needed to fully seat the acetabular cup in the presence of a Kryptonite reconstructed defect and different levels of osteoporosis. The results show that for an otherwise healthy bone with a reconstructed acetabular wall defect, the cup insertion force is on the same order as that seen in the previous studies, where no defect was present. For a reconstructed defect in the presence of osteoporosis, the amount of force needed to seat the acetabular cup decreases (Figure 64).

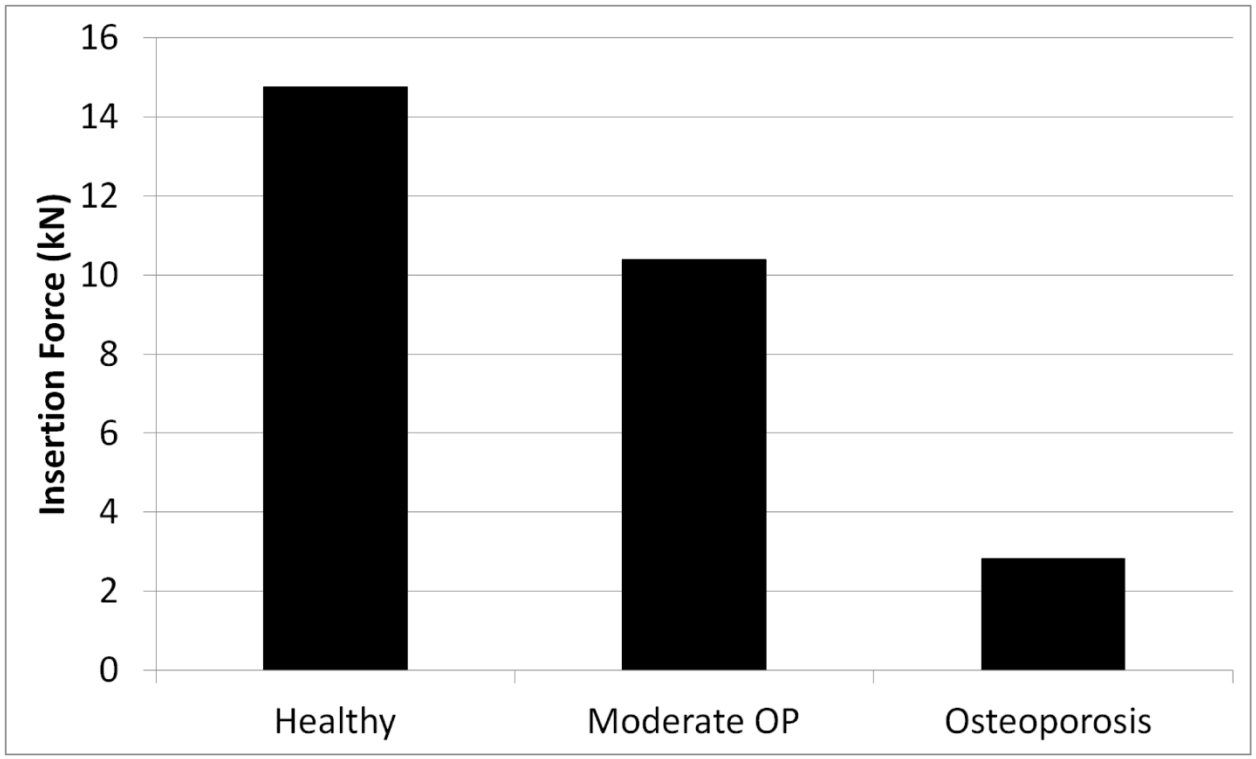

Figure LXIV. Force needed to press-fit insert the acetabular cup in the presence of a reconstructed acetabular wall defect and varying levels of osteoporosis.

4.4.1 Change of peak stress with varying apparent density

Analysis of the peak stress on the Kryptonite bone cement at the interface reveals that for differing apparent density values to mimic healthy, mildly osteoporotic and osteoporotic bone reveals that von Mises stress values were within the linear portion of the stress-strain curve and therefore less than the yield stress for Kryptonite.

Results of this study indicate that in osteoporosis and moderate osteoporosis, the resulting von Mises stress on the bone is less than the peak stress seen in the healthy bone. For decreasing apparent density/elastic modulus to simulate healthy, mild osteoporosis and osteoporosis, peak stress occurred below 55 MPa in 90%, 95%, and

98% of the bone, respectively. Peak stresses were noted primarily on the cortical bone near the peripheral rim of the acetabular cup (Figure 65-67).

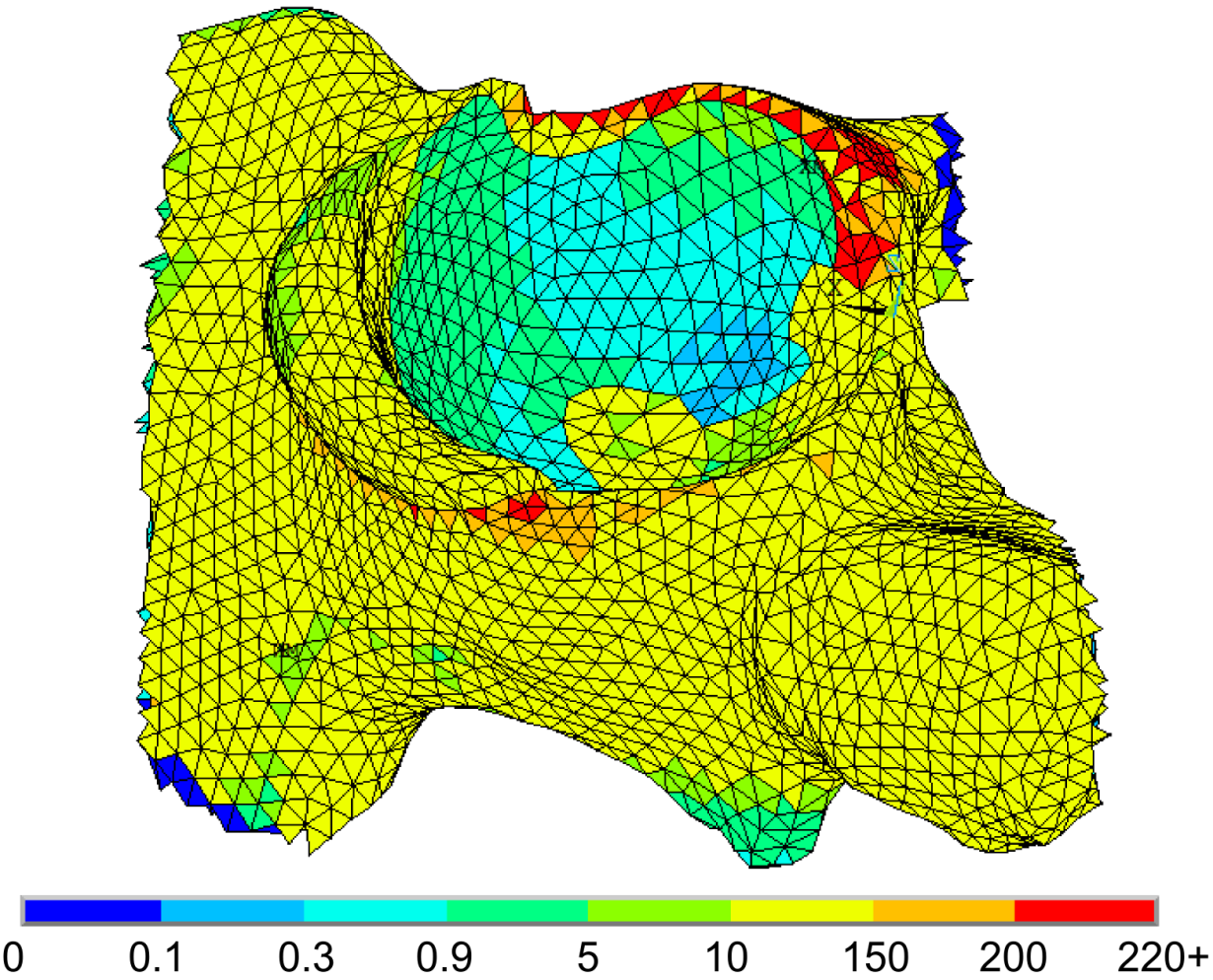

Figure LXV. Resulting von Mises stress (MPa) on a healthy hemi-pelvis and Kryptonite bone cement with reconstructed defect during post-operative loading.

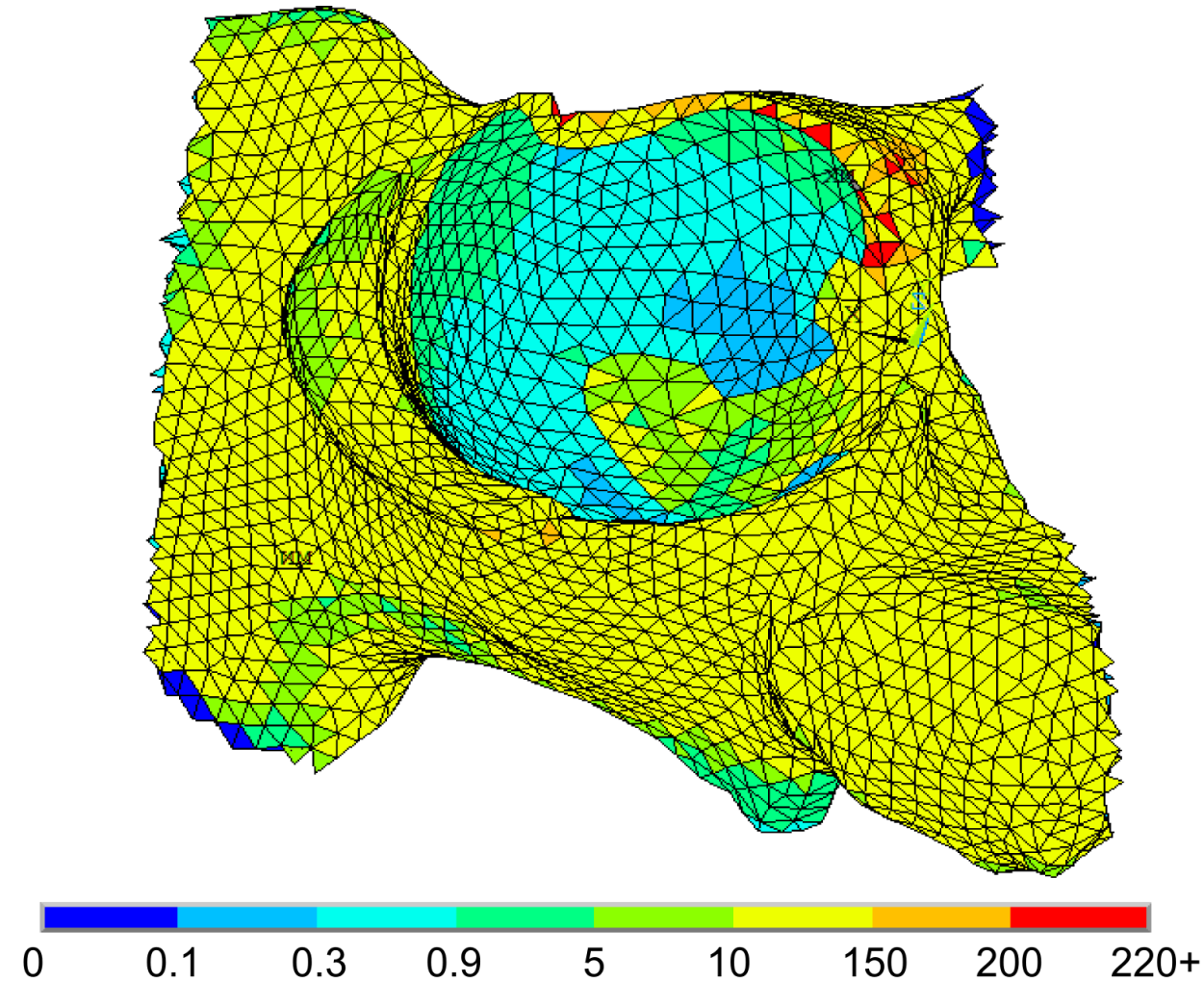

Figure LXVI. Resulting von Mises stress (MPa) on a hemi-pelvis and Kryptonite bone cement with reconstructed defect affected by moderate osteoporosis during post-operative loading.

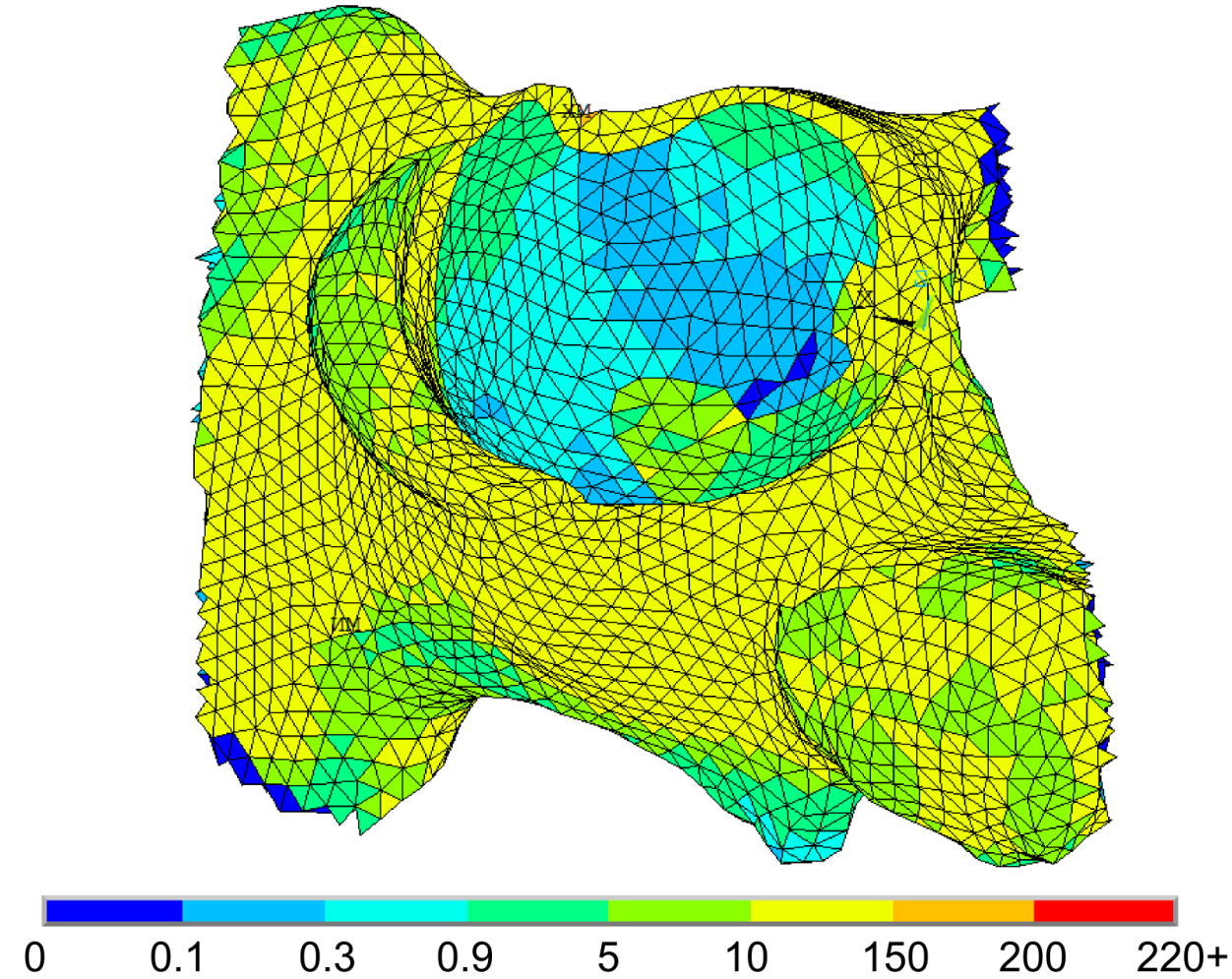

Figure LXVII. Resulting von Mises stress (MPa) on a hemi-pelvis and Kryptonite bone cement with reconstructed defect affected by osteoporosis during post-operative loading.

Analysis of the resulting von Mises stress at the screw-Kryptonite and screw-bone interface reveals that higher stresses occur near the site of the screw (Figures 68-70). However, the resulting stress values remain below the yield limit for both Kryptonite and bone for all cases.

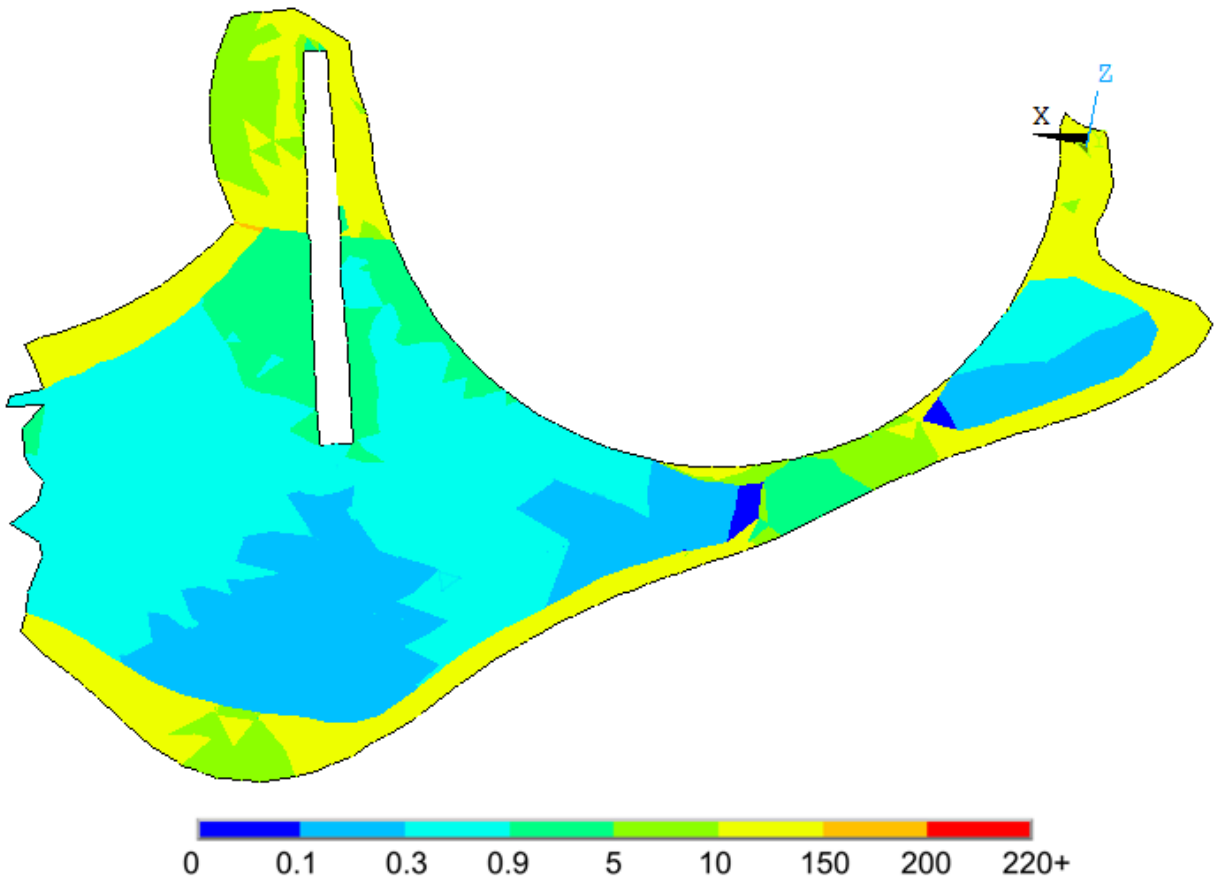

Figure LXVIII. Cross section showing the resulting von Mises stress (MPa) on a healthy hemi-pelvis and Kryptonite bone cement with reconstructed defect during post-operative loading.

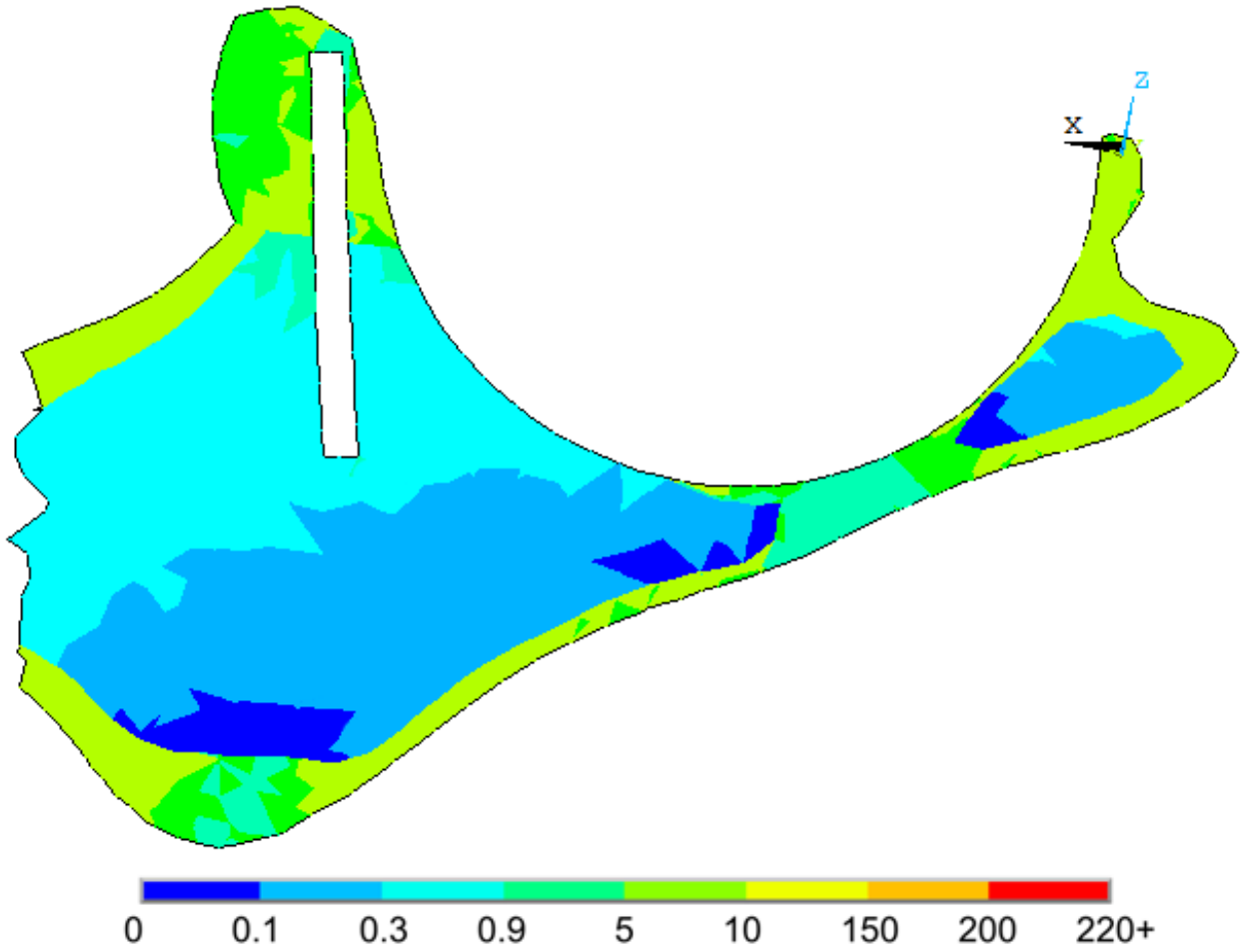

Figure LXIX. Cross section showing the resulting von Mises stress (MPa) on a hemi-pelvis and Kryptonite bone cement with reconstructed defect affected by moderate osteoporosis during post-operative loading.

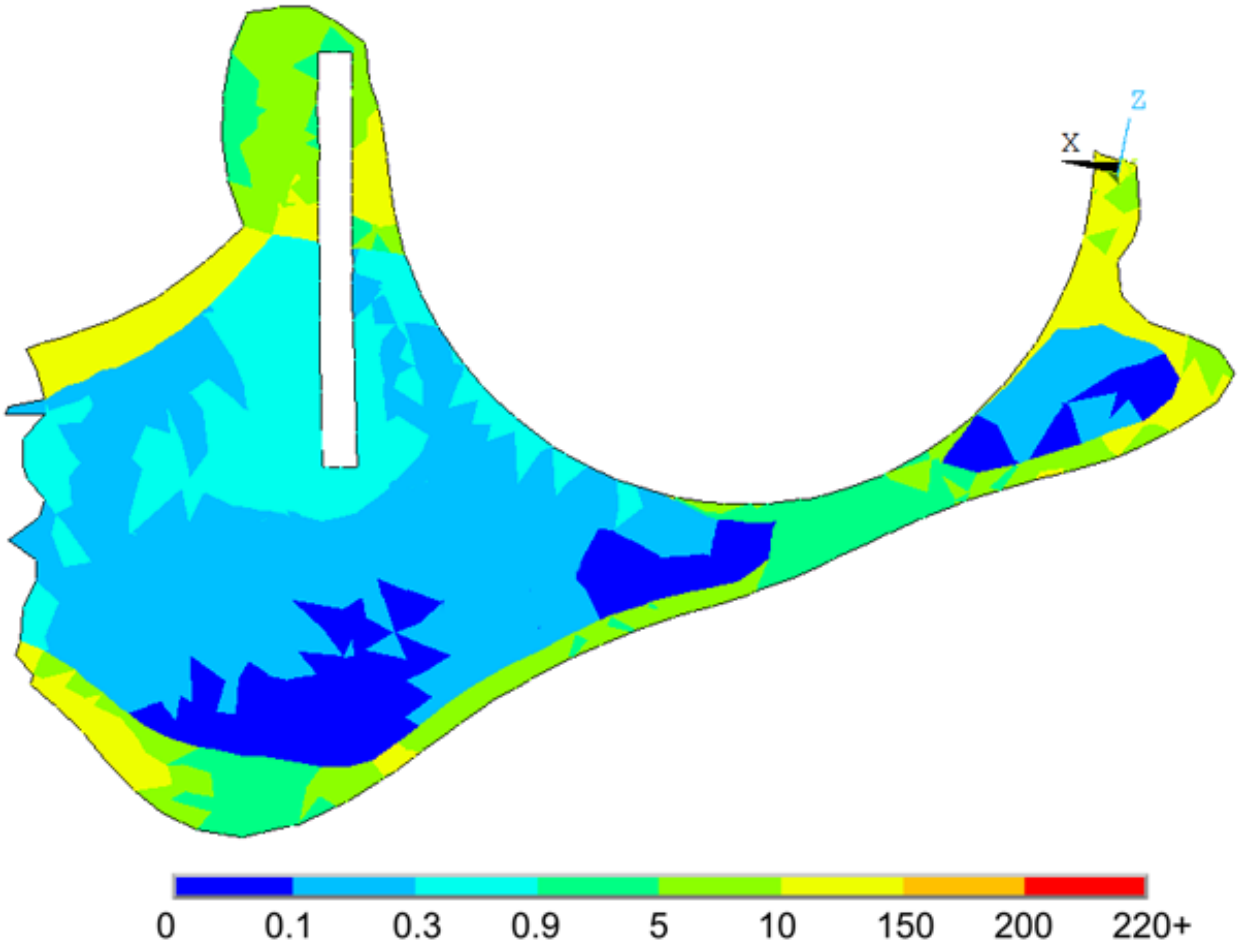

Figure LXX. Cross section showing the resulting von Mises stress (MPa) on a hemi-pelvis and Kryptonite bone cement with reconstructed defect affected by osteoporosis during post-operative loading.

4.4.2 Acetabular cup fixation in the presence of reconstructed defect

An analysis of the stability of the acetabular cup at the interface reveals that for all cases of osteoporosis in the presence of a reconstructed acetabular defect the percentage of surface contact at the interface differs by less than 1%. The analysis shows that for decreasing levels of apparent density of bone, displacement of the acetabular cup increases over loading (Figure 71). Additionally, the rotation of the

acetabular cup about an Euler axis increases as a function of decreased apparent density over loading (Figure 72).

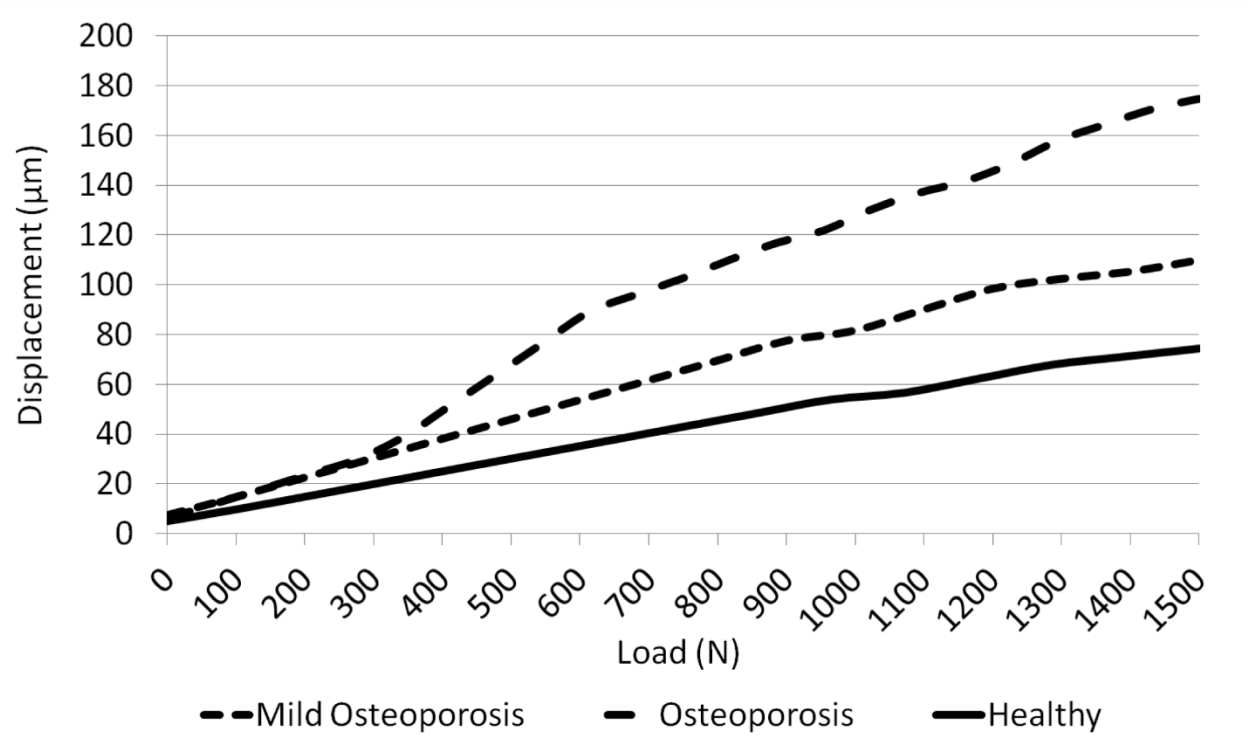

Figure LXXI. Displacement of the center of the acetabular cup along the z-axis into the acetabulum over loading for various levels of osteoporosis in the presence of a reconstructed acetabular defect.

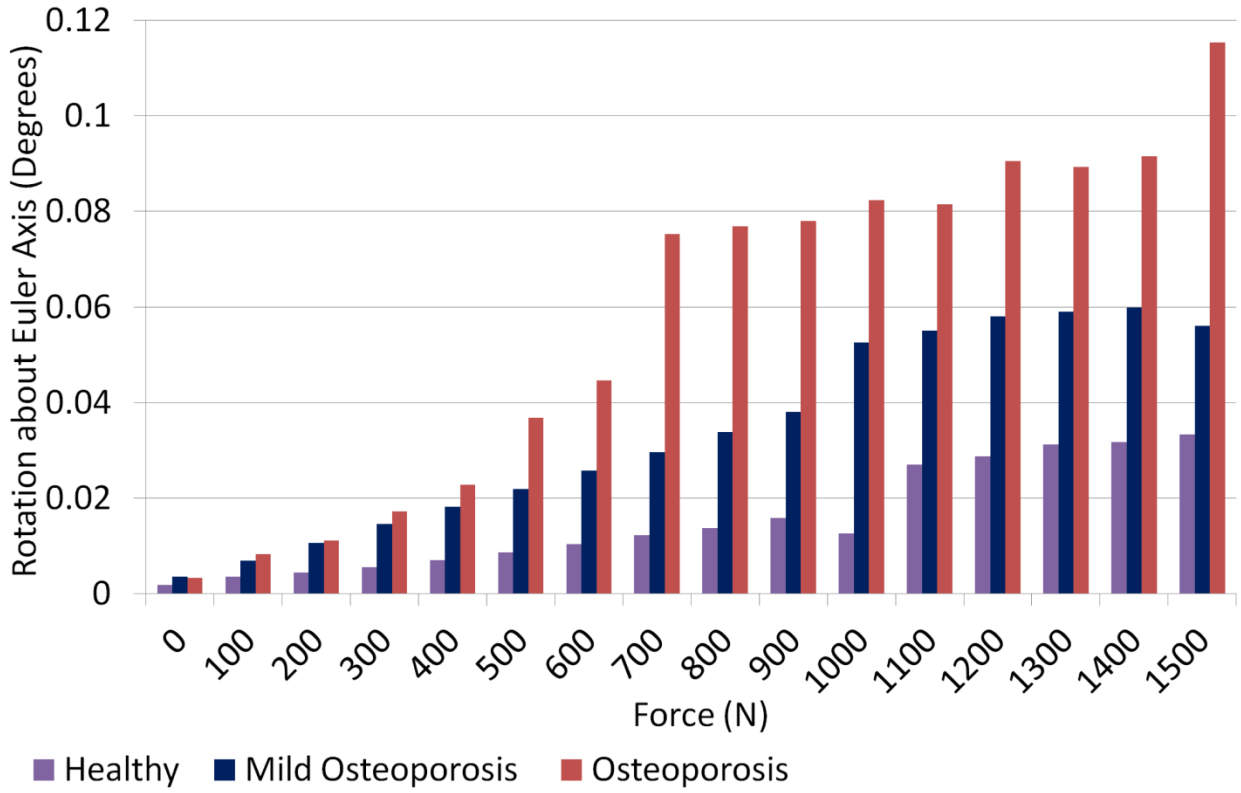

Figure LXXII. Displacement of the center of the acetabular cup along the z-axis into the acetabulum over loading for various levels of osteoporosis in the presence of a reconstructed acetabular defect.

4.5 Discussion

This study investigates the initial stability and fixation of the acetabular cup in the presence of an acetabular wall defect reconstructed with bone screws and augmented with Kryptonite bone cement. Because defects may also occur in conjunction with decreased apparent bone density, it is of interest to have an understanding of the influence of various levels of simulated osteoporosis.

A patient specific finite element model is especially useful because it allows for an understanding of where peak stresses may occur into the bone during loading. While

the majority of peak stresses seen on the bone were well below the elastic yield limit of bone, a small percentage of peak von Mises stress neared the yield limit in the healthy bone and mildly osteoporotic bone. In both cases, these stresses were located in the cortical bone around the peripheral rim of the acetabular cup opposite of the reconstructed defect location.

A comparison of the stress seen during loading between the model with an augmented acetabular defect and the model of the healthy bone from Chapter 4 reveals an alteration in the distribution of stress (Figure 72). In the healthy bone, peak stresses on the cortical bone were seen in the posterior superior region. However, the presence of the Kryptonite reconstructed defect located in the posterior superior region resulted in peak stresses of the anterior inferior region of the acetabulum.

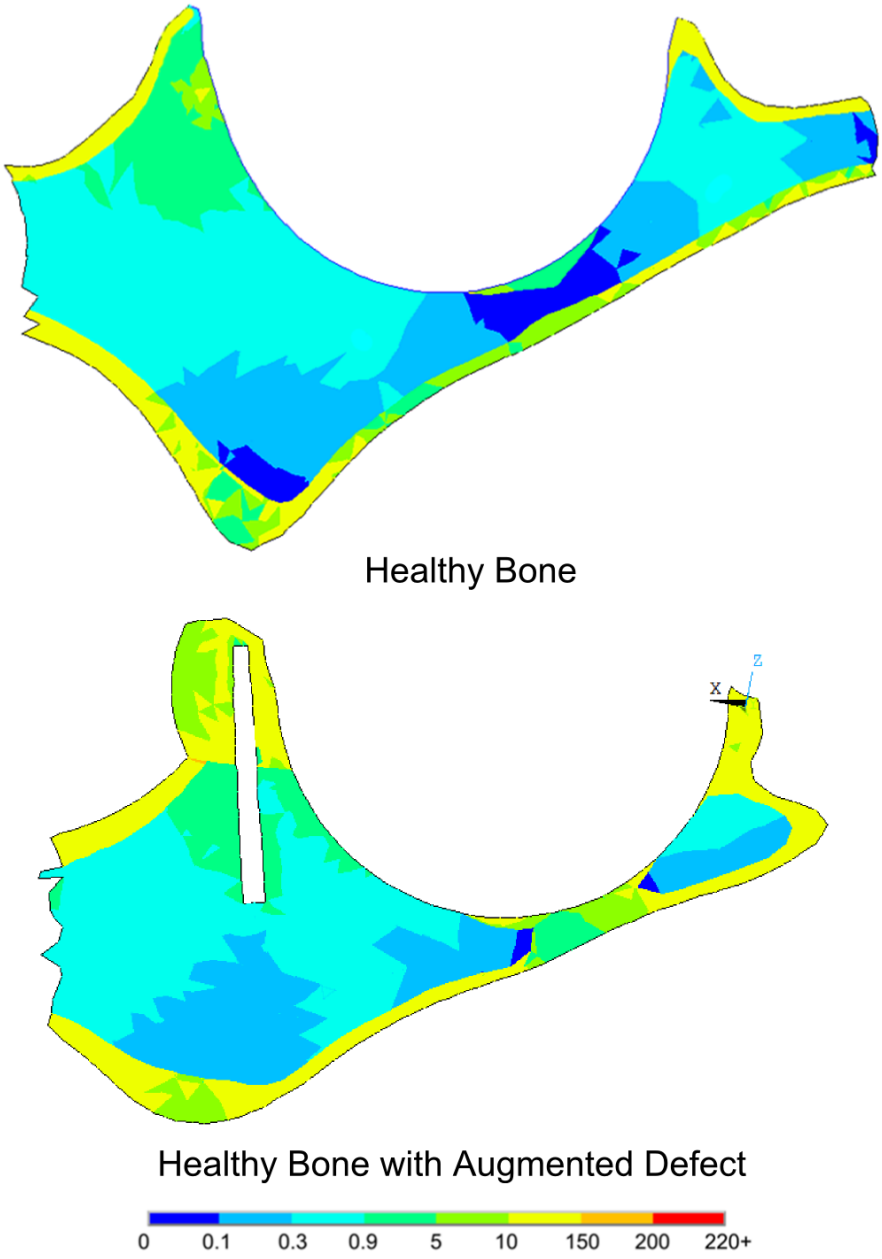

Figure LXXIII. Comparison of von Mises stress in a cross section of bone for a healthy hemi-pelvis and hemi-pelvis with augmented defect.

The distribution of stress is further altered due to the reconstructed defect, particularly in the trabecular bone due to the addition of bone screws. It is interesting to note that higher von Mises stress was seen at and near the bone-screw interface compared to the distribution of trabecular bone stress elsewhere. As previously discussed in Chapter 2, a bony fracture was seen in one specimen near the site of the bone-screw interface. These results further support the notation that during THR in the presence of a reconstructed acetabular defect, more caution should be exercised regarding screw placement and acetabular cup insertion so as not to result in excessive stresses on the acetabulum.

A comparison of the relative displacement of the acetabular cup into the acetabulum seen in the mechanical testing with imposed augmented defect and the displacement seen in the model discussed in this chapter can provide insight into the health of the actual bone. The displacement into the bone predicted in the model with simulated healthy bone and augmented defect is more than 50% less than that seen in the in-vitro experiment in the presence of augmented defect. In contrast, the displacement predicted by the model with the least amount of apparent density with augmented defect only differs from the in-vitro experiment by 11%. These results may indicate that the apparent density of the cadaveric hemi-pelvis specimen with augmented defect was actually less than the apparent density assumed here for healthy bone.

This model can provide insight into the stresses on the bone due to varying structural and material differences along with an acetabular defect. Using the model, we

can evaluate the best combination of wall reconstruction dimensions for various patients in order to reduce the amount of resulting stress on the bone.

Limitations exist in the current study. The current model takes into account only a uniform bone apparent density to simulate osteoporosis in the presence of a reconstructed acetabular defect. Additionally, this study assumes a uniform cylindrical geometrical representation of the bone screws with no relative motion at the bone-screw, bone-Kyrptonite and Kryptonite-screw interfaces. Taking into account the exact screw dimensions and relative motion could enhance provide a more accurate representation of possible in-vivo or in-vitro conditions. Additionally, we have imposed a specific dimensioning of Kyrptonite without considering different wall reconstruction thickness.

5. CONCLUSION

5.1 Clinical significance

This study aims to quantify stability and fixation of a press-fit acetabular cup implant during total hip replacement with and without the presence of an acetabular wall defect reconstructed with Kryptonite bone cement and to define a methodology to simulate those alterations within a patient-specific model for clinical usage. The goals of this study are two-fold – to have a complete understanding of the fixation following acetabular defect augmentation during THR, and also an understanding of the key factors influencing initial cup stability following THR in an otherwise healthy bone.

This study addresses a methodology in which a patient-specific acetabular defect was created in cadaveric specimens and then reconstructed using bone screws and Kryptonite bone cement. Mechanical testing of the cup-bone interface in a hemi-pelvis with and without reconstructed defect allowed us to quantify the differences between a healthy bone and a bone with augmented defect during immediate post-operative loading.

A patient-specific computer model of one of the specimens tested was created and validated with the results of mechanical testing and was used to have an understanding of the key factors during cup insertion which may affect initial cup stability and fixation. Essentially, parameters of interest were the amount of under-reaming, the insertion force needed to insert the cup, the allowable displacement, and rotation due to loading. An evaluation of the stress seen on the bone in the finite element model allowed for an understanding of where stress might occur in-vivo.

An acetabular defect was introduced to the validated model and a Kryptonite-screw reinforcement wall was reconstructed over the defect according to the patient-specific dimensions outlined in Chapter 2 during specimen preparation. This model was used to have an understanding of the influence of an augmented acetabular defect of the posterior superior wall on the displacement, rotation, and stress on the bone near the acetabulum.

The methodology developed can provide information useful for clinical situations. In particular, it is of clinical interest to have an understanding of the amount of surface contact at the cup-bone interface as a result of varying forces used to seat the acetabular cup, as well as the fixation during post-operative loading. An optimization of the amount of reaming needed can be used clinically because it gives a better understanding of the reaming characteristics which provide a stable fixation of the acetabular cup while reducing the amount of stress into the pelvic bone. In deciding the optimal geometry of a surface reconstruction due to acetabular wall defect, a model can provide insight into the dimensioning of augmented reconstruction wall, which includes the actual dimensions as well as the chemical formulation of Kryptonite in order to result in the least amount of cup displacement and rotation without approaching the yield stress of bone at the cup-bone and bone-screw interface.

6.2 Future considerations

The statistical significance of this work could be greatly enhanced through the use of additional mechanical testing of a greater number of specimens. Because of the relatively small number of cadaveric specimens tested, some variability was seen between the results of each group tested. Furthermore, some variability in the size of

specimens was seen, the significance of which could be greatly reduced through a larger sample size.

Future development of the methodology created in this work could be the increase of increment using a refinement of the thresholding used for material segmentation of material properties considered here. The model could be improved through the use of time-dependant material properties of bone or an introduction of anisotropic properties. In particular, the influence of osteoporosis in conjunction with an acetabular wall defect reinforced with Kryptonite bone cement could be more accurately understood if a non-uniform distribution of the material properties of trabecular bone was used.

The introduction of a fracture criterion could help to explore different load cases which are more extreme than the cases simulated in this study. Future studies on the post-operative activities could give us a better understanding of the effective loads over different gait cycles. This could be used for an optimization of the augmented defect properties in order to reduce stress and increase stability during different post-operative activities.

REFERENCES

Aaron, R.K.: Osteonecrosis: etiology, pathophysiology, and diagnosis. In: Callahan JJ, Rosenberg AG, Rubash HE, eds. The Adult Hip. Philadelphia, PA: Lippincott-Raven Publishers; 451-466, 1998.

Abdullah, A.H., Asri, M.A., Alias, M.S., and Giha, T.: Finite element analysis of cemented hip arthroplasty: influence of stem tapers. Proceedings of the International Multi Conference of Engineers and Computer Scientists. 3: 1-5, 2010.

ACR.: Recommendations for the medical management of osteoarthritis of the hip and knee: 2000 update. American College of Rheumatology Subcommittee on Osteoarthritis Guidelines. Arthritis Rheum. 43: 1905–1915, 2000.

Adams, P., Davies, G. T., and Sweetnam, P.: Cortical Bone-Loss with Age. Lancet. 1201-1202, 1971.

Ahnfelt, L., Herberts, P., Malchau, H., and Andersson, G.B.: Prognosis of total hip replacement. A Swedish multicenter study of 4,664 revisions. Acta Orthop Scand Suppl. 238: 1-26, 1990.

Anderson, J. J. and Felson, D. T.: Factors Associated with Osteoarthritis of the Knee in the First National Health and Nutrition Examination Survey (Hanes I). Evidence for an Association with Overweight, Race, and Physical Demands of Work. Am J Epidemiol. 128: 179-189, 1988.

August, A.C., Aldam, C.H., and Pynsent, P.B.: The McKee-Farrar hip arthroplasty: a long term study. J Bone Joint Surg Br. 68: 520-527, 1986.

Ausiello, J.C. and Stafford, R.S.: Trends in medication use for osteoarthritis treatment. J Rheumatol. 29, 999-1005, 2002.

Badley, E., Rasooly, I., and Webster, G.: Relative importance of musculoskeletal disorders as cause of chronic health problems, disability and health care utilization: Findings from the 1990 Ontario Health Survey. J Rheumatol. 21: 505-514, 1994.

Barden, R.M.: Osteonecrosis of the femoral head. Orthop Nurs. 4(4):45-51, 1985.

Baron, J.A., Barett, J.A., and Karagas, M.R.: The epidemiology of peripheral fractures. Bone. 18: S209–S13, 1996.

Bartel, D. L., Burstein, A. H., and Toda, M. D.: The effect of conformity and plastic thickness on contact stress in metal backed plastic implants. J Biomech Eng. 107: 193-199, 1985.

Bayraktar, H.H., Morgan, E.F., Niebur, G.L., Morris, G.E., Wong, E.K., and Keaveny, T.M.: Comparison of the elastic and yield properties of human femoral trabecular and cortical bone tissue. J Biomech. 37(1): 27-35, 2004.

Beaupre, G.S., Orr, T.E., and Carter, D.R.: An approach for time-dependent bone modeling and remodelling: theoretical development. J Orthop Res. 8: 651-661, 1990.

Bergman, G., Graichen, F., Rohlmann, A.: Hip joint loading during walking and running, measured in two patients. J. Biomech. 26(8): 969-990, 1993.

Bergmann, G., Deuretzbacher, G., Heller, M., Graichen, F., Rohlmann, A., Strauss, J., and Duda, G.N.: Hip contact forces and gait patterns from routine activities. J Biomech. 34(7): 859-871, 2001.

Blackley, H.R.L., Davis, A.M., Hutchison, C.R., et al.: Proximal femoral allografts for reconstruction of bone stock in revision arthroplasty of the hip. J Bone Joint Surg Am. 83: 346-354, 2001.

Bobyn, J. D., Pilliar, R. M., Cameron, H. U., and Weatherly, G. C.: The Optimum Pore Size for the Fixation of Porous Surfaced Metal Implants the Ingrowth of Bone. Clin. Orthop. Relat. Res. 150: 263–70, 1980.

Bohm, P. and Banzhaf, S.: Acetabular revision with allograft bone: 103 revisions with 3 reconstruction alternatives, followed for 0.3-13 years. Acta Orthop Scand. 70:240, 1999.

Boxberger, J.I., Adams, D.J., Diaz-Doran, V., Akkarapaka, N.B., and Kolb, E.D.: Radius fracture repair using volumetrically expanding polyurethane bone cement. J Hand Surg. 36A: 1297-1302, 2011.

Bozic, K.J., Kurtz, S.M., Lau, E., Ong, K., Thoams, P.V., Berry, D.J.: The epidemiology of revision total hip arthroplasty in the United States. J Bone Joint Surg. 91: 128-133, 2009.

Breusch, S. and Henrik M.: The Well-Cemented Hip Arthroplasty. New York: Springer, 2005.

Brodner, W., Grubl, A., Jankovsky, R., Meisinger, V., Lehr, S., and Gottsauner-Wolf, F.: Cup inclination and serum concentration of cobalt and chromium after metal-on-metal total hip arthroplasty. J Arthroplasty. 19: 66–70, 2004.

Brooker, A.F. and Collier, J.P.: Evidence of bone ingrowth into a porous - coated metal total hip prosthesis: a case report. J Bone Joint Surg 66A: 619-621, 1984.

Burgers, T.A., Mason, J., Niebur, G., Ploeg, H.L.: Compressive properties of trabecular bone in the distal femur. J Biomech. 41(5): 1077-1085, 2008.

Burnstein, A.H., Reilly, D.T., and Martens, M.: Aging of bone tissuemechanical properties. J Bone Joint Surg. 58(A): 82-86, 1976.

Burr, D.B.: Subchondral bone, microdamage and trabecular microfracture. Joint and Muscle Dysfunction of the Temporomandibular Joint: The Second Scientific Meeting of the TMJ Association. Bethesda, 2002.

Turner, C.H., Rho, J., Takano, Y., Tsui, T.Y., and Pharr, G.M.: The elastic properties of trabecular and cortical bone tissues are similar results from two microscopic measurement techniques. J Biomech. 32: 437–441, 1999.

Callaghan, J. J., Rosenberg, A. G., and Rubash, H. E.: The Adult Hip. 2nd. Lippincott Williams and Wilkins, Philadelphia, PA, 2007.

Carter, D.R.: Mechanical loading histories and cortical bone remodeling. Calcified Tissue International. 36: S19-S24, 1984.

Cezayirlioglu, H., Bahniuk, E., Davy, D. T., and Heiple, K. G.: Anisotropic yield behavior of bone under combined axial force and torque. J Biomech. 19: 61-66, 1985.

Chabaud, M., Fossiez, F., Taupin, J. L., and Miossec, P.: Enhancing effect of IL-17 on IL-1-induced IL-6 and leukemia inhibitory factor production by rheumatoid arthritis synoviocytes and its regulation by Th2 cytokines. J. Immunol. 161: 409–414, 1998.

Chandran N, Optimization of the Design of Posterior Stabilizer in Total Knee Arthroplasty through Finite Element Method, Master Thesis, University of Illinois at Chicago, Chicago, Illinois, 2003.

Chen, W.M., Engh, A., Hopper, R.H., Mcauly, J.P., and Engh, C.A..: Acetabular revision with use of a bilobed component inserted without cement in patients who have acetabular bonestock deficiency. J Bone Joint Surg Am. 82:197-206, 2000.

Choi, K., Kuhn, J.L., Ciarelli, M.J., and Goldstein, S.A.: The elastic moduli of human subchondral, trabecular, and cortical bone tissue and the size-dependency of cortical bone modulus. J Biomech. 23(11): 1103-1113, 1990.

Coathup, M.J., Blunn, G.W., Flynn, N., Williams, C., and Thomas N.P.: A comparison of bone remodeling around hydroxyapatie-coated, porous-coated and grit-blasted hip replacements retrieved at post-mortem. J Bone Joint Surg. 82: 118-123, 2000.

Curtis, M.J., Jinnah, R.H., Wilson, V.D., and Hungerford, D.S.: The initial stability of uncemented acetabular cups. J Bone Joint Surg Br. 74: 372-376, 1992.

D'Lima, D.D., Urquhart, G., Buehler, K.O., Walker, R.H., and Colwell, C.W. Jr.: The effect of the orientation of the acetabular and femoral components on the range of motion of the hip at different head-neck ratios. J Bone Joint Surg Am. 82: 315–321, 2000.

Dalstra, M. and Huiskes, R.:The Pelvic Bone as a Sandwich Construction; a Three Dimensional Finite Element Study. Proc. ESB. 1990; 7, B32.

Dalstra, M., Huiskes, R., and Van Erning, L.: Development and Validation of a Three-Dimensional Finite Element Model of the Pelvic Bone. J Biomech Eng. 117: 272–278, 1995.

Dalstra, M., Huiskes, R., Odgaard, A., and van Erning, L.: Mechanical and textural properties of pelvic trabecular bone. J Biomech. 26: 523-535, 1993.

Dammak, M., Shirazi-Adl, A., Schwartz Jr, M. and Gustavson, L.: Friction properties at the bone-metal interface -- comparison of four different porous metal surfaces. J Biomed Mater Res. 39: 329-336, 1997.

Della Valle, C.J., Shuaipaj, T., Berger, R.A., Rosenberg, A.G., Shott, S., Jacobs, J.J., and Galante, J.O.: Revision of the acetabular component without cement after total hip arthroplasty. J Bone Joint Surg Am. 87:1795-1800, 2005.

DeWal, H., Su, E., and DiCesare, P.E.: Instability following total hip arthroplasty. Am J Orthop. 32: 377–382, 2003.

Dowson, D.:Effect of start-up conditions on elastohydrodynamic lubrication of metal-on-metal hip implants. Proc. Instn. Mech. Engrs. 220: 143-150, 2001.

Echeverri, S., Leyvraz, P.F., Zambelli, P.Y., and Jolles, B.M.: Reliable acetabular cup orientation with a new gravity-assisted guidance system. J Arthroplasty. 21: 413–419, 2006.

Eftekhar, N.S., Kiernan, H.A. Jr, and Stinchfield, F.E.: Systemic and local complications following low-friction arthroplasty of the hip joint : a study of 800 consecutive operations. Arch Surg. 111: 150-5, 1976.

Fedak, P.M., Kieser, T.M., Maitland, A.M., Holland, M., Kasatkin, A., LeBlanc, P., Kim, J.K., and King, K.M.: Adhesive-enhanced sternal closure to iprove postoperative functional recovery: a pilot, randomized control study. Ann Thorac Surgery. 92: 1444-1450, 2011.

Fedak, P.M., Kolb, E., Borsato, G., Frohlich, D.E., Kasatkin, A., Narine, K., Akkarapaka, N., and King, K.M.: Kryptonite bone cement prevents pathologic sternal displacement. Ann Thorac Surgery. 90: 979-985, 2010.

Felson, D. T.: Do Occupation-Related Physical Factors Contribute to Arthritis?, Baillieres Clin Rheumatol. 8: 63-77, 1994.

Ficat, R.P.: Idiopathic bone necrosis of the femoral head. Early diagnosis and treatment. J Bone Joint Surg Br. 67(1): 3-9, 1985.

Firestein, G.S.: Evolving concepts of rheumatoid arthritis. Nature Clinical Practice Rheumatology. 423: 356-361, 2003.

Fritsche, A., Zietz, C., Teufel, S., Kolp, S., Tokar, I., Mauch, C., Mittlemier, W., and Bader, R.: In-vitro and in-vivo investigations of the impaction and pull-out behavior of metal backed acetabular cups. J Bone Joint Surg Br. 93, 2011.

Garvin, K.L. and Hanssen, A.D.: Current concepts review infection after total hip arthroplasty. J Bone Joint Surg. 77: 1576-1588, 1995.

Geesink, R.G. and Hoefnagels, N.H.: Six-year results of hydroxyapatite-coated total hip replacement. J. Bone Joint Surg. 77: 34-37, 1995.

Geesink, R.G., de Grott, K.l., and Klein, C.P.: Chemical implant fixation using hydroxyl-apatite coatings. The development of human total hip prosthesis for chemical fixation to bone using hyroxyl-apatite coatings on titanium substrates. Clin Orthop. 225: 147-170, 1987.

Gefen, A.: Optimizing the biomehcnical compatibility of orthopedic screws for bone fracture fixation. Med Eng Phys. 24: 337-347, 2002.

Gibson, L.J.: The mechanical behavior of cancellous bone. J Biomech. 18: 317-328, 1985.

Goldberg, V.M.: Selection of bone grafts for revision total hip arthroplasty. Clin Orthop. 381:68-76, 2000.

Goldsmith, A.A., Dowson, D., Isaac, G.H., and Landcaster, J.G.: A comparative joint simulator study of the wear of metal-on-metal and alternative material combinations in hip replacements. Proc Instn Mech Engrs. 214: 39-47, 2000.

Goodman, S.B. and Carter, D.R.: Acetabular lucent lines and mechanical stress in total hip arthroplasty. J Arthroplasty. 2: 219-224, 1987.

Griffin, T.M. and Guilak, F.: The role of mechanical loading in the onset and progression of osteoarthritis. Exercise and Sports Science Reviews. 33(4): 195-200, 2005.

Griss, P. and Heimke, G.: Five years experience with ceramic-metal composite hip prosthesis. Clinical evaluation. Arch Orthop Traum Surg. 98: 157-164, 1981.

Gross, A. E. and Goodman, S. The Current Role of Structural Grafts and Cages in Revision Arthroplasty of the Hip. Clin Orthop Relat Res. 429: 193–200, 2004.

Haaker, R.G., Tiedjen, K., Ottersbach, A., Rubenthaler, F., Stockheim, M., and Stiehl, J.B.: Comparison of conventional versus computer-navigated acetabular component insertion. J Arthroplasty. 22: 151–159, 2007.

Haidukeqych, G.J., Jacofsky, D.J., Hanssen, A.D. and Lewallen, D.G: Intraoperative fractures of the acetabulum during primary total hip arthroplasty. J Bone Joint Surg Am. 88(9): 1952-1956, 2006.

Hallel T, Salvati, E.A., and Botero, P.M.: Polymethylmethacrylate in the knee. J Bone Joint Surg Am. 58-A : 556-557, 1976.

Harris, W. H.: Factors Controlling Optimal Bone Ingrowth of Total Hip Replacement Components. Instr Course Lect. 35: 184–187, 1986.

Hastings, D.E. and Parker, S.M.: Protrusio acetabuli in rheumatoid arthritis. Clin Orthop. 108: 76-83, 1975.

Haydon, C.M., Mehin, R., Burnett, S., et al.: Revision total hip arthroplasty with use of a cemented femoral component: results at a mean of ten years. J Bone Joint Surg Am. 86: 1179-1185, 2004.

Hayes, W. C: Biomechanical measurements of bone. In: CRC Handbook of Engineering in Medicine and Biology: Section B. Instruments and Measurements, eds. A. Burstein, 333-372, 1991.

Heijink, A., Zobitz, M.E., Nuyts, R., Morrey, B.F., and An, K.N.: Prosthesis design and stress profile after hip resurfacing: a finite element analysis. J Orthopaedic Surgery. 16(3): 326-332, 2008.

Helgason, B., Perilli, E., Schileo, E., Taddei, F., Brynjólfsson,and B., Viceconti, M.: Mathematical relationships between bone density and mechanical properties: A literature review. C Biomech. 23: 135-146, 2008.

Herberts, P.: Hip arthroplasty revision. Acta Orthop Scand. 63: 109-110, 1992.

Hoshino, A. and Wallace, W. A.: Impact-absorbing properties of the human knee. J Bone Joint Surg. 69B: 807–811, 1987.

Howell, J. and Bolland, B. Bone loss around the acetabular component. European Instructional Lectures. Ed. George Bentley. Springer. 11: 155-166, 2011.

Hsu, J.T., Chang, C.H., Huang, H.L., Zobitz, M.E., Chen, W.P., and Lai, K.A., An, K.N.: The number of screws, bone quality, and friction coefficient affect acetabular cup stability. Medical Engineering & Physics. 1089-1095, 2007.

Hui, S.L., Slemenda, C.W., and Johnston, C.C.: Age and bone mass as predictors of fracture in a prospective study. J Clin Invest. 81: 1804, 1809, 1988.

Huiskes, R. Finite element analysis of acetabular reconstruction: noncemented threaded cups. Acta Orthop Scand. 58: 620-625, 1987.

Jacob, H.A.C, Huggler, A.H., Dietschi, C., and Schreiber, A.: Mechanical Function of Subchondral Bone as Experimentally Determined on the Acetabulum of the Human Pelvis. J. Biomech. 9: 625-627, 1976.

Jepson, K.J., Davy, D.T.,and Krzypow, D.J.: The role of lamellar interface during torsional yielding of human cortical bone. J Biomech. 32: 303-310, 1999.

Jiang, Y., Zhao, J., Augat, P., Ouyang, X., Lu, Y., Majumdar, S., and Genant, H.K. : Trabecular bone mineral and calculated structure of human bone specimens scanned by peripheral quantitative computed tomography: relation to biomechanical properties. J Bone Miner Res. 13(11): 1783-1790, 1998.

Johanson, N.A., Driftmier, K.R., Cerynik, D.L., and Stehman, C.C.: Grading Acetabular Defects. The need for a universal and valid system. J Arthroplasty. 25: 425-431, 2010.

Jolles, B.M., Zangger, P., and Leyvraz, P.F.: Factors predisposing to dislocation after primary total hip arthroplasty: a multivariate analysis. J Arthroplasty. 17: 282–288, 2002.

Joshi, R.V., Eftekhar, N.S., Mcmahon, D.J., and Nercessian, O.A.: Osteolysis after Charnley primary low-friction arthroplasty; a comparison of two matched paired groups. J Bone Joint Surg. 80B (4): 585-590, 1998.

Kanis, J.A., Melton, L.J., Christianson, C., Johnston, C.C., and Khaltaev, N.: The diagnosis of osteoporosis. J Bone Miner Res. 9(8): 1137-1141, 1994.

Kanis, J.A. and Pitt, F.: Epidemiology of osteoporosis. Bone. 31: S7-S15, 1992.

Katti, KS.: Biomaterials in total joint replacement. Colloids and Surfaces B: Biointerfaces. 39: 133-142, 2004.

Kaufer, H.: Mechanics of the treatment of hip injuries. Clin Orthop Rel Res. 146: 53-51, 1980.

Kavanagh, B.F., Ilstrup, D.M., and Fitzgerald, R.H.: Revision total hip arthroplasty. J Bone Joint Surg Am. 67: 517, 1985.

Kennedy, J.G., Rogers, W.B., SoVe, K.E., Sullivan, R.J., GriVen, D.G., and Sheehan, L.J.: Effect of acetabular component orientation on recurrent dislocation, pelvic osteolysis, polyethylene wear, and component migration. J Arthroplasty. 13: 530–534, 1998.

Kim, Y.S., Callaghan, J.J., Ahn, P.B., Brown, T.D.: Fracture of the acetabulum during insertion of an oversized hemispherical component. J Bone Joint Surg Am. 77: 111-7, 1995.

Knahr, K., Bohler, M., Frank, P., Plenk, H,. and Salzer, M.: Survival analysis of an uncemented ceramic acetabular component in total hip replacement. Arch Orthop Trauma Surg. 106: 297-300, 1987.

Kroon, P.O. and Freeman, M.A.: Hydroxyapatite coating of hip prosthesis. Effect on migration into the femur. J Bone Joint Surg Br. 74: 518-522, 1992.

Kuiper, J.H., van Uem, B., Nekkers, G.J., and Cheah, K.: Early mechanical stability of impaction-grafted prostheses correlates strongly with degree of impaction. Trans EORS. 8:6, 1998.

Kummer, F.J., Shah, S., Iyer, S., and DiCesare, P.E.: The effect of acetabular cup orientations on limiting hip rotation. J Arthroplasty. 14: 509–513, 1999.

Kurtz, S.M., Ochoa, J.A., Hovey, C.B., and White, C V.: Simulation of initial frontside and backside wear rates in a modular acetabular component with multiple screw holes. J Biomech. 32: 967-976, 1992.

Kurtz, S.M., Ong, K.L., Schmier, J., et al.: Future clinical and economic impact of revision total hip and knee arthroplasty. J Bone Joint Surg. 89: 144-151, 2007.

Kwong, L.M., Jasty, M., and Harris, W.H.: High Failure Rate of Bulk Femoral Head Allografts in Total Hip Acetabular Reconstruction at 10 Years. J Arthroplasty. 8(4): 341-346, 1993.

Kwong, L.M., O'Connor, D.O., Sedlacek, R.C., Krushell, R.J., Maloney, W.J., and Harris, W.H.: A quantitative in vitro assessment of fit and screw fixation on the stability of a cementless hemispherical acetabular component. J Arthroplasty. 9(2): 163–170, 1994.

Lewis, R.: Arthritis: modern treatment for that old pain in joints. FDA Consumer. 25: 1991.

Li, B. and Aspden, R.M.: Material properties of bone from the femoral neck and calcar femorale of patients with osteoporosis and osteoarthritis. Osteoporos Int. 7: 450-456, 1997.

Li, B.and Aspden, R.M.: Mechanical and material properties of cancellous bone from the femoral head of patients with osteoarthritis and osteoporosis. Annals of the Rheumatic Diseases. 12(4): 641-651, 1997a.

Li, B. abd Aspden, R.M.: Mechanical and material properties of the subchondral bone plate from the femoral head of patients with osteoarthritis and osteoporosis. Annals of the Rheumatic Diseases. 56: 247-254, 1997b.

Linde, F., Norgaard, P., Hvid, I., Odgaard, A., and Soballe, K.: Mechanical properties of trabecular bone: dependency on strain rate. J Biomech. 24: 803-809, 1991.

Linde, F. and Sorensen, H.C.: The effect of different storage methods on the mechanical properties of trabecular bone. J Biomech. 26: 1249-1252, 1993.

Linde, F.: Elastic and Viscoelastic Properties of Trabecular Bone by a Compression Testing Approach. Dan Med Bull. 4: 119-138, 1994.

Lowell, J.D. Scheller, A.D., and Turner, R.H.: Complications of arthroplasty and total joint replacement in the hip. In: Epps CH, ed. Complications in orthopaedic surgery. Philadelphia: J. B. Lippincott, 919-944, 1978.

MacDonald W., Swarts E., and Beaver .: Penetration and shear strength of cement-bone interfaces in vivo. Clin Orthop Relat Res 286: 283-288, 1993.

Macirowski, T., Tepic, S., and Mann, R. W.: Cartilage Stresses in the Human Hip Joint. J Biomech Eng. 116: 10-18, 1994.

MacKenzie, J.R., Callaghan, J.J., Pedersen, D.R., and Brown, T.D.: Areas of contact and extent of gaps with implantation of oversized acetabular components in total hip arthroplasty. Clin Orthop Relat Res. 298: 127-136, 1994.

Malchau, H., Herberts, P., Eisler, T., Garellick, G., and Soderman, P.: The Swedish Total Hip Replacement Register. J Bone Joint Surg Am. 84:2-20, 2002.

Mallory, T.H: Rupture of the common iliac vein from reaming the acetabulum during total hip replacement. J Bone Joint Surg Am. 54: 276-277, 1972.

Mann K.A., Ayers D.C., Werner F.W., Nicoletta R.J., and Fortino M.D.:Tensile strength of the cement-bone interface depends on the amount of bone interdigitated with PMMA cement. J Biomech. 30:339-346, 1997.

Mann, K.A., Bartel, K.A., Wright, T.M.,and Burstein, A.H.: Coulumb frictional interfaces in modeling cemented total hip replacements, a more realistic model. J Biomech. 28(9): 1067-1078, 1995.

Mantwill, F., Schulz, A.P., Faber, A., Hollstein, D., Kammal, M., Fay, A., and Jurgens, C.: Robotic systems in total hip arthroplasty—is the time ripe for a new approach? Int J Med Robot. 1: 8–19, 2005.

Marcus, R., Feldman, D., Nelson, D.A., and Rosen, C.J.: Osteoporosis. Elsevier Academic Press, 2008.

Martens, M., Audekerche, R.V., Delport, P., De Meester, P., and Mulier, J.C.: The mechanical characteristics of cancellous bone at the upper femoral region. J Biomech. 16(12): 971-983, 1983.

McCollum, D.E., and Nunley, J.A.: Bone grafting in acetabular protrusio: a biological buttress. In: Nelson CL, editor. The hip: proceedings of the sixth open scientific meeting of the hip society. St. Louis: CV Mosby. 124-46, 1978.

McMinn, D., Treacy, R., Lin, K., and Pynsent, P.B.: Metal on metal surface replacement of the hip: experience of the McMinn prosthesis. Clin Orthop. 329: 89-98, 1996.

Meghini, R.M., Stultz, A.D., Watson, J.S., Davis, M.Z., and Buckley, C.S.: Does ischial screw fixation improve mechanical stability in revision total hip arthroplasty? J Arthroplasty. 25(7): 1157-1161, 2009.

Melton, L.J: Atkinson, E.J., O'Fallon, W.M., Wahner, H.W., and Riggs, B.L.: Long-term fracture prediction by bone mineral assessed at different skeletal sites. J Bone Miner Res. 8: 11227-1233, 1993.

Mendes, D.G., Roffman, M., and Silbermann, M.: Reconstruction of the acetabular wall with bone graft in arthroplasty of the hip. Clin Orthop. 186:29-37, 1984.

Michaeli, D.A., Murphy, S.B., and Hipp, J.A.: Comparison of predicted and measured contact pressures in normal and dysplastic hips. Med Eng Phys. 19(2): 180-186, 1997.

Milner, P.F., Kraus, A.P., Sebes, J.I., et al.: Sickle cell disease as a cause of osteonecrosis of the femoral head. N Engl J Med. 325(21):1476-1481, 1991.

Mjoberg, B.: Fixation and loosening of hip prostheses. A review. Acta Orthop Scand. 62: 500-508, 1991.

Mont, M.A., Marker, D.R., Smith, J.M., Ulrich, S.D., and McGrath, M.S.: Resurfacing is comparable to total hip arthroplasty at short-term followup. Clinic Orthop Relat. Res. 467: 66-71, 2009.

Moskal, J.T. and Shen, F.H.: The use of bilobed porous-coated acetabular components without structural bone graft for type III acetabular defects in revision total hip arthroplasty. J Arthroplasty. 19: 867-873, 2004.

Noguchi, Y., Miura, H., Takasugi, S., and Iwamoto, Y.: Cartilage and labrum degeneration in the dysplastic hip generally originates in the anterosuperior weight-bearing area: an arthroscopic observation. Arthroscopy: J of Arth and Rel Surg. 15(5): 496-506, 1999.

Nehme, A., Lewallen, D. G., and Hanssen, A. D. Modular Porous Metal Augments for Treatment of Severe Acetabular Bone Loss During Revisions Hip Arthroplasty. Clin Orthop Relat Res. 429: 201–208, 2004.

Nuzzo, G., Luongo, M., Parlato, C., and Moraci, A.: Cranial reconstruction using bioaabsorbable calcified triglyceride bone cement. Journal of Craniofacial Surgery. 21: 1170-1174, 2010.

Paprosky, W. G. and Burnett, S. J.: Assessment and Classification of Bone Stock efficiency in Revision Total Hip Arthroplasty. Am J Orthop. 26: 459–464, 2002.

Paprosky, W.G. and Sekundiak, T.D.: Instructional Course Lectures, The American Academy of Orthopaedic Surgeons—Total Acetabular Allografts, J Bone Joint Surg Am. Vol. 81: 280–291, 1999.

Paprosky, W.G., Perona, P.G., and Lawrence, J.M.: Acetabular defect classification and surgical reconstruction in revision arthroplasty. A 6-year follow-up evaluation. J Arthroplasty. 9: 33-44, 1994.

Parfitt, A.M., Villanueva, A.R., Foldes, J., and Rao, D.S.: Relations between histologic indices of bone formation: implications for the pathogenesis of spinal osteoporosis. J Bone Miner Res. 10: 466–473, 1995.

Pearcy, M.J.: A new generation of artificial hip joints. Eng Med. 17: 199-201, 1988.

Periasami, K., Watson, W.S., Mohammed, A., Murray, H., Walker, B., Patil, S., and M, R.M.D.: A randomized study of peri-prosthetic bone density after cemented versus trabecular fixation of a polyethylene acetabular component. J Bone Joint Surg. 93: 1033-1044, 2011.

Perona, P.G., Lawrence, J., Paprosky, W.G., Patwardhan, A.G., and Sartori, M.: Acetabular micromotion as a measure of initial implant stabimlity in primary hip arhtroplasty. J Arthroplasty. 7(4): 537-547, 1992.

Pilliar, R.M., Lee, J.M., and Maniatopoulos, C.: Observations on the effect of movement on bone ingrowth into porous-surfaced implants. Clin Orthop Relat Res. 208: 108–113, 1986.

Pinnacle Acetabular System: Surgical Technique. DePuy Orthopaedics 2006.

Poss, R., Ewald, F.C., Thomas, W.H., and Sledge, C.B.: Complications of total hip-replacement in patients with rheumatoid arthritis. J Bone Joint Surg Am. 58(8): 1130-1133, 1976.

Radin, E. L.: Osteoarthrosis--the Orthopedic Surgeon's Perspective. Acta Orthop Scand Suppl. 266: 6-9, 1995.

Radin, E. L., Burr, D. B., Caterson, B., Fyhrie, D., Brown, T. D., and Boyd, R. D.: Mechanical Determinants of Osteoarthrosis, Semin Arthritis Rheum. 21: 12-21, 1991.

Raisz, L.G.: Pathogensis of osteoporosis: concepts, conflicts, and prospects. Science in Medicine. 115(12): 3318-3324, 2005.

Ranawat, A., Zelken, J., Helfet, D., and Buly, R.: Total hip arthroplasty for posttraumatic arthritis after acetabular fracture. J Arthroplasty. 24(5): 757-567, 2009.

Rees, H.W., Fung, D.A., Cerynik, D.L., Amin, N.H., and Johanson, N.A.: Revision total hip arthroplasty without graft of high-grade acetabular defects. J Arthroplasty. 00: 1-7, 2011.

Rice, J.C., Cowin, S.C., and Bowman, J.A.: On the dependence of the elasticity and strength of cancellous bone on apparent density. J Biomech. 21: 155-168, 1988.

Richards, A.M., Coleman, N.W., Knight, T.A., Belkoff, S.M., and Mears, S.C.: Bone density and cortical thickness in normal, osteopenic, and osteoporotic sacra. J Osteoporosis. 2010: 1-5, 2010.

R.M., Stultz, A.D., Watson, J.S., Davis, M.Z., Buckley, C.S.: Does ischial screw fixation improve mechanical stability in revision total hip arthroplasty? J Arthroplasty. 25: 1157-1161, 2010.

Roder, C., Bach, B., Berry, D.J., Eggli, S., Langenhahn, R., and Buato, A.: Obesity, age, sex, diagnosis, and fixation mode differently affect early cup failure in total hip arthroplasty. J Boint Joint Surg. 95: 1954-1963, 2010.

Roffman, M., Silbermann, M., and Mendes, D.G.: Incorporation of bone graft covered with methylmethacrylate onto the acetabular wall. An experimental study. Acta Orthop Scand. 54:580-3, 1983.

Rohrl, S.M., Nivbrant, B., Strom, H., and Nilsson, K.G.: Effect of augmented cup fixation on stability, wear, and osteolysis. J. Arthroplasty. 19(8): 962-971, 2004.

Roth, A., Winzer, T., Sander, K., Anders, J.O., and Venbrocks, R.A.: Press fit fixation of cementless cups: how much stability do we need? Arch Orthop Trauma Surg. 126: 77-81, 2006.

Saikko, V. and Calonius, O.: Slide track analysis of the relative motion between femoral head and acetabular cup in walking and in hip simulators. J Biomech. 35: 455-464, 2002.

Santanglo, S.A. and Mazzocca, A.D.: University of Connecticut Health Center. Data on file at Doctors Research Group, Inc.

Santavirta, S., Bohler, M., Harris, W.H., Konttinen, Y.T., Lappalainen, R., Muratoglu, O., Rieker, C., and Salzer, M.: Alternative materials to improve total hip replacement tribology. Acta Orthop Scand. (74): 380-388, 2003.

Schreurs, B.W., Busch, V., Welten, M.L., et al.: Acetabular reconstruction with impaction bone-grafting and a cemented cup in patients younger than fifty years old. J Bone Joint Surg Am. 86:2385. 2004.

Schutzer, S.F. and Harris, W.H.: Deep wound infection after total hip replacement under contemporary aseptic conditions. J Bone Joint Surg. 70(5): 724-727, 1988.

Sedel, L., Nizard, R. S., Kerboull, L., and Witvoet, J.: Alumina-alumina hip replacement in patients younger than 50 years old. Clin Orthop Rel Res. 298: 175-183, 1994.

Semlitsch, M. and Willert, H.G.: Clinical wear behaviour of ultra-high molecular weight polyethylene cups paired with metal and ceramic ball heads in comparison to metal-on-metal pairings of hip joint replacements . Proc. Instn. Mech. Engrs, Part H, 211: 73-88, 1997.

Sharkey, P.F., Hozack, W.J., Callaghan, et. al.: Acetabular fracture associated with cementless acetabular component insertion. J Arthroplasty. 14: 426-431, 1999.

Shifrin, L.Z., Reis, N.D., Zinman, H., and Besser, M.I.: Idiopathic transient osteoporosis of the hip. J Bone Joint Surg. 69(5): 769-773, 1987.

Shimmin, A., Beaule, P.E., and Campbell, P.: Metal-on-metal hip replacing arthroplasty. J Bone Joint Surg. 90: 637-654, 2009.

Simonian, P. T. and Routt, M. L.: Biomechanics of Pelvic Fixation. J Am Acad Orthop Sug. 28 (3): 351–367, 1997.

Slooff, T.J., Huiskes, R., van Horn, J., and Lemmens, A.J.: Bone grafting in total hip replacement for acetabular protrusion. Acta Orthop Scand. 55:593-596, 1984.

Soballe, K., Hansen, E.S., Brockstedt-Rasmussen, H., Jorgensen, P.H., and Bunger, C.: Tissue ingrowth into titanium and hydroxyapatite-coated implants during stable and unstable mechanical conditions. J Orthop Res. l0: 285-299, 1992.

Soballe, K.: Hydroxyapatite ceramic coating for bone implant fixation. Acta Orthop Scand. 255: 1-58, 1993.

Spears, I.R., Pfleiderer, M., Schneider, E., Hille, E., and Morlock, M.M.: The effect of interfacial parameters on cup-bone relative micromotions. A finite element investigation. J Biomech. 31: 113-120, 2001.

Sporer, S.M., Paprosky, W.G., and O'Rourke, M.: Managing bone loss in acetabular revision. J Bone Joint Surg Am. 87: 1620-1630, 2005.

Stephenson , P.K., Freeman, M.A.R., Revell, P.A., et al.: The effect of a hydroxyapatite coating on ingrowth of bone into cavities in an implant. J Arthroplasty. 6: 5l-58, 1991.

Stiehl, J.B.: Revascularization of a Total Bulk Acetabular Allograft at 14 Years. J. Arthroplasty, 19: 508–512, 2004.

Stiehl, J.B., MacMillan, E., and Skrade, D.A.: Mechanical stability of porous-coated acetabular components in total hip arthroplasty. J Arthroplasty. 6(4): 295-300, 1991.

Stolarski, T., Nakasone, Y., Yoshimoto, S.: Engineering Analysis with ANSYS Software. Elsevier. Burlington, MA. 2006.

Tanaka, K., Tamura, J., Kawanabe, K., Shimizu, M., and Nakamura, T.: Effect of aluina femoral heads on polyethylene wear in cemented total hip arthroplasty. Old versus current alumina. J Bone Joint Surg Br. 85: 655-660, 2003.

Theory reference for ANSYS and ANSYS Workbench, P. 734, ANSYS Release 11, ANSYS Inc.

Thompson, M.S., Northmore-Ball, M.D., and Tanner, K.E.: Effects of acetabular resurfacing component material and fixation on the strain distrubtion in the pelvis. Journal of Engineering in Medicine. 216(4): 237-245, 2002.

Toms, A.D., Barker, R.L., Jones, R.S., et al.: Impaction bone grafting in revision joint replacement surgery. J Bone Joint Surg Am. 86:2050, 2004.

van der Heijde, D.M.F.M.: Joint erosions and patients with early rheumatoid arthritis. Rheum. 34(2): 74-78, 1995.

van der Linde, M. and Tonino, A.: Acetabular revision with impacted grafting and a reinforcement ring. Acta Orthop Scand. 72: 221-227, 2001.

Vasu, R., Carter, D.R., and Harris, W.H.: Stress distributions in the acetabular region. I: before and after total joint replacement. J Biomech. 15: 155-164, 1982.

Vicentonti, M., Muccini, R., Bernakiewicz, M., Baleani, M., and Cristofolini., L.: Large-slidding contact elements accurately predict levels of bone-implant micromotion relevant to osseointegration. J Biomech. 33: 1611-1618, 2000.

Wachter, N.J., Krischak, G.D., Mentzel, M., Sarkar, M.R., Ebinger, T., Kinzl, L., Claes, L., and Augat, P.: Correlation of bone mineral density with strength and microstructural parameters of cortical bone in vitro. Bone. 31: 90-95, 2002.

Wasielewski, R. C; Cooperstein, L. A.; Kruger, M. P.; and Rubash, H. E.: Acetabular anatomy and the transacetabular fixation of screws in total hip arthroplasty. J. Bone and Joint Surg. 12-A: 501-508, 1990.

Widmer, K.H.: Containment versus impingement: finding a compromise for cup placement in total hip arthroplasty. Int Othop. 31: S29-S33, 2007.

Wirtz, D.C., Schiffers, N., Pandorf, T., Raderacher, K., Weichert, D., and Forst, R.: Critical evaluation of known bone material properties to realize anisotropic FE-simulation of the proximal femur. J Biomech. 33: 1325-1330, 2000.

Won, C.H., Hearn, T.C., and Tile, M.: Micromotion of cementless hemispherical acetabular components. J Bone Joint Surg Br. 77: 484-489, 1995.

Wright, J.W., Pellicci, P.M., Salvati, E.A., et al.: Bone density adjacent to press-fit acetabular components: a prospective analysis with quantitative computed tomography. J Bone Joint Surg Am. 83-A: 529-536, 2001.

www.orthopaedics.about.com September 2011

Zipfel, G.J., Guiot, B.H., and Fessler, R.G.: Bone grafting. Neurosurg Focus 14: e8, 2003.

Zivkovic, I.: Initial stability of the press-fit acetabular implant: experimental and finite element study. Ph.D. Thesis, University of Illinois at Chicago, Chicago, 2006.

Zivkovic I, Gonzalez, M, Amirouche, F., 2010. The Effect of Under-Reaming on the Cup/Bone Interface of a Press Fit Hip Replacement. J. Biomech. Eng. Volume 13(4), 041008 .

Zywiel, M.G., McGrath, M.S., and Mont, M.A.: A Clinician's Pearls and Myths in Rheumatology. Springer Science, 2009.

VITA

NAME: Stefanie Broviak

EDUCATION: B.A., Bioengineering, University of Illinois at Chicago, Chicago, Illinois, 2010

M.S., Bioengineering, University of Illinois at Chicago, Chicago, Illinois, 2012

PROFESSIONAL MEMBERSHIP: Tau Beta Pi Engineering Honor Society

Engineering Council

ABSTRACTS: Amirouche, F., Broviak, S., Solitro, G.F.: Does the position of the cup affect THR fixation and stability? An in-vitro validation and FEM modeling of patient-specific orientations. Abstr., 2011.

Amirouche, F., Gusdou, Y., Goldstein, W., Upadhyay, A., Broviak, S.: Augmentation of acetabular defect with Kyrptonite bone cement in total hip arthroplasty. Abstr. Annu. Meet. Ortho. Res. Soc., 2010.